

INFERRING MANIFOLDS FROM NOISY DATA USING GAUSSIAN PROCESSES

DAVID B DUNSON AND NAN WU

ABSTRACT. In analyzing complex datasets, it is often of interest to infer lower dimensional structure underlying the higher dimensional observations. As a flexible class of nonlinear structures, it is common to focus on Riemannian manifolds. Most existing manifold learning algorithms replace the original data with lower dimensional coordinates without providing an estimate of the manifold in the observation space or using the manifold to denoise the original data. This article proposes a new methodology for addressing these problems, allowing interpolation of the estimated manifold between fitted data points. The proposed approach is motivated by novel theoretical properties of local covariance matrices constructed from noisy samples on a manifold. Our results enable us to turn a global manifold reconstruction problem into a local regression problem, allowing application of Gaussian processes for probabilistic manifold reconstruction. In addition to theory justifying the algorithm, we provide simulated and real data examples to illustrate the performance.

Data denoising; Dimension reduction; Manifold learning; Manifold reconstruction; Nonparametric regression; Gaussian processes

1. INTRODUCTION

Data are often observed as moderate to high-dimensional but in many cases have a lower dimensional structure. As this structure may be non-linear, it is common to characterize it mathematically as a Riemannian manifold. This has led to a rich literature on manifold learning algorithms, which reconstruct the observed data in a low dimensional space, while maintaining as much of the geometry of the underlying manifold as possible. Some well known manifold learning algorithms include isomap [39], Laplacian eigenmaps [4], locally linear embeddings [35], diffusion maps [8] and t-distributed stochastic neighbor embedding [40]. In practice, for the manifold assumption to be realistic, it is typically necessary to allow measurement error. Although some manifold learning algorithms are robust to noise [14, 36, 13, 10], these algorithms focus on providing lower-dimensional features and not on reconstructing the manifold and providing fitted values in the original sample space. The goal of this article is to address these limitations of classical manifold learning algorithms.

We describe a real life motivation behind the manifold reconstruction problem. Ecologists investigating bird species biodiversity heavily rely on the classification of vocalizations within audio files gathered from various spatial locations. These audio files are converted via discrete short time Fourier transform into spectrograms, which are matrices of huge dimensions. Submatrices representing vocalizations of bird species are then extracted and annotated by experts. In Figure 1, we present 5 annotated spectrograms corresponding to a specific call type of *Anthus trivialis* (tree pipit) from [32]. In recent years, machine learning algorithms have shown success in constructing classifiers for bird vocalizations [25], particularly when a substantial number of annotated spectrograms are available. However, expert annotations are expensive, and the quantity of audio data for rare bird species remains limited. Consequently, one approach to augmenting the training data [23] involves simulating new spectrograms through a small amount of annotated spectrograms corresponding to a vocalization. We delve into this data augmentation strategy by reconstructing the underlying low dimensional structure of the annotated spectrograms identified in a high dimensional space. By interpolating on this low dimensional structure, we generate new samples corresponding to the vocalization.

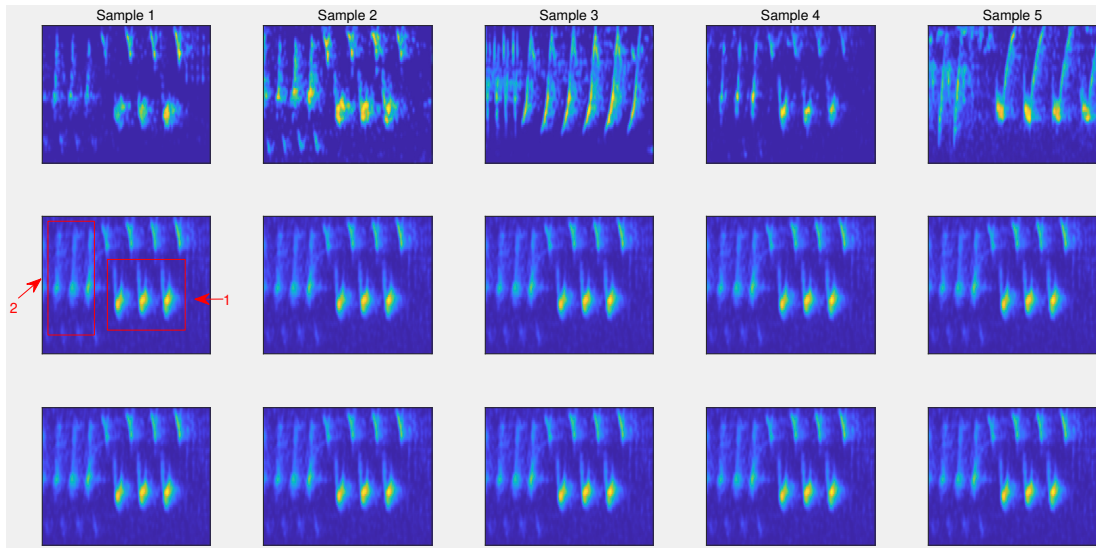


FIGURE 1. Top row: 5 out of 83 annotated spectrograms corresponding to a call type of *Anthus trivialis*. The rows of the matrices correspond to frequency (kHz), and the columns correspond to time (ms). Each entry in a matrix represents the amplitude of the signal at the given time and frequency. They are matrices in $\mathbb{R}^{75 \times 197}$ and identified in \mathbb{R}^{14775} . Samples 2 and 4 are near Sample 1. Second and third rows: 10 generated samples near Sample 1. Region 2 in the generated sample is similar to Sample 1, while region 1 is similar to Samples 2 and 4.

In this article, we propose a Manifold reconstruction via Gaussian processes (MrGap) algorithm, which estimates a submanifold of the observation space from samples on the manifold corrupted by Gaussian noise. MrGap builds upon our theoretical analysis of the spectral behavior of the local covariance matrix of noisy samples on a manifold. Our theoretical results enable us to turn a global manifold reconstruction problem into a local regression problem so that we can apply Gaussian process (GP) regression. The predictors and the response variables of the regression problem are constructed from the Euclidean coordinates of the noisy samples. MrGap provides a probabilistic method to reconstruct a manifold in the sense that for each noisy sample, we obtain a probability distribution whose mean is a denoised point on the manifold. Moreover, we can interpolate between different denoised points. To provide a teaser illustrating practical advantages of our algorithm, we apply it to 83 spectrograms corresponding to a call type of *Anthus trivialis*. The spectrograms are identified in \mathbb{R}^{14775} and exhibit an underlying 1 dimensional manifold structure. We interpolate 10 points near each sample on the manifold through MrGap and present 10 corresponding spectrograms near sample 1 in Figure 1. The generated new samples incorporate the audio information from sample 1 and its neighboring samples, while preserving the clean noise level. Refer to section 5 for a detailed procedure and the performance of the algorithm on noisy spectrograms.

We briefly review some related literature. The spectral properties of the local covariance matrix constructed from samples on an embedded submanifold in Euclidean space have been extensively studied. [37] analyzes the bias and variance of the local covariance matrix constructed by a smooth kernel supported on $[0, 1]$, assuming samples without noise from a closed submanifold. [42, 44] study spectral behavior of the local covariance matrix constructed from a $0-1$ kernel, assuming samples without noise from a closed submanifold and a submanifold with a boundary. [21] studies the local covariance matrix constructed from k nearest neighbors, assuming the embedded submanifold can be locally parametrized

by quadratic functions in the tangent spaces and samples are images of uniform samples in the domain of their parameterization with Gaussian noise. This is a quite restricted setting, and we consider much more general sampling conditions. Our theory on the local covariance matrix generalizes [42] to allow Gaussian noise.

In addition to manifold learning algorithms that provide a low dimensional representation of a data set, there are also algorithms developed to reconstruct a manifold from noisy samples in the original high dimensional space. [31] propose an algorithm to recover the homology groups of the manifold, assuming samples fall in an ε neighborhood of the manifold. [19] assumes noise in the normal direction to the manifold, developing a method similar to [31] and proving the convergence rate when the variance of the noise is known. The principal curve algorithm is an iterative method to fit a curve through the data [20, 22, 26]. [38] and [27] propose principal manifold methods extending principal curves to higher dimensions. These methods incorporate a penalty argument and kernel approaches to select model complexity, avoiding overfitting. [17, 18] consider samples from a manifold with Gaussian noise. By using the partition of unity, they construct a vector bundle in the neighborhood of the samples to approximate the normal bundle of the manifold. The manifold is reconstructed in a deterministic way by using the vector bundle. [1] and [2] apply local polynomial fitting to reconstruct a manifold from noisy samples. [1] assumes bounded noise in the normal direction, while [2] consider uniformly distributed noise in a tubular neighborhood of the manifold. In the most recent work, [45] consider uniform samples on an unknown manifold contaminated by Gaussian noise with a known variance. The manifold is reconstructed from the noisy data through an estimation of the orthogonal projection map.

The remainder of the paper is structured as follows. We begin by defining the problem and stating our goals in Section 2. In Section 2.1, we introduce the local covariance matrix and its associated operators. A brief overview of GP regression is presented in Section 2.2. Section 2.3 describes the primary challenges and the motivation of MrGap. The denoising and interpolation phases of the algorithm are detailed in Sections 2.4 and 2.5, respectively. The selection of parameters is discussed in Section 2.6. The theoretical analysis of MrGap is provided in Section 3. Within Section 3.1, we introduce geometric preliminaries. In Section 3.2, we provide the bias and the variance analysis of the local covariance matrix. Section 3.3 focuses on constructing charts of a manifold based on the operators associated with the local covariance matrix. We relate the reconstruction of these charts to a regression problem in Section 3.4 and discuss the theoretical aspects of the algorithm based on our earlier findings in Section 3.5. Section 3.6 introduces a geometric root mean square error to evaluate the algorithm's performance. A numerical simulation is presented in Section 4. In Section 5, we apply MrGap to augment bird vocalization data. We summarize our notations in Table 1.

2. MANIFOLD RECONSTRUCTION VIA GAUSSIAN PROCESSES

In this section, we propose an algorithm to reconstruct an embedded submanifold of Euclidean space from noisy samples. We first make the following assumption about the samples.

Assumption 2.1. *Suppose we are given the observed data $\{y_i\}_{i=1}^n \subset \mathbb{R}^D$ around a subset S of \mathbb{R}^D . S is a d -dimensional smooth, closed and connected submanifold of \mathbb{R}^D with the induced metric. Therefore, there exists a d -dimensional smooth, closed and connected Riemannian manifold M with a Riemannian metric g and an isometric embedding $\iota : M \rightarrow \mathbb{R}^D$ such that $S = \iota(M)$. Suppose P is a probability density function on M . We assume P is smooth and is bounded from below by $P_m > 0$ and bounded from above by P_M . We introduce the model that $y_i = \iota(x_i) + \eta_i$ and x_i are i.i.d samples based on P for $i = 1, \dots, n$. We further assume η_i are i.i.d sampled from $\mathcal{N}(0, \sigma^2 I_{D \times D})$ independently of x_i .*

In this work, the geometric information of $\iota(M)$ is not accessible and we are only given the Euclidean coordinates of $\{y_i\}_{i=1}^n$. However, our aim is to develop an algorithm that ensures the denoised samples lie on this submanifold. Specifically, we have the following two goals:

TABLE 1. Commonly used notations in this paper.

<i>Symbol</i>	<i>Meaning</i>
D	Dimension of the ambient space
d	Dimension of the low-dimensional Riemannian manifold
$\{e'_i\}_{i=1}^d, \{e_i\}_{i=1}^D$	The standard orthonormal basis of \mathbb{R}^d and \mathbb{R}^D respectively
M	d -dimensional smooth Riemannian manifold
P	Probability density function on M
ι	An isometric embedding of M in \mathbb{R}^D
$\{x_i\}_{i=1}^n$	Points sampled based on P from M
$\{\eta_i\}_{i=1}^n$	Noise sampled from a Gaussian distribution in \mathbb{R}^D
$\{y_i\}_{i=1}^n$	Noisy data points around $\iota(M)$
$\{\hat{y}_i\}_{i=1}^n$	Denoised data points corresponding to $\{y_i\}_{i=1}^n$
ε	The bandwidth of the local covariance matrix
$C_{n,\varepsilon}(\mathbf{y}_k)$	The local covariance matrix at \mathbf{y}_k constructed from a 0-1 kernel with bandwidth ε
J, \bar{J}	The projections from \mathbb{R}^D to the subspaces \mathbb{R}^d and \mathbb{R}^{D-d} respectively
$\mathcal{P}_{\mathbf{y}_k}, \mathcal{P}_{\mathbf{y}_k}^\perp$	Two major operators in the algorithm
δ	A scale in \mathbb{R}^D to perform $\mathcal{P}_{\mathbf{y}_k}, \mathcal{P}_{\mathbf{y}_k}^\perp$ in the algorithm

- (1) For each \mathbf{y}_k , find a corresponding $\hat{\mathbf{y}}_k \in \iota(M)$ while controlling $\frac{1}{n} \sum_{i=1}^n \|\iota(x_i) - \hat{\mathbf{y}}_k\|_{\mathbb{R}^D}^2$.
- (2) For each $\hat{\mathbf{y}}_k$, find a local parametrization of $\iota(M)$ around $\hat{\mathbf{y}}_k$ so that we can interpolate on $\iota(M)$.

For simplicity, we consider the dimension d of the manifold as known throughout the paper. Under Assumption 2.1, we provide a method to estimate the dimension d in Appendix G. There are two major ingredients in our algorithm: the local covariance matrix and GP regression. Before we describe the algorithm, we review these ingredients briefly in the following two subsections.

2.1. Local covariance matrix. Let $\{e_i\}_{i=1}^D$ be the standard orthonormal basis of \mathbb{R}^D , where $e_i = [0, \dots, 1, \dots, 0]^\top$ with 1 in the i -th entry. Similarly, let $\{e'_i\}_{i=1}^d$ be the standard orthonormal basis of \mathbb{R}^d . Letting $\chi(t) = 1$ for $t \in [0, 1]$ and $\chi(t) = 0$ for $t > 1$ denote a 0-1 kernel, we define a local covariance matrix at a sample point \mathbf{y}_k based on data $\{\mathbf{y}_1, \dots, \mathbf{y}_n\} \subset \mathbb{R}^D$,

$$(1) \quad C_{n,\varepsilon}(\mathbf{y}_k) = \frac{1}{n} \sum_{i=1}^n (\mathbf{y}_i - \mathbf{y}_k)(\mathbf{y}_i - \mathbf{y}_k)^\top \chi\left(\frac{\|\mathbf{y}_i - \mathbf{y}_k\|_{\mathbb{R}^D}}{\varepsilon}\right),$$

where $\varepsilon > 0$, and $C_{n,\varepsilon}$ is the covariance matrix used in local Principal Components Analysis (PCA); $C_{n,\varepsilon}$ and its eigenvectors are major ingredients of our algorithm. Consider the eigen decomposition

$$(2) \quad C_{n,\varepsilon}(\mathbf{y}_k) = U_{n,\varepsilon}(\mathbf{y}_k) \Lambda_{n,\varepsilon}(\mathbf{y}_k) U_{n,\varepsilon}(\mathbf{y}_k)^\top,$$

with $U_{n,\varepsilon}(\mathbf{y}_k) \in \mathbb{O}(D)$ and $\Lambda_{n,\varepsilon}(\mathbf{y}_k) \in \mathbb{R}^{D \times D}$ a diagonal matrix containing the eigenvalues of $C_{n,\varepsilon}(\mathbf{y}_k)$ in decreasing order on the diagonal, $e_1^\top \Lambda_{n,\varepsilon}(\mathbf{y}_k) e_1 \geq e_2^\top \Lambda_{n,\varepsilon}(\mathbf{y}_k) e_2 \geq \dots \geq e_D^\top \Lambda_{n,\varepsilon}(\mathbf{y}_k) e_D$. The column vectors of $U_{n,\varepsilon}(\mathbf{y}_k)$ are the orthonormal eigenvectors of $C_{n,\varepsilon}(\mathbf{y}_k)$ corresponding to decreasing order of the eigenvalues. The eigenvectors form an orthonormal basis of \mathbb{R}^D . We define two operators on \mathbb{R}^D associated with $U_{n,\varepsilon}(\mathbf{y}_k)$ as follows.

Let $J \in \mathbb{R}^{D \times d}$ be a projection matrix such that $J_{ij} = 1$ when $i = j$ and $J_{ij} = 0$ when $i \neq j$. Let $\bar{J} \in \mathbb{R}^{D \times (D-d)}$ be another projection matrix such that $\bar{J}_{ij} = 1$ when $i = d + j$ and $\bar{J}_{ij} = 0$ otherwise. Note that J and \bar{J} are the projections from \mathbb{R}^D to the subspaces \mathbb{R}^d and \mathbb{R}^{D-d} respectively. For any $\mathbf{y} \in \mathbb{R}^D$, let $\mathcal{P}_{\mathbf{y}_k}(\mathbf{y}) : \mathbb{R}^D \rightarrow \mathbb{R}^d$ with

$$(3) \quad \mathcal{P}_{\mathbf{y}_k}(\mathbf{y}) = J^\top U_{n,\varepsilon}(\mathbf{y}_k)^\top (\mathbf{y} - \mathbf{y}_k).$$

Let $\mathcal{P}_{\mathbf{y}_k}^\perp : \mathbb{R}^D \rightarrow \mathbb{R}^{D-d}$ with

$$(4) \quad \mathcal{P}_{\mathbf{y}_k}^\perp(\mathbf{y}) := \mathbf{J}^\top U_{n,\varepsilon}(\mathbf{y}_k)^\top (\mathbf{y} - \mathbf{y}_k).$$

The operators $\mathcal{P}_{\mathbf{y}_k}$ and $\mathcal{P}_{\mathbf{y}_k}^\perp$ are key pieces in our algorithm.

2.2. Gaussian process regression. Suppose $F : \mathbb{R}^d \rightarrow \mathbb{R}^q$ is an unknown regression function with $F = (f_1, \dots, f_q)^\top$. Letting $\mathbf{z}_i \in \mathbb{R}^q$ denote the response vector and $\mathbf{u}_i \in \mathbb{R}^d$ denote the predictor vector, for $i = 1, \dots, N$, and allowing for measurement error, we have

$$(5) \quad \mathbf{z}_i = F(\mathbf{u}_i) + \eta_i, \quad \eta_i \sim \mathcal{N}(0, \sigma^2 I_{q \times q}).$$

We assume all the component functions of F are not correlated and apply the techniques in GP regression for functions $f : \mathbb{R}^d \rightarrow \mathbb{R}$ [33] to each component of F . Specifically, we assign a GP prior to each f_j with mean 0 and covariance function

$$(6) \quad C(\mathbf{u}, \mathbf{u}') = A \exp\left(-\frac{\|\mathbf{u} - \mathbf{u}'\|_{\mathbb{R}^d}^2}{\rho}\right).$$

Denote $\mathbf{f}_j \in \mathbb{R}^N$ to be the discretization of f_j over $\{\mathbf{u}_i\}_{i=1}^N$ so that $\mathbf{f}_j = [f_j(\mathbf{u}_1), \dots, f_j(\mathbf{u}_N)]^\top$ for $j = 1, \dots, q$. A GP prior for f_j implies $p(\mathbf{f}_j | \mathbf{u}_1, \mathbf{u}_2, \dots, \mathbf{u}_N) = \mathcal{N}(0, \Sigma_1)$, where $\Sigma_1 \in \mathbb{R}^{N \times N}$ is the covariance matrix induced from C , with the (j, k) element of Σ_1 corresponding to $C(\mathbf{u}_j, \mathbf{u}_k)$, for $1 \leq j, k \leq N$. Prior distribution $\mathcal{N}(0, \Sigma_1)$ can be combined with information in the likelihood function under model (5) to obtain the posterior distribution, which will be used as a basis for inference.

Suppose we want to predict F at $\{\mathbf{u}_i\}_{i=N+1}^{N+m}$. Define $\mathbf{f}_j^* \in \mathbb{R}^m$ as $\mathbf{f}_j^* = [f_j(\mathbf{u}_{N+1}), \dots, f_j(\mathbf{u}_{N+m})]^\top$ for $j = 1, \dots, q$. Denote $\mathbf{F} \in \mathbb{R}^{m \times q}$ with j th column \mathbf{f}_j^* . Under a GP prior for f_j , the joint distribution of \mathbf{f}_j and \mathbf{f}_j^* is $p(\mathbf{f}_j, \mathbf{f}_j^*) = \mathcal{N}(0, \Sigma)$, where $\Sigma = \begin{bmatrix} \Sigma_1 & \Sigma_2 \\ \Sigma_3 & \Sigma_4 \end{bmatrix}$, with $\Sigma_2 \in \mathbb{R}^{N \times m}$, $\Sigma_3 \in \mathbb{R}^{m \times N}$, and $\Sigma_4 \in \mathbb{R}^{m \times m}$ induced from covariance function C .

Denote $\mathbf{Z} \in \mathbb{R}^{N \times q}$ with i th row \mathbf{z}_i^\top for $i = 1, \dots, N$. Denote $\tilde{\mathbf{z}}_j$ for $j = 1, \dots, q$ to be the j th column of \mathbf{Z} which consists of the responses of f_j over $\{\mathbf{u}_i\}_{i=1}^N$. Under model (5) and a GP prior, we have $p(\tilde{\mathbf{z}}_j, \mathbf{f}_j^*) = \mathcal{N}(0, \tilde{\Sigma})$, where

$$\tilde{\Sigma} = \Sigma + \begin{bmatrix} \sigma^2 I_{N \times N} & 0 \\ 0 & 0 \end{bmatrix} = \begin{bmatrix} \Sigma_1 + \sigma^2 I_{N \times N} & \Sigma_2 \\ \Sigma_3 & \Sigma_4 \end{bmatrix}.$$

For $j = 1, \dots, q$, the predictive distribution of \mathbf{f}_j^* is

$$(7) \quad p(\mathbf{f}_j^* | \tilde{\mathbf{z}}_j) = \mathcal{N}(\Sigma_3(\Sigma_1 + \sigma^2 I_{N \times N})^{-1} \tilde{\mathbf{z}}_j, \Sigma_4 - \Sigma_3(\Sigma_1 + \sigma^2 I_{N \times N})^{-1} \Sigma_2).$$

Then, prediction for \mathbf{F} can be expressed using the means of the above distributions:

$$(8) \quad \Sigma_3(\Sigma_1 + \sigma^2 I_{N \times N})^{-1} \mathbf{Z}.$$

In the special case $m = 1$, so we want to predict F at only one point \mathbf{u}_{N+1} , we have $\mathbf{F}^\top = F(\mathbf{u}_{N+1}) \in \mathbb{R}^q$. By (7), the predictive distribution of \mathbf{F}^\top is

$$(9) \quad p(\mathbf{F}^\top | \mathbf{Z}) = \mathcal{N}((\Sigma_3(\Sigma_1 + \sigma^2 I_{N \times N})^{-1} \mathbf{Z})^\top, (\Sigma_4 - \Sigma_3(\Sigma_1 + \sigma^2 I_{N \times N})^{-1} \Sigma_2) I_{q \times q}).$$

For each $\tilde{\mathbf{z}}_j$, the covariance parameters A , ρ and σ can be estimated by maximizing the natural log of the marginal likelihood, obtained by marginalizing over the GP prior,

$$\log p_j(\tilde{\mathbf{z}}_j | A, \rho, \sigma) = -\tilde{\mathbf{z}}_j^\top (\Sigma_1 + \sigma^2 I_{N \times N})^{-1} \tilde{\mathbf{z}}_j - \log(\det(\Sigma_1 + \sigma^2 I_{N \times N})) - \frac{N}{2} \log(2\pi).$$

To determine the parameters A , ρ and σ , we maximize $\log(\prod_{j=1}^q p_j(\tilde{\mathbf{z}}_j|A, \rho, \sigma))$,

$$\begin{aligned} \log p(\mathbf{Z}|A, \rho, \sigma) &:= \log(\prod_{j=1}^q p_j(\tilde{\mathbf{z}}_j|A, \rho, \sigma)) = \sum_{j=1}^q \log p_j(\tilde{\mathbf{z}}_j|A, \rho, \sigma) \\ &= - \sum_{j=1}^q \tilde{\mathbf{z}}_j^\top (\Sigma_1 + \sigma^2 I_{N \times N})^{-1} \tilde{\mathbf{z}}_j - q \log(\det(\Sigma_1 + \sigma^2 I_{N \times N})) - \frac{qN}{2} \log(2\pi) \\ (10) \quad &= - \text{tr}(\mathbf{Z}^\top (\Sigma_1 + \sigma^2 I_{N \times N})^{-1} \mathbf{Z}) - q \log(\det(\Sigma_1 + \sigma^2 I_{N \times N})) - \frac{qN}{2} \log(2\pi). \end{aligned}$$

This empirical Bayes approach for parameter estimation protects against over-fitting.

Remark 2.1. *In the general setup when the component functions of F are correlated, the covariance function in (6) is not appropriate and a matrix valued covariance function should be used; the above results can be easily generalized to such cases as discussed in [3].*

2.3. Main challenges and the motivation of the algorithm. Suppose \mathbf{y} is a point on the embedded manifold $\iota(M)$. The tangent space of $\iota(M)$ at \mathbf{y} , $T_{\mathbf{y}}\iota(M)$, is a subspace of \mathbb{R}^D . $\mathbf{y} + T_{\mathbf{y}}\iota(M)$ is the affine subspace tangent to $\iota(M)$ at \mathbf{y} . It is well known that $\iota(M)$ can be locally parametrized as a graph of a function over $\mathbf{y} + T_{\mathbf{y}}\iota(M)$. More precisely, consider the neighborhood $B_\delta^{\mathbb{R}^D}(\mathbf{y}) \cap \iota(M)$ for some $\delta > 0$. Then, there is function $F(\mathbf{u}) : O \subset \mathbb{R}^d \rightarrow \mathbb{R}^{D-d}$ with $F(0) = 0$ and $\nabla F(0) = 0$ such that the graph of F over O , after a rotation and a translation in \mathbb{R}^D , is a parametrization of $B_\delta^{\mathbb{R}^D}(\mathbf{y}_k) \cap \iota(M)$. The parametrization can be expressed formally as $\Phi(\mathbf{u}) : O \rightarrow \mathbb{R}^D$, where

$$\Phi(\mathbf{u}) = \mathbf{y} + U \begin{bmatrix} \mathbf{u} \\ F(\mathbf{u}) \end{bmatrix}.$$

$U \in O(D)$ is an orthogonal matrix which maps from the subspace generated by e_1, \dots, e_d to $T_{\mathbf{y}}\iota(M)$. Refer to Figure 2. A more technical description of the above fact is provided in Proposition A.1 in the Appendix.

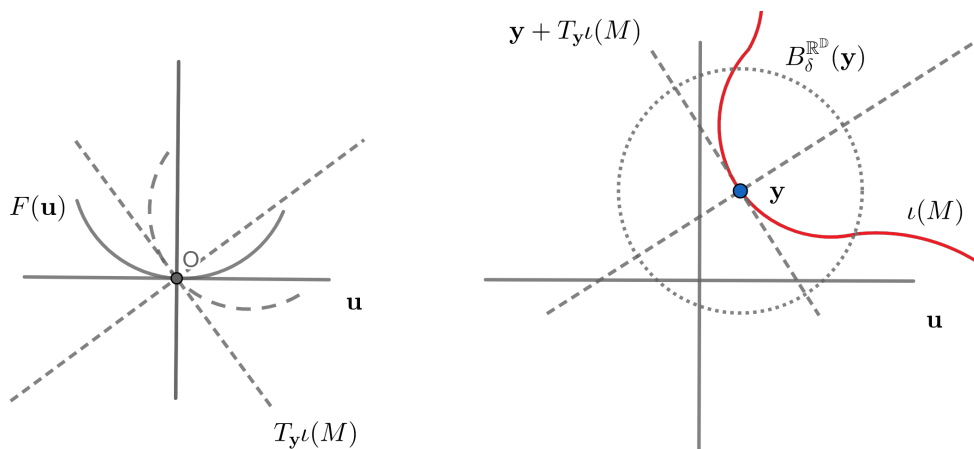


FIGURE 2. Left Panel: The solid lines are the standard coordinates of \mathbb{R}^D . The solid curve is the plot of $[\mathbf{u}, F(\mathbf{u})]^\top$. The dashed lines show the rotation of the coordinates under U and the plot of $U[\mathbf{u}, F(\mathbf{u})]^\top$. Right Panel: The red curve is $\iota(M)$. After a translation by \mathbf{y} , the graph of $\mathbf{y} + U[\mathbf{u}, F(\mathbf{u})]^\top$ gives a parametrization of $B_\delta^{\mathbb{R}^D}(\mathbf{y}) \cap \iota(M)$.

However, since $\iota(M)$ is unknown and we are only given the noisy data around $\iota(M)$, we can not recover the tangent spaces of $\iota(M)$, i.e. we do not know the matrix U or the function F . On the other hand, if we choose an arbitrary d dimensional affine subspace through a point \mathbf{y} around $\iota(M)$, then we can find a matrix U which maps the subspace generated by e_1, \dots, e_d to the subspace corresponding to the affine space, but $\iota(M)$ may not be parametrized locally by the graph of any function over the affine space. For example, let $\iota(M)$ be the graph of $y = x^2$ in \mathbb{R}^2 . Let \mathbf{y} be the origin. If we choose the affine subspace to be the y -axis, then no matter what δ we choose, $B_\delta^{\mathbb{R}^2}(\mathbf{y}) \cap \iota(M)$ can not be expressed as the graph of any function over the y -axis. Fortunately, inferring the tangent space is not necessary. The above facts can be applied to reconstruct $\iota(M)$ as long as we can find an affine subspace where $\iota(M)$ can be parametrized locally by the graph of a function over that affine space.

2.4. Denoising phase of the MrGap algorithm. Under Assumption 2.1, let \mathcal{T}_k be the subspace generated by the first d eigenvectors of $C_{n,\varepsilon}(\mathbf{y}_k)$ constructed from the noisy data as defined in (1). Let $\mathcal{H}_k = \mathbf{y}_k + \mathcal{T}_k$ be the affine subspace through \mathbf{y}_k . In section 3, we show that under certain relations between the bandwidth ε , the variance of the noise σ^2 , and the sample size n , with high probability, the neighborhood $B_{3\delta}^{\mathbb{R}^D}(\mathbf{y}_k) \cap \iota(M)$ can be parametrized as the graph of a function over \mathcal{H}_k for $\delta > \varepsilon$. The parametrization can be expressed similarly as when the affine subspace is tangent to the manifold:

$\Phi_k(\mathbf{u}) = \mathbf{y}_k + U_{n,\varepsilon}(\mathbf{y}_k) \begin{bmatrix} \mathbf{u} \\ F_k(\mathbf{u}) \end{bmatrix}$ where $F_k(\mathbf{u}) : O_k \rightarrow \mathbb{R}^{D-d}$ for a connected open set O_k containing 0 in \mathbb{R}^d and $U_{n,\varepsilon}(\mathbf{y}_k)$ is the orthogonal matrix which maps the subspace generated by e_1, \dots, e_d to \mathcal{T}_k as defined in (2). The parametrization $\Phi_k(\mathbf{u})$ is constructed from a rotation under $U_{n,\varepsilon}(\mathbf{y}_k)$ and a translation under \mathbf{y}_k of the graph of $F_k(\mathbf{u})$. On the other hand, for $0 \in \mathbb{R}^D$, we have $\mathbf{y}_k + U_{n,\varepsilon}(\mathbf{y}_k) \begin{bmatrix} 0 \\ 0 \end{bmatrix} = \mathbf{y}_k$ which may be not on $\iota(M)$. Based on the parametrization $\Phi_k(\mathbf{u})$,

$$(11) \quad \hat{\mathbf{y}}_k = \mathbf{y}_k + U_{n,\varepsilon}(\mathbf{y}_k) \begin{bmatrix} 0 \\ F_k(0) \end{bmatrix}$$

is a point on $\iota(M)$. Hence, unlike when all the points are on the manifold, $F_k(0)$ may not be 0. But if we can predict $F_k(0)$, then (11) provides us the denoised output $\hat{\mathbf{y}}_k$ corresponding to \mathbf{y}_k .

To predict $F_k(0)$, we infer the function F_k through GP regression. The operations $\mathcal{P}_{\mathbf{y}_k}$ and $\mathcal{P}_{\mathbf{y}_k}^\perp$ in (3) and (4) are compositions of (a) a translation under $-\mathbf{y}_k$, (b) a rotation under $U_{n,\varepsilon}(\mathbf{y}_k)^\top$, and (c) projections onto \mathbb{R}^d and \mathbb{R}^{D-d} respectively. Since $\Phi_k(\mathbf{u})$ is a parametrization of $B_{3\delta}^{\mathbb{R}^D}(\mathbf{y}_k) \cap \iota(M)$ and there is noise in the data, we use points in a smaller neighborhood of \mathbf{y}_k to estimate $F_k(0)$: $B_\delta^{\mathbb{R}^D}(\mathbf{y}_k) \setminus \mathbf{y}_k \cap \{\mathbf{y}_1, \dots, \mathbf{y}_n\} = \{\mathbf{y}_{k,1}, \dots, \mathbf{y}_{k,N_k}\}$. Refer to Section 3 for details. Then, $\mathbf{w}_{k,j} = \mathcal{P}_{\mathbf{y}_k}(\mathbf{y}_{k,j})$ are the inputs for F_k and $\mathbf{z}_{k,j} = \mathcal{P}_{\mathbf{y}_k}^\perp(\mathbf{y}_{k,j})$ are the corresponding response variables for $j = 1, \dots, N_k$. Refer to Figure 3.

In conclusion, the denoising phase of the MrGap algorithm consists of the following steps. Inputs of the algorithm include data $\{\mathbf{y}_i\}_{i=1}^n$, a bandwidth ε of the local covariance matrix $C_{n,\varepsilon}(\mathbf{y}_k)$, and a scale δ of the maps $\mathcal{P}_{\mathbf{y}_k}$ and $\mathcal{P}_{\mathbf{y}_k}^\perp$. The output of the algorithm is the denoised data $\{\hat{\mathbf{y}}_1, \dots, \hat{\mathbf{y}}_n\}$. In Step 1, for each noisy data point \mathbf{y}_k , we find the noisy data $\{\mathbf{y}_{k,1}, \dots, \mathbf{y}_{k,N_k}\}$ in $B_\delta^{\mathbb{R}^D}(\mathbf{y}_k) \setminus \mathbf{y}_k$. We construct the inputs and response variables for a regression function F_k as described above. In Step 2, we calculate the GP covariance matrix across 0 and $\{\mathbf{w}_{k,j}\}_{j=1}^{N_k}$. In Step 3, we apply GP regression, while estimating the tuning parameters, to recover $F_k(0)$ in order to denoise the data. Recovery of F_k involves a challenging errors in variables regression problem, so that in Step 4, we apply Steps 1 to 3 iteratively to refine the results. Figure 3 illustrates the first 3 steps and Step 4 is further discussed theoretically in Section 3. We summarize the denoising phase as Algorithm 1 in the following table.

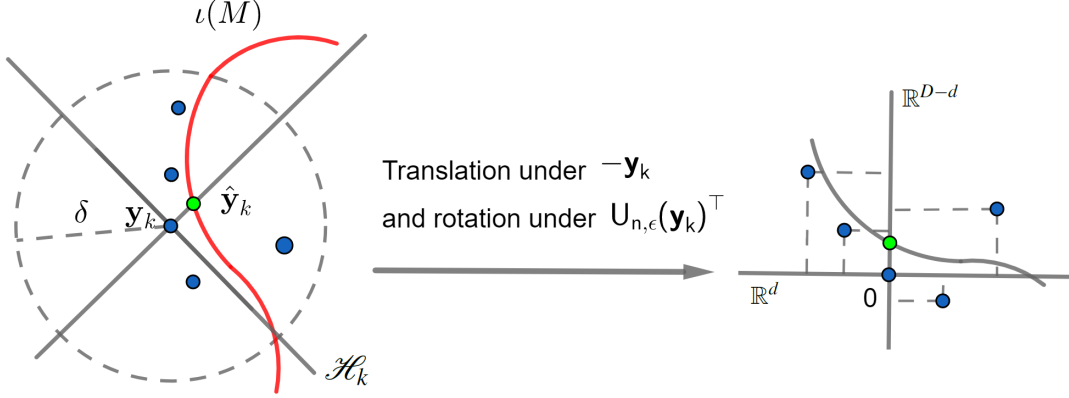


FIGURE 3. Left Panel: The red curve is $\iota(M)$. The solid lines are the affine subspace \mathcal{H}_k and the affine normal subspace of \mathcal{H}_k . The blue points are the noisy data points in the δ neighborhood of \mathbf{y}_k . Right Panel: The solid lines are the coordinates in \mathbb{R}^D and the graph of the function F_k . After (1) a translation under $-\mathbf{y}_k$ and (2) a rotation under $U_{n,\varepsilon}(\mathbf{y}_k)^\top$, the blue points in the left panel (the noisy data points) are mapped to the blue points in the right panel. In particular, \mathbf{y}_k is mapped to the origin. If we project the blue points except $0 \in \mathbb{R}^D$ in the right panel onto \mathbb{R}^d and \mathbb{R}^{D-d} which are the last operations (3) in $\mathcal{P}_{\mathbf{y}_k}$ and $\mathcal{P}_{\mathbf{y}_k}^\perp$, then we have the inputs $\mathbf{w}_{k,j}$ and the response variables $\mathbf{z}_{k,j}$ for F_k respectively. The green point in the right panel is $[0, F_k(0)]^\top$. We apply equation (11) to get the denoised output $\hat{\mathbf{y}}_k$ indicated by the green point in the left panel.

2.5. Interpolation phase of the MrGap algorithm. For simplicity, suppose $\sigma \approx 0$, so that the variance of the noise is very small and one iteration in Algorithm 1 suffices. We interpolate K points iteratively around each denoised output $\hat{\mathbf{y}}_k$ on $\iota(M)$ for k from 1 to n .

Suppose $C_{n,\varepsilon}(\mathbf{y}_k)$ is the local covariance matrix defined in (1). Recall that for each \mathbf{y}_k , the neighborhood $B_{3\delta}^{\mathbb{R}^D}(\mathbf{y}_k) \cap \iota(M)$ has the parametrization: $\Phi_k(\mathbf{u}) = \mathbf{y}_k + U_{n,\varepsilon}(\mathbf{y}_k) \begin{bmatrix} \mathbf{u} \\ F_k(\mathbf{u}) \end{bmatrix}$ where $F_k(\mathbf{u}) : O_k \rightarrow \mathbb{R}^{D-d}$ for a connected open set O_k in \mathbb{R}^d and $U_{n,\varepsilon}(\mathbf{y}_k)$ is the orthogonal matrix defined in (2). We find $B_{3\delta}^{\mathbb{R}^D}(\mathbf{y}_k) \setminus \mathbf{y}_k \cap \{\mathbf{y}_1, \dots, \mathbf{y}_n\} = \{\mathbf{y}_{k,1}, \dots, \mathbf{y}_{k,N_k}\}$. Then, $\mathbf{w}_{k,j} = \mathcal{P}_{\mathbf{y}_k}(\mathbf{y}_{k,j})$ are the inputs for F_k and $\mathbf{z}_{k,j} = \mathcal{P}_{\mathbf{y}_k}^\perp(\mathbf{y}_{k,j})$ are the corresponding response variables for $j = 1, \dots, N_k$. We use the inputs $\mathbf{w}_{k,j}$ for $j = 1, \dots, N_k$ to estimate a small round ball contained in the domain O_k with the center of the ball the mean of $\{\mathbf{w}_{k,j}\}_{j=1}^{N_k}$. We uniformly randomly sample K points $\{\tilde{\mathbf{u}}_{k,1}, \dots, \tilde{\mathbf{u}}_{k,K}\}$ in the ball as a straightforward way to generate points in the domain of each chart. In step 3 of Algorithm 1, the GP parameters are estimated through maximizing the sum of log marginal likelihoods. We then estimate $F_k(0)$ and $F_k(\tilde{\mathbf{u}}_{k,j})$ for $j = 1, \dots, K$. Hence,

$$(14) \quad \mathbf{y}_k + U_{n,\varepsilon}(\mathbf{y}_k) \begin{bmatrix} \tilde{\mathbf{u}}_{k,j} \\ F_k(\tilde{\mathbf{u}}_{k,j}) \end{bmatrix}$$

is a point interpolated in $B_{3\delta}^{\mathbb{R}^D}(\mathbf{y}_k) \cap \iota(M)$ for $j = 1, \dots, K$.

However, it is possible that $B_{3\delta}^{\mathbb{R}^D}(\mathbf{y}_k) \cap \iota(M)$ and $B_{3\delta}^{\mathbb{R}^D}(\mathbf{y}_{k'}) \cap \iota(M)$ intersect when $k \neq k'$. We want to make sure that the points interpolated in $B_{3\delta}^{\mathbb{R}^D}(\mathbf{y}_k) \cap \iota(M)$ and $B_{3\delta}^{\mathbb{R}^D}(\mathbf{y}_{k'}) \cap \iota(M)$ are glued together smoothly along the intersecting region. Suppose we interpolated $K(k-1)$ points around $\hat{\mathbf{y}}_1, \dots, \hat{\mathbf{y}}_{k-1}$

Algorithm 1: MrGap denoising steps to produce estimates of $\hat{\mathbf{y}}_1, \dots, \hat{\mathbf{y}}_n$ from $\mathbf{y}_1, \dots, \mathbf{y}_n$.

- 1 For each \mathbf{y}_k , construct $C_{n,\varepsilon}(\mathbf{y}_k)$ as in (1). Denote the N_k samples in $B_{\delta}^{\mathbb{R}^D}(\mathbf{y}_k) \setminus \mathbf{y}_k$ as $\{\mathbf{y}_{k,1}, \dots, \mathbf{y}_{k,N_k}\}$. Let $\mathbf{w}_{k,j} = \mathcal{P}_{\mathbf{y}_k}(\mathbf{y}_{k,j})$ and $\mathbf{z}_{k,j} = \mathcal{P}_{\mathbf{y}_k}^{\perp}(\mathbf{y}_{k,j})$ for $j = 1, \dots, N_k$, with $\mathcal{P}_{\mathbf{y}_k}(\mathbf{y})$ and $\mathcal{P}_{\mathbf{y}_k}^{\perp}(\mathbf{y})$ defined in (3) and (4). The k th local GP regression has responses $\mathbf{z}_{k,j}$ and predictors $\mathbf{w}_{k,j}$.
- 2 For each \mathbf{y}_k , construct covariance $\Sigma_k = \begin{bmatrix} \Sigma_{k,1} & \Sigma_{k,2} \\ \Sigma_{k,3} & \Sigma_{k,4} \end{bmatrix} \in \mathbb{R}^{(N_k+1) \times (N_k+1)}$ over $\{\mathbf{w}_{k,1}, \dots, \mathbf{w}_{k,N_k}, \mathbf{0}\}$ induced by C in (6), with $\Sigma_{k,1} \in \mathbb{R}^{N_k \times N_k}$. Denote $\mathbf{Z}_k \in \mathbb{R}^{N_k \times (D-d)}$ with i th row $\mathbf{z}_{k,i}^{\top}$.
- 3 For the k th local GP regression, the log marginal likelihood is calculated using (10) for $\mathbf{Z} = \mathbf{Z}_k$, $\Sigma_1 = \Sigma_{k,1}$ and $N = N_k$. We choose A , ρ and σ to maximize the sum of these log marginal likelihoods over $k = 1, \dots, n$,

$$(12) \quad \sum_{k=1}^n \log p_k(\mathbf{Z}_k | A, \rho, \sigma) = - \sum_{k=1}^n \left(\text{tr}(\mathbf{Z}_k^{\top} (\Sigma_{k,1} + \sigma^2 I_{N_k \times N_k})^{-1} \mathbf{Z}_k) - (D-d) \log(\det(\Sigma_{k,1} + \sigma^2 I_{N_k \times N_k})) - \frac{qN_k}{2} \log(2\pi) \right).$$

We then obtain the denoised output data using

$$(13) \quad \mathbf{y}_k^{(1)} = \mathbf{y}_k + U_{n,\varepsilon}(\mathbf{y}_k) \begin{bmatrix} \mathbf{0} \\ (\Sigma_{k,3} (\Sigma_{k,1} + \sigma^2 I_{N_k \times N_k})^{-1} \mathbf{Z}_k)^{\top} \end{bmatrix},$$

where $U_{n,\varepsilon}(\mathbf{y}_k)$ is the orthonormal eigenvector matrix of $C_{n,\varepsilon}(\mathbf{y}_k)$ defined in (2). The upper index (1) indicates that $\mathbf{y}_k^{(1)}$ are the results from the first round of the iterations.

- 4 Repeat Steps 1-3 using the denoised data in Step 3 as the input in Step 1. Stop iterating when the change in σ between iterations is below a small tolerance and output the final denoised data.
-

and we denote the union of these points as \tilde{M}_{k-1} . We explain how to interpolate K points in $B_{3\delta}^{\mathbb{R}^D}(\mathbf{y}_k) \cap \iota(M)$ and glue them smoothly with \tilde{M}_{k-1} . We find $\tilde{M}_{k-1} \cap B_{\delta}^{\mathbb{R}^D}(\mathbf{y}_k) = \{\tilde{\mathbf{y}}_{k,1}, \dots, \tilde{\mathbf{y}}_{k,L_k}\}$. Hence, instead of only using $\{\mathbf{w}_{k,j}\}_{j=1}^{N_k}$ and $\{\mathbf{z}_{k,j}\}_{j=1}^{N_k}$ for the prediction, we use both $\{\mathbf{w}_{k,j}\}_{j=1}^{N_k}$ and $\tilde{\mathbf{w}}_{k,j} = \mathcal{P}_{\mathbf{y}_k}(\tilde{\mathbf{y}}_{k,j})$ for $j = 1, \dots, L_k$ as the inputs for F_k . We use both $\{\mathbf{z}_{k,j}\}_{j=1}^{N_k}$ and $\tilde{\mathbf{z}}_{k,j} = \mathcal{P}_{\mathbf{y}_k}^{\perp}(\tilde{\mathbf{y}}_{k,j})$ for $j = 1, \dots, L_k$ as the corresponding response variables for F_k . The tuning parameters that we estimated in Step 3 of Algorithm 1 determine the covariance structure for F_k so that we can apply GP regression to the inputs and the response variables to recover $F_k(\tilde{\mathbf{u}}_{k,j})$ for $j = 1, \dots, K$. Refer to Figure 4 for an illustration.

The interpolation phase is described in Algorithm 2 as follows. Inputs consist of K , the GP parameters A, ρ, σ from the *last round* of Algorithm 1, and the denoised data from the *second to last round* of Algorithm 1.

2.6. Selection of the parameters ε and δ . Appropriate choice of ε and δ depends on geometric properties of $\iota(M)$ and the distribution of the data. Since $\iota(M)$ is unknown, we propose a practical approach for selecting ε and δ . The sum of marginal likelihoods in (12) is $L(\varepsilon, \delta) = \sum_{k=1}^n \log p_k(\mathbf{Z}_k | A, \rho, \sigma)$. We propose choosing ε and δ by maximizing $L(\varepsilon, \delta)$ over all $\varepsilon \leq \delta$ in the first round of Algorithm 1: $\varepsilon, \delta = \arg \max_{\varepsilon \leq \delta} L(\varepsilon, \delta)$. Although $L(\varepsilon, \delta)$ has an analytic expression in terms of the GP parameters A, ρ , and σ , it is not explicitly expressed in ε and δ . Hence, we apply a grid search over $\varepsilon \leq \delta$. To improve efficiency, a lower bound b on ε is imposed in the search such that each $C_{n,b}(\mathbf{y}_k)$ has at least d positive eigenvalues for all k . Refer to Appendix H for an example.

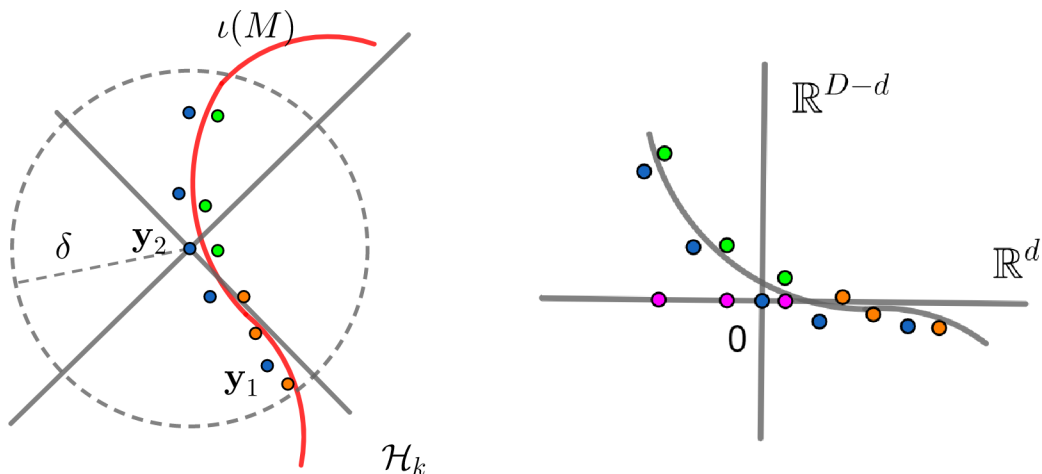


FIGURE 4. In this case $\sigma \approx 0$ and Algorithm 1 stops after the first round. We focus our discussion on the point \mathbf{y}_2 . Left Panel: The blue points are the noisy data points in $B_{\delta}^{\mathbb{R}^D}(\mathbf{y}_2)$. Suppose we interpolated K points around \mathbf{y}_1 on $\iota(M)$; \tilde{M}_1 is the union of these K points. We find $\tilde{M}_1 \cap B_{\delta}^{\mathbb{R}^D}(\mathbf{y}_2)$ which are the orange points. Right Panel: The solid lines are the coordinates in \mathbb{R}^D and the graph of the function F_2 . After a translation under $-\mathbf{y}_2$ and a rotation under $U_{n,\varepsilon}(\mathbf{y}_2)^{\top}$, the blue points and the orange points in the left panel are mapped to the blue points and orange points in the right panel. The purple points $\{\tilde{\mathbf{u}}_{2,j}\}_{j=1}^K$ are generated in the domain of F_2 in \mathbb{R}^d for the prediction. The blue points except 0 and the orange points are projected onto \mathbb{R}^d and \mathbb{R}^{D-d} to be the inputs and the response variables for the prediction of $\{F_2(\tilde{\mathbf{u}}_{2,j})\}_{j=1}^K$. The green points in the right panel are the predictions whose coordinates are $[\tilde{\mathbf{u}}_{2,j}, F_2(\tilde{\mathbf{u}}_{2,j})]^{\top}$. The green points in the right panel are mapped back to green points in the left panel through (14) which are the interpolations around \mathbf{y}_2 .

3. THEORETICAL ANALYSIS

3.1. Geometric preliminaries. Suppose M is a d -dimensional smooth, closed and connected Riemannian manifold isometrically embedded in \mathbb{R}^D through ι . Let ι_* be the differential of ι . Suppose $x \in M$ and $\mathbf{y} = \iota(x)$. Let $T_x M$ be the tangent space of M at x and $T_{\mathbf{y}} \iota(M)$ be the tangent space of $\iota(M)$ at \mathbf{y} which is a subspace of \mathbb{R}^D . ι_* at x denoted as $\iota_*(x)$ is a linear map from $T_x M$ to $T_{\mathbf{y}} \iota(M)$. Moreover, since ι is an isometry, $\iota_*(x)$ is a linear isomorphism between $T_x M$ and $T_{\mathbf{y}} \iota(M)$. Hence, $\iota_*(x)(T_x M) = T_{\mathbf{y}} \iota(M)$. For simplicity, we write $\iota_*(x)(T_x M)$ as $\iota_* T_x M$.

Recall the definition of a chart for $\iota(M)$. For any $x \in M$, we can find an open set $U_x \subset \mathbb{R}^D$ with $\iota(x) \in U_x$. V_x is an open topological ball in \mathbb{R}^d . A chart of $\iota(M)$ over $U_x \cap \iota(M)$ is a map $\Phi_x : V_x \rightarrow U_x \cap \iota(M)$ such that Φ_x is a diffeomorphism. Refer to Appendix A for a detailed introduction about diffeomorphisms between subsets in Euclidean space and the charts of the embedded submanifold $\iota(M)$. Next, we recall the definition of the reach of an embedded submanifold in the Euclidean space [16], which is an important concept in the reconstruction of the manifold.

Definition 3.1. For any point $\mathbf{y} \in \mathbb{R}^D$, the distance between \mathbf{y} and $\iota(M)$ is $\text{dist}(\mathbf{y}, \iota(M)) = \inf_{\mathbf{y}' \in \iota(M)} \|\mathbf{y} - \mathbf{y}'\|_{\mathbb{R}^D}$. The reach of $\iota(M)$ is the supremum of all ℓ such that if $\mathbf{y} \in \mathbb{R}^D$ and $\text{dist}(\mathbf{y}, \iota(M)) < \ell$ then there is a unique $\mathbf{y}' \in \iota(M)$ with $\text{dist}(\mathbf{y}, \iota(M)) = \|\mathbf{y} - \mathbf{y}'\|_{\mathbb{R}^D}$. We denote the reach of $\iota(M)$ as $\tau_{\iota(M)}$.

Algorithm 2: MrGap steps to iteratively interpolate K points around each $\hat{\mathbf{y}}_k$.

- 1 **for** $k = 1, \dots, n$ **do**
 - 2 Let \tilde{M}_{k-1} be the union of the $K(k-1)$ points already interpolated around $\{\hat{\mathbf{y}}_1, \dots, \hat{\mathbf{y}}_{k-1}\}$.
 For notation simplicity, we use $\{\mathbf{y}_1, \dots, \mathbf{y}_n\}$ to denote the denoised output from *the second to last round* iteration in Algorithm 1.
 - 3 Use $\{\mathbf{y}_1, \dots, \mathbf{y}_n\}$ to repeat Step 1 of Algorithm 1. Construct $C_{n,\varepsilon}(\mathbf{y}_k)$ and find $U_{n,\varepsilon}(\mathbf{y}_k)$.
 Obtain $\mathbf{z}_{k,j}, \mathbf{w}_{k,j}$, for $j = 1, \dots, N_k$.
 - 4 Let $\mathcal{U}_k = \frac{1}{N_k} \sum_{j=1}^{N_k} \mathbf{w}_{k,j}$, and (m_k, s_k) denote the mean and standard deviation of $\{\|\mathbf{w}_{k,1} - \mathcal{U}_k\|_{\mathbb{R}^d}, \dots, \|\mathbf{w}_{k,N_k} - \mathcal{U}_k\|_{\mathbb{R}^d}\}$. Let $\{\tilde{\mathbf{u}}_{k,1}, \dots, \tilde{\mathbf{u}}_{k,K}\}$ be K samples generated uniformly in $B_{m_k - s_k}^{\mathbb{R}^d}(\mathcal{U}_k)$. Suppose $B_{\xi}^{\mathbb{R}^D}(\mathbf{y}_k) \cap \tilde{M}_{k-1} = \{\tilde{\mathbf{y}}_{k,1}, \dots, \tilde{\mathbf{y}}_{k,L_k}\}$, and let $\tilde{\mathbf{w}}_{k,j} = \mathcal{P}_{\mathbf{y}_k}(\tilde{\mathbf{y}}_{k,j})$, $\tilde{\mathbf{z}}_{k,j} = \mathcal{P}_{\mathbf{y}_k}^{\perp}(\tilde{\mathbf{y}}_{k,j})$ for $j = 1, \dots, L_k$.
 - 5 Construct covariance $\tilde{\Sigma}_k = \begin{bmatrix} \tilde{\Sigma}_{k,1} & \tilde{\Sigma}_{k,2} \\ \tilde{\Sigma}_{k,3} & \tilde{\Sigma}_{k,4} \end{bmatrix}$ over $\{\mathbf{w}_{k,1}, \dots, \mathbf{w}_{k,N_k}, \tilde{\mathbf{w}}_{k,1}, \dots, \tilde{\mathbf{w}}_{k,L_k}, \tilde{\mathbf{u}}_{k,1}, \dots, \tilde{\mathbf{u}}_{k,K}\}$ using covariance \mathbf{C} in (6) and the covariance parameters that we find in *the last round* iteration of Algorithm 1, with $\tilde{\Sigma}_{k,1}$ corresponding to $\{\mathbf{w}_{k,1}, \dots, \mathbf{w}_{k,N_k}, \tilde{\mathbf{w}}_{k,1}, \dots, \tilde{\mathbf{w}}_{k,L_k}\}$. Denote $\mathbf{Z}_k \in \mathbb{R}^{N_k \times (D-d)}$ with j th row $\mathbf{z}_{k,j}^{\top}$, and $\tilde{\mathbf{Z}}_k \in \mathbb{R}^{L_k \times (D-d)}$ with j th row $\tilde{\mathbf{z}}_{k,j}^{\top}$.
 - 6 Let $\mathbf{1}_K$ denote a K -vector of ones. Then, the column vectors of

$$(15) \quad \mathbf{y}_k \mathbf{1}_K^{\top} + U_{n,\varepsilon}(\mathbf{y}_k) \left[\begin{array}{c} \tilde{\mathbf{u}}_{k,1}, \dots, \tilde{\mathbf{u}}_{k,K} \\ \left(\tilde{\Sigma}_{k,3} (\tilde{\Sigma}_{k,1} + \sigma^2 I_{(N_k+L_k) \times (N_k+L_k)})^{-1} \begin{bmatrix} \mathbf{Z}_k \\ \tilde{\mathbf{Z}}_k \end{bmatrix} \right)^{\top} \end{array} \right] \in \mathbb{R}^{D \times K},$$
 give the Euclidean coordinates of the points that we interpolate around $\hat{\mathbf{y}}_k$.
 - 7 **end**
-

The reach $\tau_{\iota(M)}$ of $\iota(M)$ is the largest number such that any point in \mathbb{R}^D at distance less than the reach from $\iota(M)$ has a unique nearest point on $\iota(M)$. The reaches of some special embedded submanifolds can be explicitly calculated. For example, the reach of a d dimensional round sphere in \mathbb{R}^D is the radius of the sphere. We have the following topological result about the reach of $\iota(M)$. A consequence of the result says that if we can find a point $\mathbf{y} \in \mathbb{R}^D$ and a radius ξ such that $B_{\xi}^{\mathbb{R}^D}(\mathbf{y}) \cap \iota(M)$ has more than one connected component, then $\tau_{\iota(M)} < \xi$. In Figure 5, we illustrate the concept of reach by using this consequence.

Proposition 3.1 (Proposition 1 [5]). *Suppose $0 < \xi < \tau_{\iota(M)}$. For any $\mathbf{y} \in \mathbb{R}^D$, If $B_{\xi}^{\mathbb{R}^D}(\mathbf{y}) \cap \iota(M) \neq \emptyset$, then $B_{\xi}^{\mathbb{R}^D}(\mathbf{y}) \cap \iota(M)$ is an open subset of $\iota(M)$ that is homeomorphic to $B_1^{\mathbb{R}^d}(0)$.*

Remark 3.1. *The concept of the reach of $\iota(M)$ depends on the isometric embedding ι , hence it is an extrinsic property. For example, let S^1 be the unit circle in \mathbb{R}^2 and $a \in S^1$. Let $\iota_1(M) = S^1 \setminus a \subset \mathbb{R}^2$ and let $\iota_2(M) = (0, 2\pi) \times \{0\}$ be the an interval on the x -axis in \mathbb{R}^2 . Then, $\iota_1(M)$ and $\iota_2(M)$ are different isometric embeddings of the same manifold, but they have different reaches.*

3.2. Local covariance matrix on manifold with noise. Note that $C_{n,\varepsilon}(\mathbf{y}_k)$ from (2) is invariant under the translation of $\iota(M)$ in \mathbb{R}^D . Hence, to simplify the notation, we make the following assumption for the results in this subsection.

Assumption 3.1. *For any fixed $x_k \in M$, we first translate $\iota(M)$ so that $\iota(x_k) = 0 \in \mathbb{R}^D$. Then, we apply an orthogonal transformation in \mathbb{R}^D so that $\{e_i\}_{i=1}^d$ form a basis of $\iota_* T_{x_k} M$.*

In the following proposition, we provide the bias and the variance analysis of $C_{n,\varepsilon}(\mathbf{y}_k)$. The proofs of the bias and variance analysis are provide in Appendix B and Appendix C respectively.

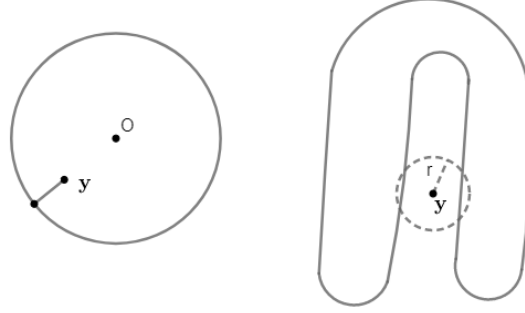


FIGURE 5. Left panel: The reach of a circle in the plane is the radius. For the center of the circle, the nearest point on the circle is the whole circle. For any point y whose distance to the circle is less than the radius, there is a unique nearest point on the circle. Right panel: A closed curve in the plane with small reach. We can find a point y and a small ball of radius r centered at y . The intersection between the ball and the curve has two connected components. Hence, by the consequence of Proposition 3.1, the reach of the curve is smaller than r .

Proposition 3.2. *Under Assumptions 2.1 and 3.1, suppose ε is small enough depending on d, D , the second fundamental form of $\iota(M)$ and the scalar curvature of M . Suppose $\sigma = \varepsilon^\alpha$ for $\alpha > \frac{3}{2}$. If $n \leq \frac{1}{2} \exp(\frac{1}{12\varepsilon^{2(\alpha-\beta)}})$ for some β such that $1 < \beta \leq \alpha - \frac{1}{2}$, then for all x_k , with probability greater than $1 - \frac{1}{n^2}$, we have $\|\eta_k\|_{\mathbb{R}^D} \leq \varepsilon^\beta$, and*

$$(16) \quad C_{n,\varepsilon}(\mathbf{y}_k) = \varepsilon^{d+2} \left(\frac{|S^{d-1}|P(x_k)}{d(d+2)} \begin{bmatrix} I_{d \times d} & 0 \\ 0 & 0 \end{bmatrix} + \mathcal{E} \right),$$

where

$$\mathcal{E} = \begin{bmatrix} O(\varepsilon^{\min(\beta-1,2)} + \sqrt{\frac{\log n}{n\varepsilon^d}}) & O(\varepsilon^{2\min(\beta-1,1)} + \sqrt{\frac{\log n}{n\varepsilon^{d-2\min(\beta-1,1)}}}) \\ O(\varepsilon^{2\min(\beta-1,1)} + \sqrt{\frac{\log n}{n\varepsilon^{d-2\min(\beta-1,1)}}}) & O(\varepsilon^{2\min(\beta-1,1)} + \sqrt{\frac{\log n}{n\varepsilon^{d-2\min(\beta-1,1)}}}) \end{bmatrix}.$$

The top left block of \mathcal{E} is a d by d matrix. The constant factors in \mathcal{E} depend on d, C^2 norm of P , the second fundamental form of $\iota(M)$ and its derivative and the Ricci curvature of M .

The following proposition describes the structure of the orthonormal eigenvector matrix of $C_{n,\varepsilon}(\mathbf{y}_k)$. The proof relies on applying the Davis-Kahan theorem [9, 46] to Proposition 3.2. For a large enough lower bound on the eigengap between the d th and $(d+1)$ th eigenvalue of $C_{n,\varepsilon}(\mathbf{y}_k)$, we need the variance of the Gaussian noise to be smaller than the requirement in Proposition 3.2, e.g. $\sigma^2 = \varepsilon^{2\alpha}$ with $\alpha \geq \frac{7}{4}$ rather than $\alpha > \frac{3}{2}$. The proof of the proposition is in Appendix C.

Proposition 3.3. *Under Assumptions 2.1 and 3.1, suppose ε is small enough depending on d, D, P_m, C^2 norm of P , the second fundamental form of $\iota(M)$ and its derivative and the Ricci curvature of M . Suppose $\sigma = \varepsilon^\alpha$ for $\alpha \geq \frac{7}{4}$. If $\varepsilon^{-d-2\min(\beta-1,1)} \leq \frac{n}{\log n}$ and $n \leq \frac{1}{2} \exp(\frac{1}{12\varepsilon^{2(\alpha-\beta)}})$ for some β such that $\frac{5}{4} \leq \beta \leq \alpha - \frac{1}{2}$, then for all x_k , with probability greater than $1 - \frac{1}{n^2}$, we have $\|\eta_k\|_{\mathbb{R}^D} \leq \varepsilon^\beta$, and*

$$(17) \quad U_{n,\varepsilon}(\mathbf{y}_k) = \begin{bmatrix} X_1 & 0 \\ 0 & X_2 \end{bmatrix} + O(\varepsilon^{2\min(\beta-1,1)}),$$

where $X_1 \in \mathbb{O}(d)$, $X_2 \in \mathbb{O}(D-d)$. $O(\varepsilon^{2\min(\beta-1,1)})$ represents a D by D matrix whose entries are of order $O(\varepsilon^{2\min(\beta-1,1)})$, where the constant factors depend on d , D , P_m , C^2 norm of P , the second fundamental form of $\iota(M)$ and its derivative and the Ricci curvature of M .

We discuss Proposition 3.3 from the following aspects.

The lower bound on n . The condition $\varepsilon^{-d-2\min(\beta-1,1)} \leq \frac{n}{\log n}$ with a lower bound of P guarantees enough points from $\{x_i\}_{i=1}^n$ in any ε geodesic ball on M with high probability.

The upper bound on n . η_k follows a Gaussian distribution, representing unbounded noise. However, the condition $n \leq \frac{1}{2} \exp(\frac{1}{12\varepsilon^{2(\alpha-\beta)}})$ with the decay of the p.d.f of the noise implies that $\|\eta_k\|_{\mathbb{R}^D} \leq \varepsilon^\beta$ with high probability. Later in the main theorem, this bound implies that the noisy data are close to the clean data compared to the reach of $\iota(M)$. This property will be used to show that we can define a chart for $\iota(M)$ through the first d eigenvectors of $C_{n,\varepsilon}(\mathbf{y}_k)$.

Relations between n , ε and σ . The upper bound on n implies $\varepsilon \rightarrow 0$ as $n \rightarrow \infty$. Since $\sigma = \varepsilon^\alpha$, the variance of the noise $\sigma^2 \rightarrow 0$ as $n \rightarrow \infty$.

If n satisfies the requirements in Proposition 3.3 so that there is β with $\frac{5}{4} \leq \beta \leq \alpha - \frac{1}{2}$, then

$$(18) \quad U_{n,\varepsilon}(\mathbf{y}_k) - \begin{bmatrix} X_1 & 0 \\ 0 & X_2 \end{bmatrix} = O(\varepsilon^{2\min(\beta-1,1)}).$$

Since $\frac{5}{4} \leq \beta$, $O(\varepsilon^{2\min(\beta-1,1)})$ should be at most order $\varepsilon^{\frac{1}{2}}$. By Assumption 3.1, $\begin{bmatrix} X_1 \\ 0 \end{bmatrix}$ forms an orthonormal basis of ι_*T_xM and $\begin{bmatrix} 0 \\ X_2 \end{bmatrix}$ forms an orthonormal basis of $\iota_*T_xM^\perp$. In our algorithm, we use the first d column vectors of $U_{n,\varepsilon}(\mathbf{y}_k)$ to construct a map $\mathcal{P}_{\mathbf{y}_k}(\mathbf{y})$ from \mathbb{R}^D to \mathbb{R}^d defined in (3). In the proof of the main theorem, we allow the first d column vectors of $U_{n,\varepsilon}(\mathbf{y}_k)$ to deviate from $\begin{bmatrix} X_1 \\ 0 \end{bmatrix}$ by an order 1 term, while $\mathcal{P}_{\mathbf{y}_k}(\mathbf{y})$ on $\iota(M)$ still remains a local diffeomorphism. Therefore, it suffices that $U_{n,\varepsilon}(\mathbf{y}_k) - \begin{bmatrix} X_1 & 0 \\ 0 & X_2 \end{bmatrix}$ is of order $O(\varepsilon^{2\min(\beta-1,1)})$.

3.3. Construction of a chart from noisy samples. In the following theorem, we show that, with high probability, the map $\mathcal{P}_{\mathbf{y}_k}(\mathbf{y})$ defined in (3) is a diffeomorphism from $B_{3\delta}^{\mathbb{R}^D}(\mathbf{y}_k) \cap \iota(M)$ onto its image for some $\delta > 0$. Consequently, its inverse defines a chart of $\iota(M)$. The proof of the theorem relies on the result of Proposition 3.3 and an analysis of the perturbations of the tangent spaces of $\iota(M)$ near \mathbf{y}_k . The proof is presented in Appendix D.

Theorem 3.1. *Under Assumption 2.1, suppose ε is small enough depending on d , D , P_m , C^2 norm of P , the second fundamental form of $\iota(M)$ and its derivative and the Ricci curvature of M . Moreover, $\varepsilon < \frac{\tau_{\iota(M)}}{16}$. Suppose $\sigma = \varepsilon^\alpha$ for $\alpha \geq \frac{7}{4}$. If $\varepsilon^{-d-2\min(\beta-1,1)} \leq \frac{n}{\log n}$ and $n \leq \frac{1}{2} \exp(\frac{1}{12\varepsilon^{2(\alpha-\beta)}})$ for some β such that $\frac{5}{4} \leq \beta \leq \alpha - \frac{1}{2}$, then for all x_k and any δ such that $\varepsilon^\beta < \delta < \frac{\tau_{\iota(M)}}{16}$, with probability greater than $1 - \frac{1}{n^2}$, we have the following facts:*

- (1) If $\mathbf{y}_i \in B_\delta^{\mathbb{R}^D}(\mathbf{y}_k)$, then $\iota(x_i) \in B_{3\delta}^{\mathbb{R}^D}(\mathbf{y}_k)$.
- (2) The map $\mathcal{P}_{\mathbf{y}_k}(\mathbf{y})$ defined in (3) is a diffeomorphism from $B_{3\delta}^{\mathbb{R}^D}(\mathbf{y}_k) \cap \iota(M)$ onto its image $O_k \subset \mathbb{R}^d$. O_k is homeomorphic to $B_1^{\mathbb{R}^d}(0)$.
- (3) There is a point $\mathbf{u}_{k,0}$ in O_k such that $0 \in B_{R_k}^{\mathbb{R}^d}(\mathbf{u}_{k,0}) \subset O_k \subset B_{3\delta}^{\mathbb{R}^d}(0)$. Let $A = 1 - \Omega\varepsilon^{2\min(\beta-1,1)}$ and $B = \frac{8\delta + 2\varepsilon^\beta}{\tau_{\iota(M)}}$, where Ω is a constant depending on d , D , P_m , C^2 norm of P , the second fundamental form of $\iota(M)$ and its derivative and the Ricci curvature of M . Then

$$R_k \geq (\sqrt{A^2 - A^2B} - \sqrt{B - A^2B})(3\delta - \varepsilon^\beta).$$

We discuss some of the conditions in the above theorem.

The relations between n , ε , and $\tau_{\iota(M)}$. From the discussion of Proposition 3.3, when the upper bound $n \leq \frac{1}{2} \exp(\frac{1}{12e^{2(\alpha-\beta)}})$ holds, we have $\|\eta_k\|_{\mathbb{R}^D} = \|\mathbf{y}_k - \iota(x_k)\|_{\mathbb{R}^D} \leq \varepsilon^\beta < \delta < \frac{\tau_{\iota(M)}}{16}$ with high probability. We illustrate in Appendix I that we may not reconstruct $\iota(M)$ properly if \mathbf{y}_k is too far away from $\iota(x_k)$ compared to the reach.

The relation between σ and the shape of the set O_k . Depending on the variance of the noise, the last part of the theorem describes how close to round O_k is. Consider the extreme case when there is no noise. Equivalently, we can take $\alpha \rightarrow \infty$ and we choose $\beta = \frac{\alpha}{2} \rightarrow \infty$ to satisfy the conditions on β in the theorem. By applying an approximation for small ε and δ , we have $R_k \geq 3(1 - \frac{4\delta}{\tau_{\iota(M)}} - \Omega'\varepsilon)\delta$ for some constant Ω' depending on $\tau_{\iota(M)}$ and Ω . Hence, O_k is close to round in the sense that O_k is contained in the round ball of radius 3δ and it contains a round ball of radius close to 3δ . In general, when σ is small, then α is large and we can choose β to be large so that for given n , the relations $\varepsilon^{-d-2\min(\beta-1,1)} \leq \frac{n}{\log n}$ and $n \leq \frac{1}{2} \exp(\frac{1}{12e^{2(\alpha-\beta)}})$ are satisfied. In this case, R_k is closer to 3δ . Consequently, when the samples are less noisy, the set O_k becomes more regular in the sense that it is always contained in $B_{3\delta}^{\mathbb{R}^d}(0)$ and it contains a round ball with radius closer to 3δ .

In conclusion, based on Theorem 3.1, if ε , δ , σ and n satisfy the conditions, then the inverse of the map $\mathcal{P}_{\mathbf{y}_k}(\mathbf{y})$ from O_k to $B_{3\delta}^{\mathbb{R}^D}(\mathbf{y}_k) \cap \iota(M)$ is a chart of $\iota(M)$. Moreover, for all $\mathbf{y}_i \in B_{\delta}^{\mathbb{R}^D}(\mathbf{y}_k)$, the corresponding $\iota(x_i)$ is in the image of the chart. When σ is smaller, the domain O_k becomes more regular. In the following subsections, we will discuss how to use $\{\mathcal{P}_{\mathbf{y}_k}(\mathbf{y}_i)\}$ and $\{\mathcal{P}_{\mathbf{y}_k}^\perp(\mathbf{y}_i)\}$ for $\mathbf{y}_i \in B_{\delta}^{\mathbb{R}^D}(\mathbf{y}_k)$ to recover information about the inverse of the map $\mathcal{P}_{\mathbf{y}_k}(\mathbf{y})$.

Remark 3.2. *The main idea of the proof of Theorem 3.1 can be summarized as follows. Consider two conditions: (1) \mathbf{y}_i should not deviate significantly from $\iota(x_i)$ compared to $\tau_{\iota(M)}$, and (2) there exists a d dimensional affine subspace through \mathbf{y}_i with an orthonormal basis deviating from an orthonormal basis of the tangent space at $\iota(x_i)$ by an order 1 term depending on d . When these conditions are met, this affine subspace can be used to construct a chart for $\iota(M)$. When η_i is a bounded error rather than Gaussian, condition (1) can be satisfied by proposing an error bound depending on the reach, while the behavior of orthonormal eigenvectors of $C_{n,\varepsilon}(\mathbf{y}_i)$ can be explored by a similar method as in Proposition 3.3. Hence, we expect the result of Theorem 3.1 to hold with suitable relations between the error bound on η_i , ε , δ , n , and $\tau_{\iota(M)}$.*

3.4. Setup of the regression functions. We describe a chart of $\iota(M)$ around $\iota(x_k)$ and an associated regression problem implied by Theorem 3.1. Suppose ε , δ , σ and n satisfy the conditions in Theorem 3.1. Then, all the following statements hold with probability greater than $1 - \frac{1}{n^2}$.

If the image of $B_{3\delta}^{\mathbb{R}^D}(\mathbf{y}_k) \cap \iota(M)$ under $\mathcal{P}_{\mathbf{y}_k}(\mathbf{y})$ is $O_k \subset \mathbb{R}^d$, then $\mathcal{P}_{\mathbf{y}_k}(\mathbf{y})$ is a diffeomorphism from $B_{3\delta}^{\mathbb{R}^D}(\mathbf{y}_k) \cap \iota(M)$ to O_k . O_k is an open set in \mathbb{R}^d homeomorphic to $B_1^{\mathbb{R}^d}(0)$. If Φ_k is the inverse of $\mathcal{P}_{\mathbf{y}_k}(\mathbf{y})$ from O_k to $B_{3\delta}^{\mathbb{R}^D}(\mathbf{y}_k) \cap \iota(M)$, then Φ_k is a chart of $\iota(M)$. Based on (3),

$$(19) \quad \Phi_k(\mathbf{u}) = \mathbf{y}_k + U_{n,\varepsilon}(\mathbf{y}_k) \begin{bmatrix} \mathbf{u} \\ F_k(\mathbf{u}) \end{bmatrix},$$

where $F_k(\mathbf{u}) : O_k \rightarrow \mathbb{R}^{D-d}$ is a smooth function. Note that

$$(20) \quad F_k(\mathbf{u}) = \mathcal{P}_{\mathbf{y}_k}^\perp(\Phi_k(\mathbf{u})).$$

Let $\eta_{i,1} = J^\top U_{n,\varepsilon}(\mathbf{y}_k)^\top \eta_i \in \mathbb{R}^d$ and $\eta_{i,2} = \bar{J}^\top U_{n,\varepsilon}(\mathbf{y}_k)^\top \eta_i \in \mathbb{R}^{D-d}$. Suppose $B_{\frac{\mathbb{R}^D}{\delta}}(\mathbf{y}_k) \cap \{\mathbf{y}_1, \dots, \mathbf{y}_n\} = \{\mathbf{y}_{k,1}, \dots, \mathbf{y}_{k,N_k}\}$. By Theorem 3.1, we have $\iota(x_{k,i}) \in B_{\frac{\mathbb{R}^D}{3\delta}}(\mathbf{y}_k)$ for $i = 1, \dots, N_k$. Hence,

$$\begin{aligned} \mathbf{u}_{k,i} &= \mathcal{P}_{\mathbf{y}_k}(\iota(x_{k,i})), & \iota(x_{k,i}) &= \Phi_k(\mathbf{u}_{k,i}), \\ \mathbf{y}_{k,i} &= \iota(x_{k,i}) + \boldsymbol{\eta}_{k,i} = \Phi_k(\mathbf{u}_{k,i}) + \boldsymbol{\eta}_{k,i}, \end{aligned}$$

with $\mathbf{u}_{k,i} \in O_k$. Moreover,

$$\begin{aligned} (21) \quad \mathcal{P}_{\mathbf{y}_k}(\mathbf{y}_{k,i}) &= J^\top U_{n,\varepsilon}(\mathbf{y}_k)^\top (\iota(x_{k,i}) + \boldsymbol{\eta}_{k,i} - \iota(x_k) - \boldsymbol{\eta}_k) \\ &= J^\top U_{n,\varepsilon}(\mathbf{y}_k)^\top (\iota(x_{k,i}) - \iota(x_k) - \boldsymbol{\eta}_k) + J^\top U_{n,\varepsilon}(\mathbf{y}_k)^\top \boldsymbol{\eta}_{k,i} \\ &= \mathbf{u}_{k,i} + \boldsymbol{\eta}_{k,i,1}. \end{aligned}$$

$$\begin{aligned} (22) \quad \mathcal{P}_{\mathbf{y}_k}^\perp(\mathbf{y}_{k,i}) &= \bar{J}^\top U_{n,\varepsilon}(\mathbf{y}_k)^\top (\iota(x_{k,i}) + \boldsymbol{\eta}_{k,i} - \iota(x_k) - \boldsymbol{\eta}_k) \\ &= \bar{J}^\top U_{n,\varepsilon}(\mathbf{y}_k)^\top (\iota(x_{k,i}) - \iota(x_k) - \boldsymbol{\eta}_k) + \bar{J}^\top U_{n,\varepsilon}(\mathbf{y}_k)^\top \boldsymbol{\eta}_{k,i} \\ &= \mathcal{P}_{\mathbf{y}_k}^\perp(\Phi_k(\mathbf{u}_{k,i})) + \bar{J}^\top U_{n,\varepsilon}(\mathbf{y}_k)^\top \boldsymbol{\eta}_{k,i} \\ &= F_k(\mathbf{u}_{k,i}) + \boldsymbol{\eta}_{k,i,2}. \end{aligned}$$

If we can recover the function F_k by using the pairs $(\mathcal{P}_{\mathbf{y}_k}(\mathbf{y}_{k,i}), \mathcal{P}_{\mathbf{y}_k}^\perp(\mathbf{y}_{k,i}))_{i=1}^{N_k}$, then, for $\mathbf{u} \in O_k$, (19) provides a point in $B_{\frac{\mathbb{R}^D}{3\delta}}(\mathbf{y}_k) \cap \iota(M)$. Therefore, we introduce the following errors-in-variables regression problem. Suppose $F = (f_1, \dots, f_p) : O \subset \mathbb{R}^d \rightarrow \mathbb{R}^q$, with $q = D - d$, is an unknown regression function, where O is an unknown open subset homeomorphic to a d dimensional open ball in \mathbb{R}^d . We observe the labeled training data $(\mathbf{w}_i, \mathbf{z}_i)_{i=1}^N$, where

$$(23) \quad \begin{aligned} \mathbf{w}_i &= \mathbf{u}_i + \boldsymbol{\eta}_{i,1}, & \boldsymbol{\eta}_{i,1} &\sim \mathcal{N}(0, \sigma^2 I_{d \times d}), \\ \mathbf{z}_i &= F(\mathbf{u}_i) + \boldsymbol{\eta}_{i,2}, & \boldsymbol{\eta}_{i,2} &\sim \mathcal{N}(0, \sigma^2 I_{q \times q}), \end{aligned}$$

and $\{\mathbf{u}_i\}_{i=1}^N \subset O$. The goal is to predict $F(\mathbf{u})$ for $\mathbf{u} \in O$.

3.5. Discussion of the main algorithm. In this subsection, by applying the previous theoretical results, we provide a discussion of the main algorithms.

Step 1 of Algorithm 1: Setup of the predictors and the response variables for charts of $\iota(M)$.

For each k , we find all the samples $\{\mathbf{y}_j\}$ in $B_{\frac{\mathbb{R}^D}{\delta}}(\mathbf{y}_k)$. Suppose there are N_k samples in $B_{\frac{\mathbb{R}^D}{\delta}}(\mathbf{y}_k) \setminus \mathbf{y}_k$, denoted $\{\mathbf{y}_{k,1}, \dots, \mathbf{y}_{k,N_k}\}$. Denote $\mathbf{w}_{k,j} = \mathcal{P}_{\mathbf{y}_k}(\mathbf{y}_{k,j})$ and $\mathbf{z}_{k,j} = \mathcal{P}_{\mathbf{y}_k}^\perp(\mathbf{y}_{k,j})$ for $j = 1, \dots, N_k$. Observe that $\mathcal{P}_{\mathbf{y}_k}(\mathbf{y}_k) = 0$. Then, by (21) and (22), we have

$$(24) \quad \begin{aligned} \mathbf{w}_{k,j} &= \mathbf{u}_{k,j} + \boldsymbol{\eta}_{k,j,1} & \boldsymbol{\eta}_{k,j,1} &\sim \mathcal{N}(0, \sigma^2 I_{d \times d}), \\ \mathbf{z}_{k,j} &= F_k(\mathbf{u}_{k,j}) + \boldsymbol{\eta}_{k,j,2} & \boldsymbol{\eta}_{k,j,2} &\sim \mathcal{N}(0, \sigma^2 I_{(D-d) \times (D-d)}), \end{aligned}$$

where $F_k : O_k \subset \mathbb{R}^d \rightarrow \mathbb{R}^{D-d}$ is described in (20). O_k is homeomorphic to a d dimensional open ball with 0 and $\{\mathbf{u}_{k,j}\}_{j=1}^{N_k}$ in O_k . The map $\Phi_k : O_k \rightarrow B_{\frac{\mathbb{R}^D}{3\delta}}(\mathbf{y}_k) \cap \iota(M)$ described in (19) is a chart of $\iota(M)$ containing $\iota(x_k)$. Our goal is to reconstruct the chart so that we can predict

$$\mathbf{y}_k + U_{n,\varepsilon}(\mathbf{y}_k) \begin{bmatrix} 0 \\ F_k(0) \end{bmatrix}.$$

Predictive distribution of the initial denoised samples (from Steps 2 to 3). We infer $F_k(0)$ by applying GP regression to (24), while ignoring the errors of $\mathbf{w}_{k,j}$. Based on (9) and (19), for each k , the predictive distribution of $\mathbf{y}_k + U_{n,\varepsilon}(\mathbf{y}_k) \begin{bmatrix} 0 \\ F_k(0) \end{bmatrix}$ is Gaussian in the $D - d$ dimensional affine subspace

$\mathcal{A}_k = \mathbf{y}_k + V_k$, where V_k is the $D - d$ dimensional subspace generated by the last $D - d$ column vectors of $U_{n,\varepsilon}(\mathbf{y}_k)$. The mean of this predictive distribution is a_k , where

$$(25) \quad a_k = \mathbf{y}_k + U_{n,\varepsilon}(\mathbf{y}_k) \begin{bmatrix} 0 \\ (\Sigma_{k,3}(\Sigma_{k,1} + \sigma^2 I_{N_k \times N_k})^{-1} \mathbf{Z}_k)^\top \end{bmatrix} \in \mathcal{A}_k,$$

and the variance is $\Sigma_{k,4} - \Sigma_{k,3}(\Sigma_{k,1} + \sigma^2 I_{N_k \times N_k})^{-1} \Sigma_{k,2} \in \mathbb{R}$. The initial denoised outputs of this step are $\{\mathbf{y}_1^{(1)}, \dots, \mathbf{y}_n^{(1)}\}$ with $\mathbf{y}_k^{(1)} = a_k$.

Step 4 of Algorithm 1: Reconstruction of the charts by iteration. For any $i > 1$, denote the denoised outputs from the $(i - 1)$ th iteration of Steps 1-3 as $\{\mathbf{y}_1^{(i-1)}, \dots, \mathbf{y}_n^{(i-1)}\}$. We assume

$$(26) \quad \mathbf{y}_k^{(i-1)} = \iota(x_k^{(i-1)}) + \boldsymbol{\eta}_k^{(i-1)} \text{ for } x_k^{(i-1)} \in M \text{ and } \boldsymbol{\eta}_k^{(i-1)} \sim \mathcal{N}(0, \sigma^{(i-1)2} I_{D \times D}),$$

where $\sigma^{(i-1)}$ decreases as i increases. In the i th iteration, for each $\mathbf{y}_k^{(i-1)}$, we construct $C_{n,\varepsilon}^{(i-1)}(\mathbf{y}_k^{(i-1)})$ by using $\{\mathbf{y}_1^{(i-1)}, \dots, \mathbf{y}_n^{(i-1)}\}$ as in (1). We find the orthonormal eigenvector matrix $U_{n,\varepsilon}^{(i-1)}(\mathbf{y}_k^{(i-1)})$ of $C_{n,\varepsilon}^{(i-1)}(\mathbf{y}_k^{(i-1)})$ as in (2) and construct the operators $\mathcal{P}_{\mathbf{y}_k^{(i-1)}}(\mathbf{y})$ and $\mathcal{P}_{\mathbf{y}_k^{(i-1)}}^\perp(\mathbf{y})$. Suppose $\{\mathbf{y}_j^{(i-1)}\}_{j=1}^n \cap B_\delta^{\mathbb{R}^D}(\mathbf{y}_k^{(i-1)}) = \{\mathbf{y}_{k,1}^{(i-1)}, \dots, \mathbf{y}_{k,N_k^{(i-1)}}^{(i-1)}\}$. Let $\mathbf{w}_{k,j}^{(i-1)} = \mathcal{P}_{\mathbf{y}_k^{(i-1)}}(\mathbf{y}_{k,j}^{(i-1)})$ and $\mathbf{z}_{k,j}^{(i-1)} = \mathcal{P}_{\mathbf{y}_k^{(i-1)}}^\perp(\mathbf{y}_{k,j}^{(i-1)})$ for $j = 1, \dots, N_k^{(i-1)}$. Then, (21) and (22) imply that

$$(27) \quad \begin{aligned} \mathbf{w}_{k,j}^{(i-1)} &= \mathbf{u}_{k,j}^{(i-1)} + \boldsymbol{\eta}_{k,j,1}^{(i-1)}, & \boldsymbol{\eta}_{k,j,1}^{(i-1)} &\sim \mathcal{N}(0, \sigma^{(i-1)2} I_{d \times d}) \\ \mathbf{z}_{k,j}^{(i-1)} &= F_k^{(i-1)}(\mathbf{u}_{k,j}) + \boldsymbol{\eta}_{k,j,2}^{(i-1)}, & \boldsymbol{\eta}_{k,j,2} &\sim \mathcal{N}(0, \sigma^{(i-1)2} I_{(D-d) \times (D-d)}) \end{aligned}$$

for $j = 1, \dots, N_k^{(i-1)}$, where $F_k^{(i-1)} : O_k^{(i-1)} \subset \mathbb{R}^d \rightarrow \mathbb{R}^{D-d}$ is in (20) and $\{\mathbf{u}_{k,1}^{(i-1)}, \dots, \mathbf{u}_{k,N_k^{(i-1)}}^{(i-1)}\}$ are in the domain $O_k^{(i-1)}$. The chart $\Phi_k^{(i-1)} : O_k^{(i-1)} \rightarrow B_{3\delta}^{\mathbb{R}^D}(\mathbf{y}_k^{(i-1)}) \cap \iota(M)$ can be expressed as in (19) by $\mathbf{y}_k^{(i-1)}$, $U_{n,\varepsilon}^{(i-1)}(\mathbf{y}_k^{(i-1)})$, and $F_k^{(i-1)}$. To find $F_k^{(i-1)}(0)$, we use the covariance function C to construct a $(N_k^{(i-1)} + 1) \times (N_k^{(i-1)} + 1)$ covariance matrix $\Sigma_k^{(i-1)}$ over $\{\mathbf{w}_{k,1}^{(i-1)}, \dots, \mathbf{w}_{k,N_k^{(i-1)}}^{(i-1)}, 0\}$. Denote the covariance parameters that we find through (12) in the i th iteration as $A^{(i-1)}$, $\boldsymbol{\rho}^{(i-1)}$ and $\sigma^{(i-1)}$. These parameters determine the covariance structure associated to all the charts $\{\Phi_k^{(i-1)}(\mathbf{u})\}_{k=1}^n$. Thus, we can use the GP to predict $F_k^{(i-1)}(0)$ and find the denoised outputs $\{\mathbf{y}_1^{(i)}, \dots, \mathbf{y}_n^{(i)}\}$ from the i th iteration through (13). Suppose the change from $\sigma^{(i-1)}$ to $\sigma^{(i)}$ is below a small tolerance when $i = I$. Then, the iterations stop at the I th round. The final denoised output corresponding to \mathbf{y}_k is $\hat{\mathbf{y}}_k = \mathbf{y}_k^{(I)}$.

Algorithm 2: Gluing the charts and interpolation within charts. We use $\{\mathbf{y}_1^{(I-1)}, \dots, \mathbf{y}_n^{(I-1)}\}$ from the $(I-1)$ th iteration in Algorithm 1 as the inputs to interpolate points on $\iota(M)$. In the I th iteration of Steps 1-3 of Algorithm 1, we construct n charts $\{\Phi_k^{(I-1)}\}_{k=1}^n$, whose domains are $\{O_k^{(I-1)}\}_{k=1}^n$. If we can generate K points in each domain $O_k^{(I-1)}$, then we can use the covariance parameters $A^{(I-1)}$, $\boldsymbol{\rho}^{(I-1)}$ and $\sigma^{(I-1)}$ estimated in the I th iteration to recover each $\Phi_k^{(I-1)}$ and interpolate K points on $\iota(M)$ through (15). However, if the K generated points are not in $O_k^{(I-1)}$, then it is possible that the corresponding interpolated points are not on $\iota(M)$.

Suppose $\{\mathbf{y}_j^{(I-1)}\}_{j=1}^n \cap B_\delta^{\mathbb{R}^D}(\mathbf{y}_k^{(I-1)}) = \{\mathbf{y}_{k,1}^{(I-1)}, \dots, \mathbf{y}_{k,N_k^{(I-1)}}^{(I-1)}\}$. Let $\mathbf{w}_{k,j}^{(I-1)} = \mathcal{P}_{\mathbf{y}_k^{(I-1)}}(\mathbf{y}_{k,j}^{(I-1)})$. We estimate a round ball contained in $O_k^{(I-1)}$ using $\{\mathbf{w}_{k,1}^{(I-1)}, \dots, \mathbf{w}_{k,N_k^{(I-1)}}^{(I-1)}\}$ and sample K points, $\{\tilde{\mathbf{u}}_{k,1}, \dots, \tilde{\mathbf{u}}_{k,K}\}$,

uniformly at random from the ball. The center of the ball is

$$\mathcal{U}_k = \frac{1}{N_k^{(\text{I-1})}} \sum_{j=1}^{N_k^{(\text{I-1})}} \mathbf{w}_{k,1}^{(\text{I-1})} = \frac{1}{N_k^{(\text{I-1})}} \sum_{j=1}^{N_k^{(\text{I-1})}} \mathbf{u}_{k,j}^{(\text{I-1})} + \frac{1}{N_k^{(\text{I-1})}} \sum_{j=1}^{N_k^{(\text{I-1})}} \eta_{k,j,1}^{(\text{I-1})} \in \mathbb{R}^d,$$

where $\mathbf{u}_{k,j}^{(\text{I-1})} \in O_k^{(\text{I-1})}$ and $\eta_{k,j,1}^{(\text{I-1})} \sim \mathcal{N}(0, \sigma^{(\text{I-1})^2} I_{d \times d})$ for $j = 1, \dots, N_k^{(\text{I-1})}$. We set the radius as $m_k - s_k$, with m_k the mean and s_k the standard deviation of $\{\|\mathbf{w}_{k,1}^{(\text{I-1})} - \mathcal{U}_k\|_{\mathbb{R}^d}, \dots, \|\mathbf{w}_{k,N_k^{(\text{I-1})}}^{(\text{I-1})} - \mathcal{U}_k\|_{\mathbb{R}^d}\}$.

Next, we discuss how the above method to construct a small round ball in $O_k^{(\text{I-1})}$ relates to the evolution of the shapes of the sets $\{O_k, O_k^{(1)}, \dots, O_k^{(\text{I-1})}\}$ through the iteration process. If $O_k^{(\text{I-1})} \subset \mathbb{R}^d$ is very close to spherical, then it is easy to verify our algorithm produces a ball contained in $O_k^{(\text{I-1})}$. On the other hand, by (26) and (3) in Theorem 3.1, all the sets $\{O_k, O_k^{(1)}, \dots, O_k^{(\text{I-1})}\}$ are contained in $B_{3\delta}^{\mathbb{R}^d}(0)$. Since $\sigma^{(i-1)}$ decreases as i increases, comparing to $\{O_k, O_k^{(1)}, \dots, O_k^{(\text{I-2})}\}$, $O_k^{(\text{I-1})}$ contains a larger ball of radius closer to 3δ . In Figure 6, we show an illustration of the sets O_k and $O_k^{(\text{I-1})}$ for a comparison. Hence, we perform the interpolation after sufficient iterations of Step 1-3 in Algorithm 1.

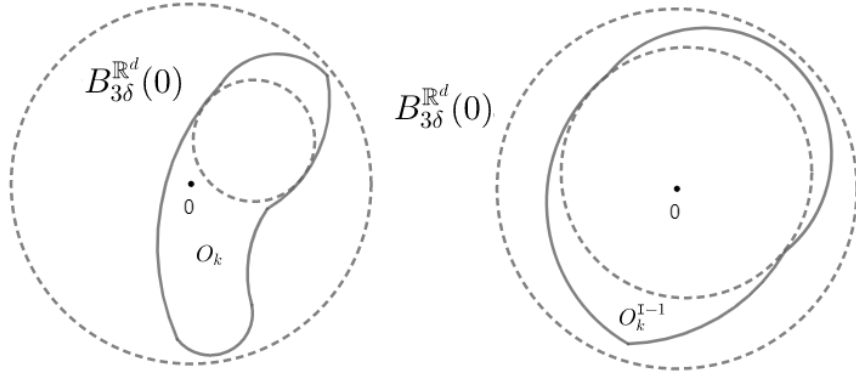


FIGURE 6. Both O_k and $O_k^{(\text{I-1})}$ are contained in $B_{3\delta}^{\mathbb{R}^d}(0)$. Left: An illustration of the set $O_k \subset \mathbb{R}^d$ where O_k containing a small round ball. Right: An illustration of the set $O_k^{(\text{I-1})} \subset \mathbb{R}^d$ where $O_k^{(\text{I-1})}$ containing a larger round ball of radius close to 3δ .

To make sure that the charts are glued together smoothly and the interpolated points lie on a smooth manifold, we iteratively interpolate the points in the charts $\Phi_i^{(\text{I-1})}$ for i from 1 to n . Suppose \tilde{M}_{k-1} is the union of $K(k-1)$ points interpolated in the charts $\{\Phi_i^{(\text{I-1})}\}_{i=1}^{k-1}$. We find $B_{\delta}^{\mathbb{R}^D}(\mathbf{y}_k^{(\text{I-1})}) \cap \tilde{M}_{k-1} = \{\tilde{\mathbf{y}}_{k,1}, \dots, \tilde{\mathbf{y}}_{k,L_k}\}$. Suppose $\tilde{\mathbf{w}}_{k,j} = \mathcal{P}_{\mathbf{y}_k^{(\text{I-1})}}(\tilde{\mathbf{y}}_{k,j})$ and $\tilde{\mathbf{z}}_{k,j} = \mathcal{P}_{\mathbf{y}_k^{(\text{I-1})}}^{\perp}(\tilde{\mathbf{y}}_{k,j})$ for $j = 1, \dots, L_k$. Since $\Phi_k^{(\text{I-1})}$ is a chart of $\iota(M)$ over $B_{3\delta}^{\mathbb{R}^D}(\mathbf{y}_k^{(\text{I-1})}) \cap \iota(M)$, we need to predict $F_k^{(\text{I-1})}$ in (20) over $\{\tilde{\mathbf{u}}_{k,1}, \dots, \tilde{\mathbf{u}}_{k,K}\}$. We use $\{\mathbf{w}_{k,1}^{(\text{I-1})}, \dots, \mathbf{w}_{k,N_k^{(\text{I-1})}}^{(\text{I-1})}, \tilde{\mathbf{w}}_{k,1}, \dots, \tilde{\mathbf{w}}_{k,L_k}\}$ as the inputs for $F_k^{(\text{I-1})}$ and $\{\mathbf{z}_{k,1}^{(\text{I-1})}, \dots, \mathbf{z}_{k,N_k^{(\text{I-1})}}^{(\text{I-1})}, \tilde{\mathbf{z}}_{k,1}, \dots, \tilde{\mathbf{z}}_{k,L_k}\}$ as the response variables. The coordinates of the interpolated points around $\hat{\mathbf{y}}_k$ are provided in (15).

3.6. Evaluation of the performance of the algorithm. In this section, we introduce an approach to evaluate performance of MrGap. The error in prediction is determined by how far the generated points deviate from the embedded submanifold $\iota(M)$. Thus, we introduce the following geometric root mean

square error. For any $\mathbf{y} \in \mathbb{R}^D$, the distance from \mathbf{y} to $S \subset \mathbb{R}^D$ is defined as

$$\text{dist}(\mathbf{y}, S) = \inf_{\mathbf{y}' \in S} \|\mathbf{y} - \mathbf{y}'\|_{\mathbb{R}^D}.$$

Given $\mathcal{Y} = \{\mathbf{y}_1, \dots, \mathbf{y}_n\} \subset \mathbb{R}^D$, the geometric root mean square error (GRMSE) from \mathcal{Y} to S is $\text{GRMSE}(\mathcal{Y}, S) = \sqrt{\frac{1}{n} \sum_{i=1}^n \text{dist}(\mathbf{y}_i, S)^2}$, with $\text{GRMSE}(\mathcal{Y}, S) = 0$ if and only if \mathcal{Y} is in the closure of S . Hence, when S is compact, $\text{GRMSE}(\mathcal{Y}, S) = 0$ if and only if $\mathcal{Y} \subset S$.

In the following proposition, we show that when $S = \iota(M)$ and $\mathcal{Y}_{\text{true}}$ is sampled on $\iota(M)$ based on a density function with a positive lower bound, if the sample size of $\mathcal{Y}_{\text{true}}$ goes to infinity, then $\text{GRMSE}(\mathcal{Y}, \mathcal{Y}_{\text{true}})$ converges to $\text{GRMSE}(\mathcal{Y}, \iota(M))$ almost surely. We also provide the convergence rate. The proof of the proposition is in Appendix E.

Proposition 3.4. *Suppose $\mathcal{Y} = \{\mathbf{y}_1, \dots, \mathbf{y}_n\} \subset \mathbb{R}^D$. $\{x_1, \dots, x_m\}$ are samples on M based on a C^1 p.d.f q on M such that $q > q_{\min} > 0$. Let $\mathcal{Y}_{\text{true}} = \{\iota(x_1), \dots, \iota(x_m)\}$. Suppose C is a constant depending on d, D, C^1 norm of q , the curvature of M and the second fundamental form of $\iota(M)$, then with probability greater than $1 - \frac{1}{m^2}$,*

$$\text{GRMSE}(\mathcal{Y}, \mathcal{Y}_{\text{true}})^2 - 2r\text{GRMSE}(\mathcal{Y}, \iota(M)) - r^2 \leq \text{GRMSE}(\mathcal{Y}, \iota(M))^2 \leq \text{GRMSE}(\mathcal{Y}, \mathcal{Y}_{\text{true}})^2,$$

where $r^d = \max(\frac{2}{q_{\min}}, (\frac{2C}{q_{\min}})^2) \frac{\log m}{m}$.

Note that $q_{\min} \leq \frac{1}{\text{Vol}(M)}$ and the equality holds when q is uniform. Therefore, the above proposition suggests an efficient way to estimate $\text{GRMSE}(\mathcal{Y}, \iota(M))$ is sampling $\mathcal{Y}_{\text{true}}$ uniformly.

4. NUMERICAL SIMULATION

In this section, $\iota(M)$ is an embedded 3-real projective space, $RP(3)$, in \mathbb{R}^{10} . Suppose S^3 is the 3 dimensional unit sphere: $S^3 = \{[z_1, z_2, z_3, z_4]^\top \mid z_1^2 + z_2^2 + z_3^2 + z_4^2 = 1\} \subset \mathbb{R}^4$. Recall that $RP(3)$ is a 3 dimensional closed connected manifold which can be topologically constructed by identifying the antipodal points $[z_1, z_2, z_3, z_4]^\top$ and $[-z_1, -z_2, -z_3, -z_4]^\top$ on S^3 . Then, we explicitly describe the construction of $\iota(M)$ through the following map:

$$(28) \quad \begin{aligned} \Phi(\mathbf{z}) : \quad S^3 &\rightarrow \iota(M) \subset \mathbb{R}^{10} \\ \mathbf{z} = [z_1, z_2, z_3, z_4]^\top &\rightarrow [z_1^2, z_2^2, z_3^2, z_4^2, z_1 z_2, z_1 z_3, z_1 z_4, z_2 z_3, z_2 z_4, z_3 z_4]^\top. \end{aligned}$$

Note that $\Phi(\mathbf{z}) = \Phi(-\mathbf{z})$. Hence, Φ induces a map $\tilde{\Phi} : RP(3) \rightarrow \iota(M) \subset \mathbb{R}^{10}$. It can be shown that $\tilde{\Phi}$ is a diffeomorphism.

Remark 4.1. *Let $SO(3) \subset \mathbb{R}^9$ be the group of all rotations about the origin of \mathbb{R}^3 :*

$$SO(3) = \{A \in \mathbb{R}^{3 \times 3} \mid AA^\top = A^\top A = I_{3 \times 3}, \quad \det(A) = 1\}.$$

Then, $SO(3)$ is a manifold diffeomorphic to $RP(3)$.

We can apply Φ to generate samples on $\iota(M)$. We first uniformly sample $\{\mathbf{z}_i\}_{i=1}^n$ on S^3 . We almost surely have $\mathbf{z}_i \neq -\mathbf{z}_j$, i.e. we will not generate antipodal points. Then, $\{\Phi(\mathbf{z}_i)\}_{i=1}^n$ are the distinct non-uniform samples on $\iota(M)$.

We uniformly sample points $\{\mathbf{z}_i\}_{i=1}^{1200}$ on S^3 to obtain non-uniform samples $\{\Phi(\mathbf{z}_i)\}_{i=1}^{1200}$ on $\iota(M)$. Suppose $\eta_i \sim \mathcal{N}(0, \sigma^2 I_{10 \times 10})$, with $\sigma = 0.04$, $\mathbf{y}_i = \Phi(\mathbf{z}_i) + \eta_i$ for $i = 1, \dots, 1200$, and $\mathcal{Y} = \{\mathbf{y}_i\}_{i=1}^{1200}$. We uniformly sample $\{\mathbf{z}_i\}_{i=1}^{10^6}$ on S^3 to obtain $\mathcal{Y}_{\text{true}} = \{\Phi(\mathbf{z}_i)\}_{i=1}^{10^6}$. We use $\mathcal{Y}_{\text{true}}$ to approximate the GRMSE from samples to $\iota(M)$ with $\text{GRMSE}(\mathcal{Y}, \mathcal{Y}_{\text{true}}) = 0.1074$.

We apply the MrGap algorithm with $\varepsilon = 0.5$ and $\delta = 0.5$. We iterate Steps 1-3 of Algorithm 1 twice. The estimated covariance parameters in the first round of the iterations are $A^{(0)} = 0.05$, $\rho^{(0)} = 1$ and $\sigma^{(0)} = \sqrt{0.0015}$. The estimated covariance parameters in the last round of the iterations are $A^{(1)} = 0.08$,

$\rho^{(1)} = 1.2$ and $\sigma^{(1)} = 0.02$. The denoised outputs are $\mathcal{X}_1 = \{\hat{\mathbf{y}}_i\}_{i=1}^{1200}$, with $GRMSE(\mathcal{X}_1, \mathcal{Y}_{true}) = 0.0532$. When we apply Algorithm 2, we choose $K = 10$, i.e. we construct 1200 charts and we interpolate 10 points in each chart. The outputs are $\mathcal{X}_2 = \{\tilde{\mathbf{y}}_i\}_{i=1}^{12000}$ with $GRMSE(\mathcal{X}_2, \mathcal{Y}_{true}) = 0.0593$. Refer to the Appendices for more numerical examples.

5. AUGMENTATION TO THE BIRD VOCALIZATION DATA

Recall the bird vocalization data introduced in Section 1. The data consists of 83 submatrices $\{A_i\}_{i=1}^{83}$ of dimensions 75×197 corresponding to a type of call of *Anthus trivialis*. Let v_i be the i th column vector of a matrix $A \in \mathbb{R}^{p \times q}$, then we can identify A as $\mathbf{v} = [v_1^\top, \dots, v_q^\top]^\top \in \mathbb{R}^{pq}$. Thus, we transform $\{A_i\}_{i=1}^{83}$ to $\{v_i\}_{i=1}^{83} \subset \mathbb{R}^{14775}$. Since we want to explore the geometric structure of the audio signals corresponding a vocalization of a species disregarding the impact of the volume of the signals, we normalize $\{v_i\}_{i=1}^{83}$ with $\mathbf{x}_i = \frac{v_i}{\|v_i\|_{\mathbb{R}^{14775}}}$. Suppose $\eta_i \sim \mathcal{N}(0, \sigma^2 I_{14775 \times 14775})$, with $\sigma = 0.005$. We add the Gaussian noise to generate more noisy data $\mathbf{x}_i^h = \mathbf{x}_i + \eta_i \in \mathbb{R}^{14775}$ for $i = 1, \dots, 83$.

As $\{\mathbf{x}_i^h\}_{i=1}^{83}$ span a subspace of dimension at most 82, to reconstruct the underlying structure of the data through MrGap efficiently, we apply PCA to isometrically embed the data in \mathbb{R}^{82} . Specifically, fixing any \mathbf{x}_k^h , the PCA matrix is equivalent to the local covariance matrix as in (1) with a large enough bandwidth. We denote it as $C(\mathbf{x}_k^h)$. Let $U(\mathbf{x}_k^h)$ be the orthonormal eigenvector matrix of $C(\mathbf{x}_k^h)$ shown in (2). Suppose that \mathcal{J} is the projection map onto the first 82 components in \mathbb{R}^{14775} , i.e. $\mathcal{J} \in \mathbb{R}^{82 \times 14775}$ with $\mathcal{J}_{ij} = 1$ when $i = j$ and $\mathcal{J}_{ij} = 0$ when $i \neq j$. The low dimensional representation of \mathbf{x}_i^h is $\mathbf{y}_i = \mathcal{J} U(\mathbf{x}_k^h)^\top (\mathbf{x}_i^h - \mathbf{x}_k^h) \in \mathbb{R}^{82}$. As all the orthonormal eigenvectors of $C(\mathbf{x}_k^h)$ are used, the 83th to the 14775th components of $U(\mathbf{x}_k^h)^\top (\mathbf{x}_i^h - \mathbf{x}_k^h)$ are 0.

We evaluate the eigenvalues of the local covariance matrix constructed through $\mathcal{Y} = \{\mathbf{y}_i\}_{i=1}^{83}$ as introduced in (45). It shows that \mathcal{Y} has an underlying 1 dimensional structure. We apply the MrGap algorithm to \mathcal{Y} with $\varepsilon = 1.27$ and $\delta = 1.27$ for one round. The estimated covariance parameters are $A^{(0)} = 0.005$, $\rho^{(0)} = 0.2$ and $\sigma^{(0)} = 0.009$. We choose $K = 10$ in Algorithm 2 and generate 830 samples $\{\tilde{\mathbf{y}}_i\}_{i=1}^{830}$ on the underlying 1 dimensional manifold. To recover the corresponding spectrograms, we add zeros to $\tilde{\mathbf{y}}_i$ and extend it to a vector $\mathbf{y}_i^h \in \mathbb{R}^{14775}$ for each i . Then, $\tilde{\mathbf{x}}_i = U(\mathbf{x}_k^h) \mathbf{y}_i^h + \mathbf{x}_k^h$ for $i = 1 \dots 830$ are the new spectrograms of the call of *Anthus trivialis*. In Figure 7, we present 10 generated samples $\{\tilde{\mathbf{x}}_i\}_{i=1}^{10}$ on the manifold around \mathbf{x}_1^h . They are less noisy compared to $\{\mathbf{x}_i^h\}_{i=1}^{83}$. In the illustrative example in section 1, we consider the case when $\eta_i = 0$. The new spectrograms are produced through the same procedure.

6. DISCUSSION

In this work, we delve into the challenge of reconstructing a manifold from a noisy dataset. Leveraging the theoretical properties of the local covariance matrix, we present a framework that defines local charts for the unknown manifold, thereby transforming the global manifold reconstruction problem into a sequence of local regression problems. We introduce the MrGap algorithm, which employs GPs to address these regression problems. We provide the following discussions and future directions.

Our theory assumes the data are distributed around a compact manifold without boundary. When the prior information about whether the manifold has boundary is not available, we illustrate and discuss the performance of MrGap for data distributed around a manifold with boundary in Appendix K. Alternatively, data may be distributed around multiple connected manifolds with or without boundary. The challenge of learning these components has been extensively explored in topological data analysis [31, 15, 34, 28]. Aided by the robustness of the Graph Laplacian to noise, spectral clustering [30] can effectively identify these components from a noisy dataset. By separating the original noisy dataset into groups corresponding to distinct connected components of the underlying manifold, MrGap can be employed to reconstruct each component. An additional future direction is generalizing MrGap beyond

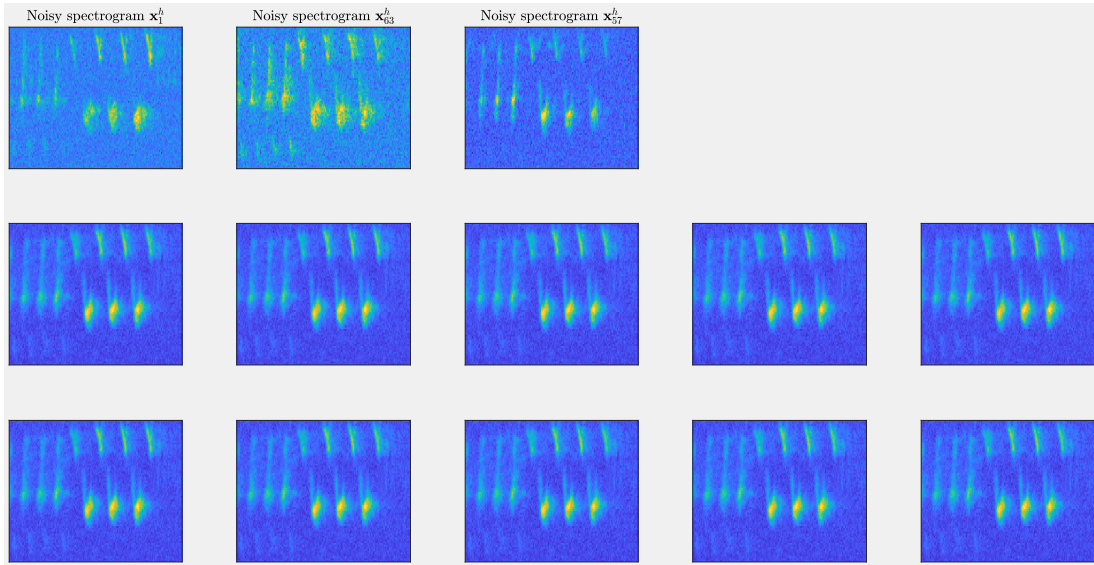


FIGURE 7. Top row: The noisy spectrograms \mathbf{x}_1^h , \mathbf{x}_{63}^h , and \mathbf{x}_{57}^h corresponding to the spectrograms Sample 1, 2 and 4 in Figure 1 . Second and third rows: 10 generated samples around \mathbf{x}_1^h .

the Gaussian noise case. In Remark 3.2, we discuss defining a similar chart through the local covariance matrix when the noise is bounded. This construction enables us to still formulate the regression problems to recover the unknown submanifold. We illustrate the performance of MrGap on a data set with bounded noise in Appendix K . Alternatively, one can consider choosing alternative non-bounded distributions for the residuals in the local regressions, such as Student-t to allow heavy tails and outliers.

Several advantages emerge from incorporating GPs into our manifold reconstruction framework. First, GP regression is flexible. Unlike the noiseless scenario in section 2.3, the regression functions associated with the charts defined through the noisy samples can be quite different from a function dominated by quadratic terms. Hence, we apply GP regression to avoid unrealistic restrictions. Second, GP regression allows the selection of various covariance functions adaptable to different smoothness levels of the manifold. While we apply the square exponential kernel under the assumption that the manifold is smooth, alternative kernels can be adopted to achieve different levels of smoothness, such as continuous or continuously differentiable, in the reconstructed manifold. Third, we propose to infer key hyperparameters by maximizing the sum of the marginal likelihood functions across all charts. The summation incorporates both local and global geometric information from the noisy dataset, protecting against over fitting. Finally, the outputs of MrGap not only encompass denoised samples but also provide posterior distributions for these samples. Future development of MrGap will extend this GP regression method so that it generates posterior distributions for interpolations as well. Thus, MrGap not only will reconstruct the underlying data structure but also will function as a probabilistic classifier from newly arrived noisy samples.

In Algorithm 1, we apply iterations to improve the performance. A potential future direction involves developing theory to analyze the convergence rate of the algorithm. This involves demonstrating that each denoised output, after each round of iteration, can be considered a clean data point on the embedded submanifold, accompanied by a new Gaussian error, as outlined in (26). Understanding the convergence rate can be achieved by investigating the variance of this new Gaussian error.

ACKNOWLEDGEMENT

David B Dunson and Nan Wu acknowledge the support from the European Research Council (ERC) under the European Union's Horizon 2020 research and innovation programme (grant agreement No 856506).

APPENDIX A. SOME BASIC CONCEPTS ABOUT SMOOTH EMBEDDED MANIFOLDS

A.1. Diffeomorphism and chart. Suppose $U \subset \mathbb{R}^p$, $V \subset \mathbb{R}^q$ where U and V are not necessarily open. Suppose $\Phi : U \rightarrow V$ is continuous. Then Φ is a smooth map, whenever it can be extended locally to a smooth map from an open set in \mathbb{R}^p to \mathbb{R}^q . More precisely, we have the following definition.

Definition A.1. *Suppose $U \subset \mathbb{R}^p$, $V \subset \mathbb{R}^q$. $\Phi : U \rightarrow V$ is a smooth map if for any $\mathbf{u} \in U$ there is an open subset $O_{\mathbf{u}}$ of \mathbb{R}^p containing \mathbf{u} and a smooth map $\tilde{\Phi} : O_{\mathbf{u}} \rightarrow \mathbb{R}^q$ such that $\Phi = \tilde{\Phi}$ on $O_{\mathbf{u}}$.*

Suppose $\Phi : U \rightarrow V$ is bijective. Then Φ^{-1} exists. We say that Φ is a diffeomorphism if both Φ and Φ^{-1} are smooth.

Suppose M is a d -dimensional smooth, closed and connected Riemannian manifold isometrically embedded in \mathbb{R}^D through ι . We define a chart of the embedded submanifold $\iota(M)$.

Definition A.2. *A map Φ is a chart (local parametrization) of $\iota(M)$, if there is an open subset U of \mathbb{R}^d and V of \mathbb{R}^D such that $\Phi : U \rightarrow V \cap \iota(M)$ is a diffeomorphism.*

We refer the readers to [29] for the above definitions. In fact, the definitions of the diffeomorphism and the chart can be generalized to the abstract manifold M . Since our proofs of the main results focus on $\iota(M)$, we only discuss the relevant definitions for $\iota(M)$. We refer the readers to [24] for the more general definitions.

A.2. Uniform construction of charts. As we introduced in the definition, for any $x \in M$, there is a chart of $\iota(M)$ over a neighborhood $U_x \cap \iota(M) \subset \mathbb{R}^D$ around $\iota(x)$. However, the size of U_x may not be uniform for all x . In the next proposition, by applying Proposition 3.1, we show that we can choose the neighborhoods $\{U_x\}$ to be uniform for all x . In particular, we can construct a chart over $B_{\xi}^{\mathbb{R}^D}(\iota(x)) \cap \iota(M)$ for any $\xi < \frac{\tau_{\iota(M)}}{2}$. The proposition will be used later in the proof of the main theorem.

Proposition A.1. *Suppose $0 < \xi < \frac{\tau_{\iota(M)}}{2}$. For any $x \in M$, there is an open set $V_x \subset B_{\xi}^{\mathbb{R}^D}(0) \subset \mathbb{R}^d$ containing 0 such that for any $\mathbf{y} \in B_{\xi}^{\mathbb{R}^D}(\iota(x)) \cap \iota(M)$, we have*

$$\mathbf{y} = \iota(x) + X(x) \begin{bmatrix} \mathbf{u} \\ G_x(\mathbf{u}) \end{bmatrix},$$

where $\mathbf{u} \in V_x$. Moreover,

- (1) $\{X e_i\}_{i=1}^d$ form a basis of $\iota_* T_x M$.
- (2) V_x is homeomorphic to $B_1^{\mathbb{R}^d}(0)$.
- (3) $G_x(\mathbf{u}) = [g_{x,1}(\mathbf{u}), \dots, g_{x,D-d}(\mathbf{u})]^{\top} \in \mathbb{R}^{D-d}$ and each $g_{x,i}$ is a smooth function on V_x .
- (4) $g_{x,i}(0) = 0$ and $\mathcal{D}g_{x,i}(0) = 0$ for $i = 1, \dots, D-d$, where $\mathcal{D}g_{x,i}$ is the derivative of $g_{x,i}$.

Proof. By Proposition 3.1, $B_{\xi}^{\mathbb{R}^D}(\iota(x)) \cap \iota(M)$ is an open subset of $\iota(M)$ which is homeomorphic to $B_1^{\mathbb{R}^d}(0)$. Let f be the projection from \mathbb{R}^D to $\iota_* T_x M$. For any $\mathbf{y} \in B_{\xi}^{\mathbb{R}^D}(\iota(x)) \cap \iota(M)$, we express $g(\mathbf{y}) = f(\mathbf{y} - \iota(x))$ in a chart around \mathbf{y} , then by Lemma 5.4 in [31], $Dg(\mathbf{y})$ is not singular. By the inverse function theorem, $g(\mathbf{y})$ is a diffeomorphism. Hence, the image of $B_{\xi}^{\mathbb{R}^D}(\iota(x)) \cap \iota(M)$ under g is the open set V_x which is homeomorphic to $B_1^{\mathbb{R}^d}(0)$. Then g^{-1} is the chart with the described properties. \square

APPENDIX B. BIAS ANALYSIS OF THE LOCAL COVARIANCE MATRIX

Recall Assumption 2.1, and let $G_\sigma(\eta)$ denote the $\mathcal{N}(0, \sigma^2 I_{D \times D})$ probability density function of η . Since the samples $\{\eta_1, \dots, \eta_n\}$ are independent of $\{x_1, \dots, x_n\}$, the pairs $\{(x_i, \eta_i)\}_{i=1}^n$ can be regarded as n i.i.d samples based on the probability density function $P(x)G_\sigma(\eta)$ on $M \times \mathbb{R}^D$. For notation simplicity, we describe the results under Assumption 3.1.

Suppose \mathbb{X} is a random variable associated with the probability density function $P(x)$ on M . Suppose \mathbb{H} is a random variable associated with the probability density function $G_\sigma(\eta)$ on \mathbb{R}^D . Since $\iota(x_k) = 0$ by Assumption 3.1, we have $\mathbf{y}_k = \iota(x_k) + \eta_k = \eta_k$. The expectation of the local covariance matrix at \mathbf{y}_k is defined as follows:

$$(29) \quad C_\varepsilon(\mathbf{y}_k) := \mathbb{E} \left[(\iota(\mathbb{X}) + \mathbb{H} - \eta_k)(\iota(\mathbb{X}) + \mathbb{H} - \eta_k)^\top \chi \left(\frac{\|\iota(\mathbb{X}) + \mathbb{H} - \eta_k\|_{\mathbb{R}^D}}{\varepsilon} \right) \right] \\ = \int_{\mathbb{R}^D} \int_M (\iota(x) + \eta - \eta_k)(\iota(x) + \eta - \eta_k)^\top \chi \left(\frac{\|\iota(x) + \eta - \eta_k\|_{\mathbb{R}^D}}{\varepsilon} \right) P(x)G_\sigma(\eta) dV d\eta.$$

Remark B.1. Suppose $f : \mathbb{R}^D \rightarrow \mathbb{R}$ is a measurable function. Then, by change of variables,

$$\int_{\mathbb{R}^D} \int_M f(\iota(x) + \eta) P(x)G_\sigma(\eta) dV d\eta = \int_{\mathbb{R}^D} \int_M f(\eta) P(x)G_\sigma(\eta - \iota(x)) dV d\eta \\ = \int_{\mathbb{R}^D} f(\eta) P \star G_\sigma(\eta) d\eta,$$

where the convolution $P \star G_\sigma(\eta) := \int_M P(x)G_\sigma(\eta - \iota(x)) dV$ is the probability density function for the random variable $\iota(\mathbb{X}) + \mathbb{H}$. Hence, the definition in (29) is equivalent to

$$(30) \quad \mathbb{E}[(\iota(\mathbb{X}) + \mathbb{H} - \eta_k)(\iota(\mathbb{X}) + \mathbb{H} - \eta_k)^\top \chi \left(\frac{\|\iota(\mathbb{X}) + \mathbb{H} - \eta_k\|_{\mathbb{R}^D}}{\varepsilon} \right)] \\ = \int_{\mathbb{R}^D} (\eta - \eta_k)(\eta - \eta_k)^\top \chi \left(\frac{\|\eta - \eta_k\|_{\mathbb{R}^D}}{\varepsilon} \right) P \star G_\sigma(\eta) d\eta.$$

In the following proposition, we provide a bias analysis for the local covariance matrix. The proposition is proved later in this section.

Proposition B.1. Under Assumptions 2.1 and 3.1, suppose ε is small enough depending on d, D , the second fundamental form of $\iota(M)$ and the scalar curvature of M . For any $\alpha > \frac{3}{2}$, suppose $1 < \beta \leq \alpha - \frac{1}{2}$. If $\sigma = \varepsilon^\alpha$ and $\|\eta_k\|_{\mathbb{R}^D} \leq \varepsilon^\beta$, then

$$C_\varepsilon(\mathbf{y}_k) = \varepsilon^{d+2} \left(\frac{|S^{d-1}|P(x_k)}{d(d+2)} \begin{bmatrix} I_{d \times d} & 0 \\ 0 & 0 \end{bmatrix} + \begin{bmatrix} O(\varepsilon^{\beta-1} + \varepsilon^2) & O(\varepsilon^{2\beta-2} + \varepsilon^2) \\ O(\varepsilon^{2\beta-2} + \varepsilon^2) & O(\varepsilon^{2\beta-2} + \varepsilon^2) \end{bmatrix} \right),$$

where the constant factors in all blocks depend on d, C^2 norm of P , the second fundamental form of $\iota(M)$ and its derivative and the Ricci curvature of M .

Suppose $\iota(x_k) = 0$ and there is no noise, then the expectation of the local covariance matrix at \mathbf{y}_k can be expressed as follows:

$$\tilde{C}_\varepsilon(\mathbf{y}_k) = \mathbb{E}[\iota(\mathbb{X})\iota(\mathbb{X})^\top \chi \left(\frac{\|\iota(\mathbb{X})\|_{\mathbb{R}^D}}{\varepsilon} \right)].$$

By Proposition 3.1 in [42],

$$(31) \quad \tilde{C}_\varepsilon(\mathbf{y}_k) = \varepsilon^{d+2} \left(\frac{|S^{d-1}|P(x_k)}{d(d+2)} \begin{bmatrix} I_{d \times d} & 0 \\ 0 & 0 \end{bmatrix} + O(\varepsilon^2) \right),$$

where $O(\varepsilon^2)$ represents a D by D matrix whose entries are of order $O(\varepsilon^2)$. The constant factors in $O(\varepsilon^2)$ depend on d, C^2 norm of P , the second fundamental form of $\iota(M)$ and its derivative and the Ricci

curvature of M . If the variance of the Gaussian noise is small enough, so that $\sigma^2 = \varepsilon^{2\alpha}$ with $\alpha \geq \frac{7}{2}$, and suppose we can choose $\beta \geq 3$, then

$$C_\varepsilon(\mathbf{y}_k) = \varepsilon^{d+2} \left(\frac{|S^{d-1}|P(x_k)}{d(d+2)} \begin{bmatrix} I_{d \times d} & 0 \\ 0 & 0 \end{bmatrix} + O(\varepsilon^2) \right).$$

Comparing to Proposition 3.1 in [42], the impact of the noise on the local covariance matrix is negligible.

Remark B.2. Since $\tilde{C}_\varepsilon(\mathbf{y}_k)$ is invariant under translation and its eigenvalues are invariant under rotation, the leading term $\varepsilon^{d+2} \frac{|S^{d-1}|P(x_k)}{d(d+2)} \begin{bmatrix} I_{d \times d} & 0 \\ 0 & 0 \end{bmatrix}$ in (31) implies that $\tilde{C}_\varepsilon(\mathbf{y}_k)$ has d large eigenvalues of order ε^{d+2} , while the rest of the eigenvalues are of order $O(\varepsilon^{d+4})$. Refer to Section G for an illustration.

B.1. Preliminary lemmas. We introduce some notation. Suppose S is a subset of M . Then $\chi_S(x)$ is the characteristic function on S . For $S_1, S_2 \subset M$, let $S_1 \Delta S_2 = (S_1 \setminus S_2) \cup (S_2 \setminus S_1)$ be the symmetric difference. Let $d_M(x, x')$ be the geodesic distance between x and x' in M . Let $B_r(x) \subset M$ be the open geodesic ball of radius r centered at $x \in M$.

First, we have the following lemma about the geodesic distance between x and x' on M and the Euclidean distance between $\iota(x)$ and $\iota(x')$ in \mathbb{R}^D . The proof of the lemma is available in [42].

Lemma B.1. Fix $x \in M$. For $\mathbf{u} \in T_x M \approx \mathbb{R}^d$ with $\|\mathbf{u}\|_{\mathbb{R}^d}$ sufficiently small, if $x' = \exp_x(\mathbf{u})$, then

$$\iota(x') - \iota(x) = \iota_* \mathbf{u} + \frac{1}{2} \mathbb{I}_x(\mathbf{u}, \mathbf{u}) + O(\|\mathbf{u}\|_{\mathbb{R}^d}^3),$$

where \mathbb{I}_x is the second fundamental form of $\iota(M)$ at x . Moreover,

$$\|\iota(x') - \iota(x)\|_{\mathbb{R}^D} = \|\mathbf{u}\|_{\mathbb{R}^d} - \frac{1}{24} \left\| \mathbb{I}_x \left(\frac{\mathbf{u}}{\|\mathbf{u}\|_{\mathbb{R}^d}}, \frac{\mathbf{u}}{\|\mathbf{u}\|_{\mathbb{R}^d}} \right) \right\|_{\mathbb{R}^D}^2 \|\mathbf{u}\|_{\mathbb{R}^d}^3 + O(\|\mathbf{u}\|_{\mathbb{R}^d}^4).$$

In other words,

$$\|\mathbf{u}\|_{\mathbb{R}^d} = \|\iota(x') - \iota(x)\|_{\mathbb{R}^D} + \frac{1}{24} \left\| \mathbb{I}_x \left(\frac{\mathbf{u}}{\|\mathbf{u}\|_{\mathbb{R}^d}}, \frac{\mathbf{u}}{\|\mathbf{u}\|_{\mathbb{R}^d}} \right) \right\|_{\mathbb{R}^D}^2 \|\iota(x') - \iota(x)\|_{\mathbb{R}^D}^3 + O(\|\iota(x') - \iota(x)\|_{\mathbb{R}^D}^4).$$

Next, we introduce the following lemma about the volume form on M . The proof of the lemma is available in [11].

Lemma B.2. Fix $x \in M$. For $\mathbf{u} \in T_x M \approx \mathbb{R}^d$ with $\|\mathbf{u}\|_{\mathbb{R}^d}$ sufficiently small, the volume form has the following expansion

$$dV = \left(1 - \sum_{i,j=1}^d \frac{1}{6} \text{Ric}_x(e'_i, e'_j) u_i u_j + O(\|\mathbf{u}\|_{\mathbb{R}^d}^3) \right) d\mathbf{u},$$

where $\mathbf{u} = \sum_{i=1}^d u_i e'_i$ and Ric_x is the Ricci curvature tensor of M at x . Consequently,

$$\text{Vol}(B_r(x)) = \text{Vol}(B_1^{\mathbb{R}^d}) r^d \left(1 - \frac{S_x}{6(d+2)} r^2 + O(r^4) \right),$$

where S_x is the scalar curvature of M at x .

Recall that $G_\sigma(\boldsymbol{\eta})$ is the $\mathcal{N}(0, \sigma^2 I_{D \times D})$ probability density function of $\boldsymbol{\eta}$:

$$G_\sigma(\boldsymbol{\eta}) = \frac{1}{(2\pi\sigma^2)^{\frac{D}{2}}} e^{-\frac{\|\boldsymbol{\eta}\|_{\mathbb{R}^D}^2}{2\sigma^2}}.$$

We have the following Lemma describing bounds on $G_\sigma(\boldsymbol{\eta})$.

Lemma B.3. (1) If $\frac{1}{\sigma} \geq \sqrt{2}(D-2)$, then $\int_{\|\boldsymbol{\eta}\|_{\mathbb{R}^D} \geq t} G_\sigma(\boldsymbol{\eta}) d\boldsymbol{\eta} \leq \frac{2}{\Gamma(\frac{D}{2})} e^{-\frac{t^2}{4\sigma^2}}$.

(2) $\int_{\mathbb{R}^D} \eta(i)^2 G_\sigma(\eta) d\eta \leq \sigma^2$, for $i = 1, \dots, D$.

Proof. (1) By the change of variables in the spherical coordinates,

$$\int_{\|\eta\|_{\mathbb{R}^D} \geq t} G_\sigma(\eta) d\eta = \frac{1}{(2\pi\sigma^2)^{\frac{D}{2}}} (2\sigma^2)^{\frac{D}{2}} |S^{D-1}| \int_{\frac{t}{\sqrt{2\sigma}}}^{\infty} r^{D-1} e^{-r^2} dr = \frac{|S^{D-1}|}{\pi^{\frac{D}{2}}} \int_{\frac{t}{\sqrt{2\sigma}}}^{\infty} r^{D-1} e^{-r^2} dr.$$

Since $\frac{t}{\sqrt{2}} \geq \log(r)$ for all $r > 0$, when $r \geq D-2$, we have $D-2 \leq \frac{r^2}{2\log(r)}$. Hence, $r^{D-2} e^{-r^2} \leq e^{-\frac{r^2}{2}}$. If $\frac{t}{\sigma} \geq \sqrt{2}(D-2)$, then

$$\int_{\|\eta\|_{\mathbb{R}^D} \geq t} G_\sigma(\eta) d\eta \leq \frac{|S^{D-1}|}{\pi^{\frac{D}{2}}} \int_{\frac{t}{\sqrt{2\sigma}}}^{\infty} e^{-\frac{r^2}{2}} r dr = \frac{2}{\Gamma(\frac{D}{2})} e^{-\frac{t^2}{4\sigma^2}}.$$

(2) follows from the change of variables in the spherical coordinates and the symmetry of \mathbb{R}^D . \square

Recall that we have $\iota(x_k) = 0 \in \mathbb{R}^D$. For $1 < \beta \leq \alpha - \frac{1}{2}$, we define the following terms which we will use in our discussion.

$$\begin{aligned} F_1(\iota(x), \eta, \eta_k) &= (\iota(x) + \eta - \eta_k)(\iota(x) + \eta - \eta_k)^\top \chi\left(\frac{\|\iota(x) + \eta - \eta_k\|_{\mathbb{R}^D}}{\varepsilon}\right), \\ E_1 &= \int_{\|\eta\|_{\mathbb{R}^D} < \varepsilon^\beta} \int_M F_1(\iota(x), \eta, \eta_k) P(x) G_\sigma(\eta) dV d\eta, \\ E_2 &= \int_{\|\eta\|_{\mathbb{R}^D} \geq \varepsilon^\beta} \int_M F_1(\iota(x), \eta, \eta_k) P(x) G_\sigma(\eta) dV d\eta, \\ E_3 &= \int_{\|\eta\|_{\mathbb{R}^D} < \varepsilon^\beta} \int_M (\iota(x) + \eta - \eta_k)(\iota(x) + \eta - \eta_k)^\top \chi_{B_\varepsilon(x_k)}(x) P(x) G_\sigma(\eta) dV d\eta. \end{aligned}$$

Lemma B.4. *Suppose ε is small enough depending on d and D . Suppose $\sigma = \varepsilon^\alpha$ and $1 < \beta \leq \alpha - \frac{1}{2}$. Then $|e_i^\top E_2 e_j| \leq \varepsilon^{d+5}$ for all $1 \leq i, j \leq D$.*

Proof. When $\|\iota(x) + \eta - \eta_k\|_{\mathbb{R}^D} \leq \varepsilon$, $\chi\left(\frac{\|\iota(x) + \eta - \eta_k\|_{\mathbb{R}^D}}{\varepsilon}\right) \leq 1$. When $\|\iota(x) + \eta - \eta_k\|_{\mathbb{R}^D} > \varepsilon$, $\chi\left(\frac{\|\iota(x) + \eta - \eta_k\|_{\mathbb{R}^D}}{\varepsilon}\right) = 0$. Hence, for all $1 \leq i, j \leq D$ and all x , we have

$$|e_i^\top (\iota(x) + \eta - \eta_k)(\iota(x) + \eta - \eta_k)^\top e_j| \chi\left(\frac{\|\iota(x) + \eta - \eta_k\|_{\mathbb{R}^D}}{\varepsilon}\right) \leq \varepsilon^2.$$

Next, we bound $|e_i^\top E_2 e_j|$,

$$\begin{aligned} |e_i^\top E_2 e_j| &\leq \int_{\|\eta\|_{\mathbb{R}^D} \geq \varepsilon^\beta} \int_M |e_i^\top (\iota(x) + \eta - \eta_k)(\iota(x) + \eta - \eta_k)^\top e_j| \\ &\quad \times \chi\left(\frac{\|\iota(x) + \eta - \eta_k\|_{\mathbb{R}^D}}{\varepsilon}\right) P(x) G_\sigma(\eta) dV d\eta \\ &\leq \int_{\|\eta\|_{\mathbb{R}^D} \geq \varepsilon^\beta} \int_M \varepsilon^2 P(x) G_\sigma(\eta) dV d\eta = \int_{\|\eta\|_{\mathbb{R}^D} \geq \varepsilon^\beta} \varepsilon^2 G_\sigma(\eta) d\eta \int_M P(x) dV \\ &\leq \int_{\|\eta\|_{\mathbb{R}^D} \geq \varepsilon^\beta} \varepsilon^2 G_\sigma(\eta) d\eta. \end{aligned}$$

We apply Fubini's theorem in the second to last step and the fact that $P(x)$ is a probability density function on M in the last step. Since $\beta \leq \alpha - \frac{1}{2}$, if $\varepsilon^{2(\beta-\alpha)} \geq \frac{1}{\varepsilon} \geq 2\sqrt{2}(D-2)$, then by Lemma B.3,

$$|e_i^\top E_2 e_j| \leq \frac{2\varepsilon^2}{\Gamma(\frac{D}{2})} e^{-\frac{1}{4\varepsilon^{2(\alpha-\beta)}}} \leq \frac{2\varepsilon^2}{\Gamma(\frac{D}{2})} e^{-\frac{1}{4\varepsilon}}.$$

We apply $\beta \leq \alpha - \frac{1}{2}$ in the last step again. Since $\Gamma(\frac{D}{2}) > 1$, when ε is small enough depending on d and D , we have $|e_i^\top E_2 e_j| \leq \varepsilon^{d+5}$. \square

Lemma B.5. *Suppose ε is small enough depending on the second fundamental form of $\iota(M)$. Let $W_{ij}(x) = |e_i^\top (\iota(x) + \eta - \eta_k)(\iota(x) + \eta - \eta_k)^\top e_j|$. Suppose $1 < \beta \leq 3$. If $\|\eta\|_{\mathbb{R}^D} \leq \varepsilon^\beta$ $\|\eta_k\|_{\mathbb{R}^D} \leq \varepsilon^\beta$, then for $x \in B_{\varepsilon+3\varepsilon^\beta}(x_k)$*

$$\begin{aligned} W_{ij}(x) &\leq 49\varepsilon^2, \quad \text{for } 1 \leq i, j \leq d, \\ W_{ij}(x) &\leq C_3(\varepsilon^3 + \varepsilon^{1+\beta}), \quad \text{for } 1 \leq i \leq d \text{ and } d+1 \leq j \leq D, \\ W_{ij}(x) &\leq C_3(\varepsilon^3 + \varepsilon^{1+\beta}), \quad \text{for } d+1 \leq i \leq D \text{ and } 1 \leq j \leq d, \\ W_{ij}(x) &\leq C_3(\varepsilon^4 + \varepsilon^{2\beta}), \quad \text{for } d+1 \leq i, j \leq D, \end{aligned}$$

where C_3 is a constant depending on the second fundamental form of $\iota(M)$.

Suppose $\beta > 3$. If $\|\eta\|_{\mathbb{R}^D} \leq \varepsilon^\beta$ $\|\eta_k\|_{\mathbb{R}^D} \leq \varepsilon^\beta$, then for $x \in B_{\varepsilon+3\varepsilon^3}(x_k)$

$$\begin{aligned} W_{ij}(x) &\leq 49\varepsilon^2, \quad \text{for } 1 \leq i, j \leq d, \\ W_{ij}(x) &\leq 2C_3\varepsilon^3, \quad \text{for } 1 \leq i \leq d \text{ and } d+1 \leq j \leq D, \\ W_{ij}(x) &\leq 2C_3\varepsilon^3, \quad \text{for } d+1 \leq i \leq D \text{ and } 1 \leq j \leq d, \\ W_{ij}(x) &\leq 2C_3\varepsilon^4, \quad \text{for } d+1 \leq i, j \leq D. \end{aligned}$$

Proof. Since $\|\eta\|_{\mathbb{R}^D} < \varepsilon^\beta$ and $\|\eta_k\|_{\mathbb{R}^D} \leq \varepsilon^\beta$, we have

$$\begin{aligned} (32) \quad &|e_i^\top (\iota(x) + \eta - \eta_k)(\iota(x) + \eta - \eta_k)^\top e_j| \\ &\leq (|e_i^\top \iota(x)| + |e_i^\top \eta| + |e_i^\top \eta_k|)(|\iota(x)^\top e_j| + |\eta^\top e_j| + |\eta_k^\top e_j|) \\ &\leq (|e_i^\top \iota(x)| + 2\varepsilon^\beta)(|\iota(x)^\top e_j| + 2\varepsilon^\beta). \end{aligned}$$

For any $x \in B_{\varepsilon+3\varepsilon^\beta}(x_k)$, suppose $x = \exp_{x_k}(\mathbf{u})$ for $\mathbf{u} \in T_{x_k}M \approx \mathbb{R}^d$. Then, $\|\mathbf{u}\|_{\mathbb{R}^d} \leq \varepsilon + 3\varepsilon^\beta$. By Lemma B.1, we have

$$\iota(x) = \iota_*\mathbf{u} + \frac{1}{2}\mathbb{I}_x(\mathbf{u}, \mathbf{u}) + O(\|\mathbf{u}\|_{\mathbb{R}^d}^3)$$

Since $\{e_1, \dots, e_d\}$ form a basis of $\iota_*T_{x_k}M$, they are perpendicular to $\mathbb{I}_x(\mathbf{u}, \mathbf{u})$. Since $1 < \beta$, when ε is small enough depending on the second fundamental form of $\iota(M)$, we have $|e_i^\top \iota(x)| \leq 5\varepsilon$ for $i = 1, \dots, d$. Similarly, since $\{e_{d+1}, \dots, e_D\}$ form a basis of $\iota_*T_{x_k}M^\perp$, they are perpendicular to $\iota_*\mathbf{u}$. When ε is small enough depending on the second fundamental form of $\iota(M)$, we have $|e_i^\top \iota(x)| \leq C_2\varepsilon^2$ for $i = d+1, \dots, D$, where C_2 is a constant depending on the second fundamental form of $\iota(M)$. If we substitute the bounds of $|e_i^\top \iota(x)|$ into (32), then after the simplification, for any $\|\eta\|_{\mathbb{R}^D} < \varepsilon^\beta$, $\|\eta_k\|_{\mathbb{R}^D} \leq \varepsilon^\beta$ and $x \in B_{\varepsilon+3\varepsilon^\beta}(x_k)$, we have

$$\begin{aligned} &|e_i^\top (\iota(x) + \eta - \eta_k)(\iota(x) + \eta - \eta_k)^\top e_j| \leq 49\varepsilon^2, \quad \text{for } 1 \leq i, j \leq d, \\ &|e_i^\top (\iota(x) + \eta - \eta_k)(\iota(x) + \eta - \eta_k)^\top e_j| \leq C_3(\varepsilon^3 + \varepsilon^{1+\beta}), \quad \text{for } 1 \leq i \leq d \text{ and } d+1 \leq j \leq D \\ &|e_i^\top (\iota(x) + \eta - \eta_k)(\iota(x) + \eta - \eta_k)^\top e_j| \leq C_3(\varepsilon^3 + \varepsilon^{1+\beta}), \quad \text{for } d+1 \leq i \leq D \text{ and } 1 \leq j \leq d \\ &|e_i^\top (\iota(x) + \eta - \eta_k)(\iota(x) + \eta - \eta_k)^\top e_j| \leq C_3(\varepsilon^4 + \varepsilon^{2\beta}), \quad \text{for } d+1 \leq i, j \leq D, \end{aligned}$$

where C_3 is a constant depending on the second fundamental form of $\iota(M)$. The proof for the case when $\beta > 3$ is similar. \square

Lemma B.6. *Suppose ε is small enough depending on the scalar curvature of M and the second fundamental form of $\iota(M)$. Suppose $1 < \beta$. If $\|\eta_k\|_{\mathbb{R}^D} \leq \varepsilon^\beta$ then*

$$E_1 = E_3 + \begin{bmatrix} O(\varepsilon^{d+1+\beta} + \varepsilon^{d+4}) & O(\varepsilon^{d+2+\beta} + \varepsilon^{d+2\beta} + \varepsilon^{d+5}) \\ O(\varepsilon^{d+2+\beta} + \varepsilon^{d+2\beta} + \varepsilon^{d+5}) & O(\varepsilon^{d+3+\beta} + \varepsilon^{d-1+3\beta} + \varepsilon^{d+6}) \end{bmatrix},$$

where the top left block is a d by d matrix and the constant factors in the four blocks depend on d , P_M and the second fundamental form of $\iota(M)$.

Proof. Let $A(\eta) = \{x \in M \mid \|\iota(x) + \eta - \eta_k\|_{\mathbb{R}^D} \leq \varepsilon \text{ for a fixed } \|\eta\|_{\mathbb{R}^D} < \varepsilon^\beta\}$. Since $\|\eta\|_{\mathbb{R}^D} < \varepsilon^\beta$ and $\|\eta_k\|_{\mathbb{R}^D} \leq \varepsilon^\beta$, by the triangle inequality, if $x \in A(\eta)$, then $\varepsilon - 2\varepsilon^\beta \leq \|\iota(x)\|_{\mathbb{R}^D} \leq \varepsilon + 2\varepsilon^\beta$. If $1 < \beta \leq 3$, when ε is small enough depending on the second fundamental form of $\iota(M)$, by Lemma B.1, we have $\varepsilon - 2\varepsilon^\beta \leq d(x, x_k) < \varepsilon + 3\varepsilon^\beta$. Hence, $B_{\varepsilon-2\varepsilon^\beta}(x_k) \subset A(\eta) \subset B_{\varepsilon+3\varepsilon^\beta}(x_k)$ which implies $A(\eta)\Delta B_\varepsilon \subset B_{\varepsilon+3\varepsilon^\beta}(x_k) \setminus B_{\varepsilon-2\varepsilon^\beta}(x_k)$. Since $1 < \beta \leq 3$, when ε is small enough depending on the scalar curvature of M , by Lemma B.2, for all $\|\eta\|_{\mathbb{R}^D} < \varepsilon^\beta$ we have

$$\text{Vol}(A(\eta)\Delta B_\varepsilon(x_k)) \leq \text{Vol}(B_{\varepsilon+3\varepsilon^\beta}(x_k)) - \text{Vol}(B_{\varepsilon-2\varepsilon^\beta}(x_k)) \leq 6\text{Vol}(B_1^{\mathbb{R}^d})d\varepsilon^{d-1+\beta} = C_1(d)\varepsilon^{d-1+\beta},$$

where $C_1(d) = 6d\text{Vol}(B_1^{\mathbb{R}^d})$ is a constant only depending on d . Similarly, if $\beta > 3$, then for all $\|\eta\|_{\mathbb{R}^D} < \varepsilon^\beta$ we have $A(\eta)\Delta B_\varepsilon \subset B_{\varepsilon+3\varepsilon^3}(x_k) \setminus B_{\varepsilon-2\varepsilon^3}(x_k)$ and

$$\text{Vol}(A(\eta)\Delta B_\varepsilon(x_k)) \leq C_1(d)\varepsilon^{d+2}.$$

Observe that for a fixed $\|\eta\|_{\mathbb{R}^D} < \varepsilon^\beta$, $|\chi_{A(\eta)}(x) - \chi_{B_\varepsilon(x_k)}(x)| \leq \chi_{A(\eta)\Delta B_\varepsilon(x_k)}(x)$. Moreover, we have $\chi_{A(\eta)}(x) = \chi\left(\frac{\|\iota(x) + \eta - \eta_k\|_{\mathbb{R}^D}}{\varepsilon}\right)$. Hence,

(33)

$$\begin{aligned} & |e_i^\top (E_1 - E_3)e_j| \\ & \leq \int_{\|\eta\|_{\mathbb{R}^D} < \varepsilon^\beta} \int_M |e_i^\top (\iota(x) + \eta - \eta_k)(\iota(x) + \eta - \eta_k)^\top e_j| |\chi_{A(\eta)}(x) - \chi_{B_\varepsilon(x_k)}(x)| P(x) G_\sigma(\eta) dV d\eta \\ & \leq \int_{\|\eta\|_{\mathbb{R}^D} < \varepsilon^\beta} \int_M |e_i^\top (\iota(x) + \eta - \eta_k)(\iota(x) + \eta - \eta_k)^\top e_j| \chi_{A(\eta)\Delta B_\varepsilon(x_k)}(x) P(x) G_\sigma(\eta) dV d\eta \\ & \leq \left(\sup_{\|\eta\|_{\mathbb{R}^D} < \varepsilon^\beta, x \in A(\eta)\Delta B_\varepsilon(x_k)} |e_i^\top (\iota(x) + \eta - \eta_k)(\iota(x) + \eta - \eta_k)^\top e_j| \right) \\ & \quad \times \int_{\|\eta\|_{\mathbb{R}^D} < \varepsilon^\beta} \int_M \chi_{A(\eta)\Delta B_\varepsilon(x_k)}(x) P(x) G_\sigma(\eta) dV d\eta \\ & \leq \left(\sup_{\|\eta\|_{\mathbb{R}^D} < \varepsilon^\beta, x \in A(\eta)\Delta B_\varepsilon(x_k)} |e_i^\top (\iota(x) + \eta - \eta_k)(\iota(x) + \eta - \eta_k)^\top e_j| \right) P_M \left(\sup_{\|\eta\|_{\mathbb{R}^D} < \varepsilon^\beta} \text{Vol}(A(\eta)\Delta B_\varepsilon(x_k)) \right) \end{aligned}$$

Recall that if $1 < \beta \leq 3$, for any $\|\eta\|_{\mathbb{R}^D} < \varepsilon^\beta$, $A(\eta)\Delta B_\varepsilon(x_k) \subset B_{\varepsilon+3\varepsilon^\beta}(x_k) \setminus B_{\varepsilon-2\varepsilon^\beta}(x_k) \subset B_{\varepsilon+3\varepsilon^\beta}(x_k)$. Hence, if we substitute the bounds in Lemma B.5 into (33), then we conclude that when $1 < \beta \leq 3$ and ε is small enough depending on the scalar curvature of M and the second fundamental form of $\iota(M)$,

$$E_1 = E_3 + \begin{bmatrix} O(\varepsilon^{d+1+\beta}) & O(\varepsilon^{d+2+\beta} + \varepsilon^{d+2\beta}) \\ O(\varepsilon^{d+2+\beta} + \varepsilon^{d+2\beta}) & O(\varepsilon^{d+3+\beta} + \varepsilon^{d-1+3\beta}) \end{bmatrix},$$

where the top left block is a d by d matrix and the constant factors depend on d , P_M and the second fundamental form of $\iota(M)$.

When $\beta > 3$ and ε is small enough depending on the scalar curvature of M and the second fundamental form of $\iota(M)$, we have $A(\eta)\Delta B_\varepsilon \subset B_{\varepsilon+3\varepsilon^3}(x_k) \setminus B_{\varepsilon-2\varepsilon^3}(x_k)$. Hence, if we substitute the bounds

in Lemma B.5 into (33), then

$$E_1 = E_3 + \begin{bmatrix} O(\varepsilon^{d+4}) & O(\varepsilon^{d+5}) \\ O(\varepsilon^{d+5}) & O(\varepsilon^{d+6}) \end{bmatrix},$$

where the top left block is a d by d matrix and the constant factors depend on d , P_M and the second fundamental form of $\iota(M)$. The statement of the lemma follows from combining the cases when $1 < \beta \leq 3$ and $\beta > 3$. \square

Lemma B.7. *Suppose ε is small enough depending on the scalar curvature of M and D . Suppose $1 < \beta \leq \alpha - \frac{1}{2}$. If $\sigma = \varepsilon^\alpha$ and $\|\eta_k\|_{\mathbb{R}^D} \leq \varepsilon^\beta$, then*

$$E_3 = \frac{|S^{d-1}|P(x_k)}{d(d+2)} \varepsilon^{d+2} \begin{bmatrix} I_{d \times d} & 0 \\ 0 & 0 \end{bmatrix} + O(\varepsilon^{d+4} + \varepsilon^{d+2\beta}),$$

where $O(\varepsilon^{d+4} + \varepsilon^{d+2\beta})$ represents a D by D matrix whose entries are of order $O(\varepsilon^{d+4} + \varepsilon^{d+2\beta})$. The constants in $O(\varepsilon^{d+4} + \varepsilon^{d+2\beta})$ depend on d , C^2 norm of P , the second fundamental form of $\iota(M)$ and its derivative and the Ricci curvature of M .

Proof.

(34)

$$\begin{aligned} E_3 &= \int_{\|\eta\|_{\mathbb{R}^D} < \varepsilon^\beta} \int_M (\iota(x) + \eta - \eta_k)(\iota(x) + \eta - \eta_k)^\top \chi_{B_\varepsilon(x_k)}(x) P(x) G_\sigma(\eta) dV d\eta \\ &= \int_{\|\eta\|_{\mathbb{R}^D} < \varepsilon^\beta} \int_M \left(\iota(x)\iota(x)^\top + \eta\iota(x)^\top - \eta_k\iota(x)^\top + \iota(x)\eta^\top + \eta\eta^\top \right. \\ &\quad \left. - \eta_k\eta^\top - \iota(x)\eta_k^\top - \eta\eta_k^\top + \eta_k\eta_k^\top \right) \chi_{B_\varepsilon(x_k)}(x) P(x) G_\sigma(\eta) dV d\eta \\ &= \int_{\|\eta\|_{\mathbb{R}^D} < \varepsilon^\beta} \int_M \left(\iota(x)\iota(x)^\top - \eta_k\iota(x)^\top + \eta\eta^\top - \iota(x)\eta_k^\top + \eta_k\eta_k^\top \right) \chi_{B_\varepsilon(x_k)}(x) P(x) G_\sigma(\eta) dV d\eta, \end{aligned}$$

where we use the symmetry of the region $\{\|\eta\|_{\mathbb{R}^D} < \varepsilon^\beta\}$ and the symmetry of the function $G_\sigma(\eta)$ in the last step.

When ε is small enough depending on the scalar curvature of M , by Lemma B.2, we have $\text{Vol}(B_\varepsilon(x_k)) \leq C_4(d)\varepsilon^d$, where $C_4(d) = 2\text{Vol}(B_1^{\mathbb{R}^d})$ is a constant only depending on d . We have

$$\begin{aligned} &\left| \int_{\|\eta\|_{\mathbb{R}^D} < \varepsilon^\beta} \int_M e_i^\top \eta \eta^\top e_j \chi_{B_\varepsilon(x_k)}(x) P(x) G_\sigma(\eta) dV d\eta \right| \\ &\leq \left| \int_{\|\eta\|_{\mathbb{R}^D} < \varepsilon^\beta} e_i^\top \eta \eta^\top e_j G_\sigma(\eta) d\eta \right| \left| \int_M \chi_{B_\varepsilon(x_k)}(x) dVP(x) \right| \\ &\leq \left| \int_{\|\eta\|_{\mathbb{R}^D} < \varepsilon^\beta} e_i^\top \eta \eta^\top e_j G_\sigma(\eta) d\eta \right| C_4(d) \varepsilon^d. \end{aligned}$$

By the symmetry of the region $\{\|\eta\|_{\mathbb{R}^D} < \varepsilon^\beta\}$ and the symmetry of the function $G_\sigma(\eta)$,

$$\int_{\|\eta\|_{\mathbb{R}^D} < \varepsilon^\beta} e_i^\top \eta \eta^\top e_j G_\sigma(\eta) d\eta = 0, \quad \text{if } i \neq j.$$

By Lemma B.3,

$$\left| \int_{\|\eta\|_{\mathbb{R}^D} < \varepsilon^\beta} e_i^\top \eta \eta^\top e_j G_\sigma(\eta) d\eta \right| \leq \sigma^2 = \varepsilon^{2\alpha}, \quad \text{if } i = j.$$

In conclusion

$$(35) \quad \int_{\|\eta\|_{\mathbb{R}^D} < \varepsilon^\beta} \int_M \eta \eta^\top \chi_{B_\varepsilon(x_k)}(x) P(x) G_\sigma(\eta) dV d\eta = O(\varepsilon^{d+2\alpha}) I_{D \times D},$$

where the constant in $O(\varepsilon^{d+2\alpha})$ depends on d .

Similarly, for $1 \leq i, j \leq D$,

$$(36) \quad \int_{\|\eta\|_{\mathbb{R}^D} < \varepsilon^\beta} \int_M e_i^\top \eta_k \eta_k^\top e_j \chi_{B_\varepsilon(x_k)}(x) P(x) G_\sigma(\eta) dV d\eta = O(\varepsilon^{d+2\beta}),$$

where the constant in $O(\varepsilon^{d+2\beta})$ depends on d .

Next, we have

$$\begin{aligned} & \left| \int_{\|\eta\|_{\mathbb{R}^D} < \varepsilon^\beta} \int_M e_i^\top \iota(x) \eta_k^\top e_j \chi_{B_\varepsilon(x_k)}(x) P(x) G_\sigma(\eta) dV d\eta \right| \\ & \leq \left| \int_M e_i^\top \iota(x) \chi_{B_\varepsilon(x_k)}(x) P(x) dV \right| \left| \int_{\|\eta\|_{\mathbb{R}^D} < \varepsilon^\beta} G_\sigma(\eta) d\eta \right| \left| \eta_k^\top e_j \right| \\ & \leq \varepsilon^\beta \left| \int_M e_i^\top \iota(x) \chi_{B_\varepsilon(x_k)}(x) P(x) dV \right|. \end{aligned}$$

Based on the proof of Lemma SI.5 in [42], $|\int_M e_i^\top \iota(x) \chi_{B_\varepsilon(x_k)}(x) P(x) dV| = O(\varepsilon^{d+2})$ for $i = 1, \dots, d$, where the constant in $O(\varepsilon^{d+2})$ depends on d and the $C^{(1)}$ norm of P . $|\int_M e_i^\top \iota(x) \chi_{B_\varepsilon(x_k)}(x) P(x) dV| = O(\varepsilon^{d+2})$ for $i = d+1, \dots, D$, where the constant in $O(\varepsilon^{d+2})$ depends on d , P_M and the second fundamental form of $\iota(M)$. In conclusion, for $1 \leq i, j \leq D$,

$$(37) \quad \int_{\|\eta\|_{\mathbb{R}^D} < \varepsilon^\beta} \int_M e_i^\top \iota(x) \eta_k^\top e_j \chi_{B_\varepsilon(x_k)}(x) P(x) G_\sigma(\eta) dV d\eta = O(\varepsilon^{d+2+\beta}),$$

where the constant in $O(\varepsilon^{d+2})$ depends on d , the $C^{(1)}$ norm of P and the second fundamental form of $\iota(M)$. Next, observe that

$$(38) \quad \begin{aligned} & \int_{\|\eta\|_{\mathbb{R}^D} < \varepsilon^\beta} \int_M \eta_k \iota(x)^\top \chi_{B_\varepsilon(x_k)}(x) P(x) G_\sigma(\eta) dV d\eta \\ & = \left(\int_{\|\eta\|_{\mathbb{R}^D} < \varepsilon^\beta} \int_M \iota(x) \eta_k^\top \chi_{B_\varepsilon(x_k)}(x) P(x) G_\sigma(\eta) dV d\eta \right)^\top. \end{aligned}$$

At last,

$$\begin{aligned} & \int_{\|\eta\|_{\mathbb{R}^D} < \varepsilon^\beta} \int_M \iota(x) \iota(x)^\top \chi_{B_\varepsilon(x_k)}(x) P(x) G_\sigma(\eta) dV d\eta \\ & = \int_M \iota(x) \iota(x)^\top \chi_{B_\varepsilon(x_k)}(x) P(x) dV \int_{\|\eta\|_{\mathbb{R}^D} < \varepsilon^\beta} G_\sigma(\eta) d\eta \\ & = \int_M \iota(x) \iota(x)^\top \chi_{B_\varepsilon(x_k)}(x) P(x) dV \left(1 - \int_{\|\eta\|_{\mathbb{R}^D} \geq \varepsilon^\beta} G_\sigma(\eta) d\eta \right). \end{aligned}$$

Based on the proof of Proposition 3.1 in [42],

$$\int_M \iota(x) \iota(x)^\top \chi_{B_\varepsilon(x_k)}(x) P(x) dV = \frac{|S^{d-1}| P(x_k)}{d(d+2)} \varepsilon^{d+2} \begin{bmatrix} I_{d \times d} & 0 \\ 0 & 0 \end{bmatrix} + \begin{bmatrix} O(\varepsilon^{d+4}) & O(\varepsilon^{d+4}) \\ O(\varepsilon^{d+4}) & O(\varepsilon^{d+4}) \end{bmatrix},$$

where the constant in $O(\varepsilon^{d+4})$ depends on d , C^2 norm of P , the second fundamental form of $\iota(M)$ and its derivative and the Ricci curvature of M . By Lemma B.3 and the fact that $\beta \leq \alpha - \frac{1}{2}$, when ε is small enough depending on D ,

$$0 < \int_{\|\eta\|_{\mathbb{R}^D} \geq \varepsilon^\beta} G_\sigma(\eta) d\eta \leq \frac{2}{\Gamma(\frac{D}{2})} e^{-\frac{1}{4\varepsilon}} \leq 2e^{-\frac{1}{4\varepsilon}} \leq \varepsilon^2.$$

In conclusion,

$$(39) \quad \int_{\|\eta\|_{\mathbb{R}^D} < \varepsilon^\beta} \int_M \iota(x) \iota(x)^\top \chi_{B_\varepsilon(x_k)}(x) P(x) G_\sigma(\eta) dV d\eta \\ = \frac{|S^{d-1}|P(x_k)}{d(d+2)} \varepsilon^{d+2} \begin{bmatrix} I_{d \times d} & 0 \\ 0 & 0 \end{bmatrix} + \begin{bmatrix} O(\varepsilon^{d+4}) & O(\varepsilon^{d+4}) \\ O(\varepsilon^{d+4}) & O(\varepsilon^{d+4}) \end{bmatrix},$$

where the constant in $O(\varepsilon^{d+4})$ depends on d , C^2 norm of P , the second fundamental form of $\iota(M)$ and its derivative and the Ricci curvature of M . If we substitute (35), (36), (37), (38) and (39) into (34) and use the fact that $\beta < \alpha$, then we have

$$E_3 = \frac{|S^{d-1}|P(x_k)}{d(d+2)} \varepsilon^{d+2} \begin{bmatrix} I_{d \times d} & 0 \\ 0 & 0 \end{bmatrix} + O(\varepsilon^{d+4} + \varepsilon^{d+2+\beta} + \varepsilon^{d+2\beta}),$$

where $O(\varepsilon^{d+4} + \varepsilon^{d+2+\beta} + \varepsilon^{d+2\beta})$ represents a D by D matrix whose entries are of order $O(\varepsilon^{d+4} + \varepsilon^{d+2+\beta} + \varepsilon^{d+2\beta})$. The constants in $O(\varepsilon^{d+4} + \varepsilon^{d+2+\beta} + \varepsilon^{d+2\beta})$ depend on d , C^2 norm of P , the second fundamental form of $\iota(M)$ and its derivative and the Ricci curvature of M . Observe that if $\beta > 2$, then $\varepsilon^{d+4} + \varepsilon^{d+2+\beta} + \varepsilon^{d+2\beta}$ is bounded by $3\varepsilon^{d+4}$. If $\beta \leq 2$, then $\varepsilon^{d+4} + \varepsilon^{d+2+\beta} + \varepsilon^{d+2\beta}$ is bounded by $3\varepsilon^{d+2\beta}$. The statement of the lemma follows. \square

B.2. Proof of Proposition B.1. Observe that

$$\mathbb{E}[(\iota(\mathbb{X}) + \mathbb{H} - \eta_k)(\iota(\mathbb{X}) + \mathbb{H} - \eta_k)^\top \chi\left(\frac{\|\iota(\mathbb{X}) + \mathbb{H} - \eta_k\|_{\mathbb{R}^D}}{\varepsilon}\right)] = E_1 + E_2 = E_3 + (E_1 - E_3) + E_2.$$

By combining Lemmas B.4, B.6 and B.7, we have

$$C_\varepsilon(\mathbf{y}_k) = \varepsilon^{d+2} \frac{|S^{d-1}|P(x_k)}{d(d+2)} \begin{bmatrix} I_{d \times d} & 0 \\ 0 & 0 \end{bmatrix} \\ + \begin{bmatrix} O(\varepsilon^{d+1+\beta} + \varepsilon^{d+2\beta} + \varepsilon^{d+4}) & O(\varepsilon^{d+2+\beta} + \varepsilon^{d+2\beta} + \varepsilon^{d+4}) \\ O(\varepsilon^{d+2+\beta} + \varepsilon^{d+2\beta} + \varepsilon^{d+4}) & O(\varepsilon^{d+3+\beta} + \varepsilon^{d-1+3\beta} + \varepsilon^{d+2\beta} + \varepsilon^{d+4}) \end{bmatrix},$$

where the constant factors in all the blocks depend on d , C^2 norm of P , the second fundamental form of $\iota(M)$ and its derivative and the Ricci curvature of M . Since $1 < \beta$, we have $\varepsilon^{d+2\beta} < \varepsilon^{d+1+\beta}$, $\varepsilon^{d+3+\beta} < \varepsilon^{d+4}$ and $\varepsilon^{d-1+3\beta} < \varepsilon^{d+2\beta}$. If $\beta > 2$, then $\varepsilon^{d+4} + \varepsilon^{d+2+\beta} + \varepsilon^{d+2\beta}$ is bounded by $3\varepsilon^{d+4}$. If $\beta \leq 2$, then $\varepsilon^{d+4} + \varepsilon^{d+2+\beta} + \varepsilon^{d+2\beta}$ is bounded by $3\varepsilon^{d+2\beta}$. Hence

$$C_\varepsilon(\mathbf{y}_k) = \varepsilon^{d+2} \frac{|S^{d-1}|P(x_k)}{d(d+2)} \begin{bmatrix} I_{d \times d} & 0 \\ 0 & 0 \end{bmatrix} + \begin{bmatrix} O(\varepsilon^{d+1+\beta} + \varepsilon^{d+4}) & O(\varepsilon^{d+2\beta} + \varepsilon^{d+4}) \\ O(\varepsilon^{d+2\beta} + \varepsilon^{d+4}) & O(\varepsilon^{d+2\beta} + \varepsilon^{d+4}) \end{bmatrix},$$

where the constant factors in all the blocks depend on d , C^2 norm of P , the second fundamental form of $\iota(M)$ and its derivative and the Ricci curvature of M .

APPENDIX C. PROOF OF PROPOSITION 3.2 AND PROPOSITION 3.3

C.1. Preliminary lemmas. Suppose $U, V \in \mathbb{R}^{m \times n}$. Recall the Hadamard product of U and V is defined as $(U \circ V)_{ij} = U_{ij}V_{ij}$ for $1 \leq i \leq m$ and $1 \leq j \leq n$. Then, $U^{(2)} = U \circ U$ is the Hadamard square of U . We start by considering the second moment of the local covariance matrix:

$$\mathbb{E}\left[\left((\iota(\mathbb{X}) + \mathbb{H} - \eta_k)(\iota(\mathbb{X}) + \mathbb{H} - \eta_k)^\top\right)^{(2)} \chi\left(\frac{\|\iota(\mathbb{X}) + \mathbb{H} - \eta_k\|_{\mathbb{R}^D}}{\varepsilon}\right)\right]$$

Next, we define the following matrices E_4 and E_5 to simplify our discussion:

$$\begin{aligned} F_2(\mathbf{t}(x), \eta, \eta_k) &= \left((\mathbf{t}(x) + \eta - \eta_k)(\mathbf{t}(x) + \eta - \eta_k)^\top \right)^{(2)} \chi\left(\frac{\|\mathbf{t}(x) + \eta - \eta_k\|_{\mathbb{R}^D}}{\varepsilon}\right), \\ E_4 &= \int_{\|\eta\|_{\mathbb{R}^D} < \varepsilon^\beta} \int_M F_2(\mathbf{t}(x), \eta, \eta_k) P(x) G_\sigma(\eta) dV d\eta, \\ E_5 &= \int_{\|\eta\|_{\mathbb{R}^D} \geq \varepsilon^\beta} \int_M F_2(\mathbf{t}(x), \eta, \eta_k) P(x) G_\sigma(\eta) dV d\eta. \end{aligned}$$

Note that for $1 \leq i, j \leq D$,

$$\begin{aligned} e_i^\top E_5 e_j &= \int_{\|\eta\|_{\mathbb{R}^D} \geq \varepsilon^\beta} \int_M \left(e_i^\top (\mathbf{t}(x) + \eta - \eta_k) \right)^2 \left((\mathbf{t}(x) + \eta - \eta_k)^\top e_j \right)^2 \\ &\quad \times \chi\left(\frac{\|\mathbf{t}(x) + \eta - \eta_k\|_{\mathbb{R}^D}}{\varepsilon}\right) P(x) G_\sigma(\eta) dV d\eta. \end{aligned}$$

When $\|\mathbf{t}(x) + \eta - \eta_k\|_{\mathbb{R}^D} \leq \varepsilon$, $\chi\left(\frac{\|\mathbf{t}(x) + \eta - \eta_k\|_{\mathbb{R}^D}}{\varepsilon}\right) \leq 1$. When $\|\mathbf{t}(x) + \eta - \eta_k\|_{\mathbb{R}^D} > \varepsilon$, $\chi\left(\frac{\|\mathbf{t}(x) + \eta - \eta_k\|_{\mathbb{R}^D}}{\varepsilon}\right) = 0$. Hence, for all $1 \leq i, j \leq D$ and all x , we have

$$\left(e_i^\top (\mathbf{t}(x) + \eta - \eta_k) \right)^2 \left((\mathbf{t}(x) + \eta - \eta_k)^\top e_j \right)^2 \chi\left(\frac{\|\mathbf{t}(x) + \eta - \eta_k\|_{\mathbb{R}^D}}{\varepsilon}\right) \leq \varepsilon^4.$$

By applying the same argument as Lemma B.4, we have the following lemma about E_5 .

Lemma C.1. *Suppose ε is small enough depending on d and D . Suppose $1 < \beta \leq \alpha - \frac{1}{2}$. If $\sigma = \varepsilon^\alpha$, then $|e_i^\top E_5 e_j| \leq \varepsilon^{d+8}$ for all $1 \leq i, j \leq D$.*

Now we are ready to bound the second moment of the local covariance matrix.

Lemma C.2. *Suppose ε is small enough depending on d , D , the scalar curvature of M and the second fundamental form of $\mathbf{t}(M)$. Suppose $1 < \beta \leq \alpha - \frac{1}{2}$. If $\sigma = \varepsilon^\alpha$ and $\|\eta_k\|_{\mathbb{R}^D} \leq \varepsilon^\beta$, then*

$$\begin{aligned} &\mathbb{E} \left[\left((\mathbf{t}(\mathbb{X}) + \mathbb{H} - \eta_k)(\mathbf{t}(\mathbb{X}) + \mathbb{H} - \eta_k)^\top \right)^{(2)} \chi\left(\frac{\|\mathbf{t}(\mathbb{X}) + \mathbb{H} - \eta_k\|_{\mathbb{R}^D}}{\varepsilon}\right) \right] \\ &= \begin{bmatrix} O(\varepsilon^{d+4}) & O(\varepsilon^{d+6} + \varepsilon^{d+2+2\beta}) \\ O(\varepsilon^{d+6} + \varepsilon^{d+2+2\beta}) & O(\varepsilon^{d+8} + \varepsilon^{d+4\beta}) \end{bmatrix}, \end{aligned}$$

where the top left block is a d by d matrix and the constant factors in all blocks depend on d , P_M and the second fundamental form of $\mathbf{t}(M)$.

Proof. Let $A(\eta) = \{x \in M \mid \|\mathbf{t}(x) + \eta - \eta_k\|_{\mathbb{R}^D} \leq \varepsilon \text{ for a fixed } \|\eta\|_{\mathbb{R}^D} < \varepsilon^\beta\}$. Since $\|\eta\|_{\mathbb{R}^D} < \varepsilon^\beta$ and $\|\eta_k\|_{\mathbb{R}^D} \leq \varepsilon^\beta$, by the triangle inequality, if $x \in A(\eta)$, then $\varepsilon - 2\varepsilon^\beta \leq \|\mathbf{t}(x)\|_{\mathbb{R}^D} \leq \varepsilon + 2\varepsilon^\beta$. If $1 < \beta \leq 3$, when ε is small enough depending on the second fundamental form of $\mathbf{t}(M)$, by Lemma B.1, we have $d(x, x_k) < \varepsilon + 3\varepsilon^\beta$. Hence, $A(\eta) \subset B_{\varepsilon+3\varepsilon^\beta}(x_k)$. Since $1 < \beta \leq 3$, when ε is small enough depending on the scalar curvature of M , by Lemma B.2, for all $\|\eta\|_{\mathbb{R}^D} < \varepsilon^\beta$, we have

$$\text{Vol}(A(\eta)) \leq \text{Vol}(B_{\varepsilon+3\varepsilon^\beta}(x_k)) \leq 4^d \text{Vol}(B_1^{\mathbb{R}^d}) \varepsilon^d = C_5(d) \varepsilon^d,$$

where $C_5(d) = 4^d \text{Vol}(B_1^{\mathbb{R}^d})$ is a constant depending on d . Similarly, if $\beta > 3$ and ε is small enough depending on the second fundamental form of $\mathbf{t}(M)$ and the scalar curvature of M , then we have $A(\eta) \subset B_{\varepsilon+3\varepsilon^3}(x_k)$ and $\text{Vol}(A(\eta)) \leq C_5(d) \varepsilon^d$.

Observe that for a fixed η , we have $\chi_{A(\eta)}(x) = \chi\left(\frac{\|\mathbf{t}(x) + \eta - \eta_k\|_{\mathbb{R}^D}}{\varepsilon}\right)$.

Let $Q_{ij}(x, \eta, \eta_k) = \left(e_i^\top (\iota(x) + \eta - \eta_k) \right)^2 \left((\iota(x) + \eta - \eta_k)^\top e_j \right)^2$, then

$$\begin{aligned}
(40) \quad |e_i^\top E_4 e_j| &= \left| \int_{\|\eta\|_{\mathbb{R}^D} < \varepsilon^\beta} \int_M e_i^\top F_2(\iota(x), \eta, \eta_k) e_j P(x) G_\sigma(\eta) dV d\eta \right| \\
&= \int_{\|\eta\|_{\mathbb{R}^D} < \varepsilon^\beta} \int_M Q_{ij}(x, \eta, \eta_k) \chi_{A(\eta)}(x) P(x) G_\sigma(\eta) dV d\eta \\
&\leq \sup_{\|\eta\|_{\mathbb{R}^D} < \varepsilon^\beta, x \in A(\eta)} Q_{ij}(x, \eta, \eta_k) \int_{\|\eta\|_{\mathbb{R}^D} < \varepsilon^\beta} \int_M \chi_{A(\eta)}(x) P(x) G_\sigma(\eta) dV d\eta \\
&\leq \sup_{\|\eta\|_{\mathbb{R}^D} < \varepsilon^\beta, x \in A(\eta)} Q_{ij}(x, \eta, \eta_k) P_M \sup_{\|\eta\|_{\mathbb{R}^D} < \varepsilon^\beta} \text{Vol}(A(\eta)) \\
&\leq \sup_{\|\eta\|_{\mathbb{R}^D} < \varepsilon^\beta, x \in A(\eta)} Q_{ij}(x, \eta, \eta_k) P_M C_5(d) \varepsilon^d.
\end{aligned}$$

If $1 < \beta \leq 3$ and $\|\eta\|_{\mathbb{R}^D} < \varepsilon^\beta$, then $x \in A(\eta) \subset B_{\varepsilon+3\varepsilon^\beta}(x_k)$. By Lemma B.5, when ε is small enough depending on the second fundamental form of $\iota(M)$, for any $\|\eta\|_{\mathbb{R}^D} < \varepsilon^\beta$, $\|\eta_k\|_{\mathbb{R}^D} \leq \varepsilon^\beta$ and $x \in B_{\varepsilon+3\varepsilon^\beta}(x_k)$, we have

$$\begin{aligned}
Q_{ij}(x, \eta, \eta_k) &\leq (49)^2 \varepsilon^4, \quad \text{for } 1 \leq i, j \leq d, \\
Q_{ij}(x, \eta, \eta_k) &\leq C_3^2 (\varepsilon^3 + \varepsilon^{1+\beta})^2 \leq 2C_3^2 (\varepsilon^6 + \varepsilon^{2+2\beta}), \quad \text{for } 1 \leq i \leq d \text{ and } d+1 \leq j \leq D, \\
Q_{ij}(x, \eta, \eta_k) &\leq C_3^2 (\varepsilon^3 + \varepsilon^{1+\beta})^2 \leq 2C_3^2 (\varepsilon^6 + \varepsilon^{2+2\beta}), \quad \text{for } d+1 \leq i \leq D \text{ and } 1 \leq j \leq d \\
Q_{ij}(x, \eta, \eta_k) &\leq C_3^2 (\varepsilon^4 + \varepsilon^{2\beta})^2 \leq 2C_3^2 (\varepsilon^8 + \varepsilon^{4\beta}), \quad \text{for } d+1 \leq i, j \leq D,
\end{aligned}$$

where C_3 is a constant depending on the second fundamental form of $\iota(M)$. Therefore, we can substitute the above bounds into (40). We conclude that when ε is small enough depending on the scalar curvature of M and the second fundamental form of $\iota(M)$,

$$E_4 = \begin{bmatrix} O(\varepsilon^{d+4}) & O(\varepsilon^{d+6} + \varepsilon^{d+2+2\beta}) \\ O(\varepsilon^{d+6} + \varepsilon^{d+2+2\beta}) & O(\varepsilon^{d+8} + \varepsilon^{d+4\beta}) \end{bmatrix},$$

where the top left block is a d by d matrix and the constant factors depend on d , P_M and the second fundamental form of $\iota(M)$.

If $\beta > 3$ and $\|\eta\|_{\mathbb{R}^D} < \varepsilon^\beta$, then $x \in A(\eta) \subset B_{\varepsilon+3\varepsilon^3}(x_k)$. By Lemma B.5, when ε is small enough depending on the second fundamental form of $\iota(M)$, for any $\|\eta\|_{\mathbb{R}^D} < \varepsilon^\beta$, $\|\eta_k\|_{\mathbb{R}^D} \leq \varepsilon^\beta$ and $x \in B_{\varepsilon+3\varepsilon^\beta}(x_k)$, we have

$$\begin{aligned}
Q_{ij}(x, \eta, \eta_k) &\leq (49)^2 \varepsilon^4, \quad \text{for } 1 \leq i, j \leq d, \\
Q_{ij}(x, \eta, \eta_k) &\leq 4C_3^2 \varepsilon^6, \quad \text{for } 1 \leq i \leq d \text{ and } d+1 \leq j \leq D, \\
Q_{ij}(x, \eta, \eta_k) &\leq 4C_3^2 \varepsilon^6, \quad \text{for } d+1 \leq i \leq D \text{ and } 1 \leq j \leq d \\
Q_{ij}(x, \eta, \eta_k) &\leq 4C_3^2 \varepsilon^8, \quad \text{for } d+1 \leq i, j \leq D,
\end{aligned}$$

where C_3 is a constant depending on the second fundamental form of $\iota(M)$. Therefore, we can substitute the above bounds into (40). We conclude that when ε is small enough depending on the scalar curvature of M and the second fundamental form of $\iota(M)$,

$$E_4 = \begin{bmatrix} O(\varepsilon^{d+4}) & O(\varepsilon^{d+6}) \\ O(\varepsilon^{d+6}) & O(\varepsilon^{d+8}) \end{bmatrix},$$

where the top left block is a d by d matrix and the constant factors depend on d , P_M and the second fundamental form of $\iota(M)$.

Since

$$\mathbb{E} \left[((\mathbf{t}(\mathbb{X}) + \mathbb{H} - \boldsymbol{\eta}_k)(\mathbf{t}(\mathbb{X}) + \mathbb{H} - \boldsymbol{\eta}_k)^\top)^{(2)} \chi \left(\frac{\|\mathbf{t}(\mathbb{X}) + \mathbb{H} - \boldsymbol{\eta}_k\|_{\mathbb{R}^D}}{\varepsilon} \right) \right] = E_4 + E_5,$$

the statement of the lemma follows from combining the cases when $1 < \beta \leq 3$ and $\beta > 3$ with Lemma C.1. \square

C.2. Proof of Proposition 3.2. Suppose $\sigma = \varepsilon^\alpha$ and $1 < \beta \leq \alpha - \frac{1}{2}$. For a fixed i , if $\varepsilon^{2(\beta-\alpha)} \geq \frac{1}{\varepsilon} \geq 2\sqrt{2}(D-2)$, then by Lemma B.3, we have

$$\Pr\{\|\boldsymbol{\eta}_i\|_{\mathbb{R}^D} \geq \varepsilon^\beta\} \leq \frac{2}{\Gamma(\frac{D}{2})} e^{-\frac{1}{4\varepsilon^{2(\alpha-\beta)}}} \leq 2e^{-\frac{1}{4\varepsilon^{2(\alpha-\beta)}}},$$

where we use $\frac{2}{\Gamma(\frac{D}{2})} \leq 2$ in the last step.

If $n \leq \frac{1}{2} \exp(\frac{1}{12\varepsilon^{2(\alpha-\beta)}})$ for some $1 < \beta < \alpha - \frac{1}{2}$, then by a straight forward calculation, we have

$$\Pr\{\|\boldsymbol{\eta}_i\|_{\mathbb{R}^D} \geq \varepsilon^\beta\} \leq 2e^{-\frac{1}{4\varepsilon^{2(\alpha-\beta)}}} \leq \frac{1}{4n^3}.$$

Since $\{\boldsymbol{\eta}_i\}_{i=1}^n$ are i.i.d. samples, by a straightforward union bound, we have

$$\Pr\{\|\boldsymbol{\eta}_i\|_{\mathbb{R}^D} \leq \varepsilon^\beta | i = 1, \dots, n\} \geq 1 - \frac{1}{4n^2}.$$

Suppose $\|\boldsymbol{\eta}_k\|_{\mathbb{R}^D} \leq \varepsilon^\beta$. Since $\mathbf{y}_k = \mathbf{t}(x_k) + \boldsymbol{\eta}_k$ with $\mathbf{t}(x_k) = \mathbf{0}$, for each $a, b = 1, \dots, D$, we denote

$$\begin{aligned} F_{a,b,i,k} &:= e_a^\top (\mathbf{y}_i - \mathbf{y}_k)(\mathbf{y}_i - \mathbf{y}_k)^\top e_b \chi \left(\frac{\|\mathbf{y}_i - \mathbf{y}_k\|_{\mathbb{R}^D}}{\varepsilon} \right) \\ &= e_a^\top (\mathbf{t}(x_i) + \boldsymbol{\eta}_i - \boldsymbol{\eta}_k)(\mathbf{t}(x_i) + \boldsymbol{\eta}_i - \boldsymbol{\eta}_k)^\top e_b \chi \left(\frac{\|\mathbf{t}(x_i) + \boldsymbol{\eta}_i - \boldsymbol{\eta}_k\|_{\mathbb{R}^D}}{\varepsilon} \right) \end{aligned}$$

$\{F_{a,b,i,k}\}$ for $i = 1, \dots, n$ and $i \neq k$ are i.i.d. realizations of the random variable

$$F_{a,b,k} := e_a^\top (\mathbf{t}(\mathbb{X}) + \mathbb{H} - \boldsymbol{\eta}_k)(\mathbf{t}(\mathbb{X}) + \mathbb{H} - \boldsymbol{\eta}_k)^\top e_b \chi \left(\frac{\|\mathbf{t}(\mathbb{X}) + \mathbb{H} - \boldsymbol{\eta}_k\|_{\mathbb{R}^D}}{\varepsilon} \right)$$

If $\|\mathbf{t}(x) + \boldsymbol{\eta} - \boldsymbol{\eta}_k\|_{\mathbb{R}^D} \leq \varepsilon$, then $\chi \left(\frac{\|\mathbf{t}(x) + \boldsymbol{\eta} - \boldsymbol{\eta}_k\|_{\mathbb{R}^D}}{\varepsilon} \right) = 1$, $|e_a^\top (\mathbf{t}(x) + \boldsymbol{\eta} - \boldsymbol{\eta}_k)| \leq \varepsilon$ and $|(\mathbf{t}(x) + \boldsymbol{\eta} - \boldsymbol{\eta}_k)^\top e_b| \leq \varepsilon$. Hence, $|F_{a,b,k}|$ is uniformly bounded by $c = \varepsilon^2$, for all $1 \leq a, b \leq D$.

By Proposition B.1, when ε is small enough depending on d, D , the second fundamental form of $\mathbf{t}(M)$ and the scalar curvature of M ,

$$\begin{aligned} & \mathbb{E}[(\mathbf{t}(\mathbb{X}) + \mathbb{H} - \boldsymbol{\eta}_k)(\mathbf{t}(\mathbb{X}) + \mathbb{H} - \boldsymbol{\eta}_k)^\top \chi \left(\frac{\|\mathbf{t}(\mathbb{X}) + \mathbb{H} - \boldsymbol{\eta}_k\|_{\mathbb{R}^D}}{\varepsilon} \right)] \\ &= \varepsilon^{d+2} \left(\frac{|S^{d-1}|P(x_k)}{d(d+2)} \begin{bmatrix} I_{d \times d} & \mathbf{0} \\ \mathbf{0} & \mathbf{0} \end{bmatrix} + \begin{bmatrix} O(\varepsilon^{\beta-1} + \varepsilon^2) & O(\varepsilon^{2\beta-2} + \varepsilon^2) \\ O(\varepsilon^{2\beta-2} + \varepsilon^2) & O(\varepsilon^{2\beta-2} + \varepsilon^2) \end{bmatrix} \right), \end{aligned}$$

where the constant factors in the four blocks depend on d, C^2 norm of P , the second fundamental form of $\mathbf{t}(M)$ and its derivative and the Ricci curvature of M . Let

$$\begin{aligned} \Omega &= \mathbb{E} \left[((\mathbf{t}(\mathbb{X}) + \mathbb{H} - \boldsymbol{\eta}_k)(\mathbf{t}(\mathbb{X}) + \mathbb{H} - \boldsymbol{\eta}_k)^\top)^{(2)} \chi \left(\frac{\|\mathbf{t}(\mathbb{X}) + \mathbb{H} - \boldsymbol{\eta}_k\|_{\mathbb{R}^D}}{\varepsilon} \right) \right] \\ &\quad - \left(\mathbb{E}[(\mathbf{t}(\mathbb{X}) + \mathbb{H} - \boldsymbol{\eta}_k)(\mathbf{t}(\mathbb{X}) + \mathbb{H} - \boldsymbol{\eta}_k)^\top \chi \left(\frac{\|\mathbf{t}(\mathbb{X}) + \mathbb{H} - \boldsymbol{\eta}_k\|_{\mathbb{R}^D}}{\varepsilon} \right)] \right)^{(2)}. \end{aligned}$$

The variance of the random variable $F_{a,b,k}$ is $e_a^\top \Omega e_b$. By combining Proposition B.1 and Lemma C.2, we have

$$\begin{aligned} e_a^\top \Omega e_b &\leq C_6 \varepsilon^{d+4} && \text{for } 1 \leq a, b \leq d, \\ e_a^\top \Omega e_b &\leq C_6 (\varepsilon^{d+6} + \varepsilon^{d+2+2\beta}) && \text{otherwise,} \end{aligned}$$

where C_6 is a constant depending on d , C^2 norm of P , the second fundamental form of $\iota(M)$ and its derivative and the Ricci curvature of M .

Observe that

$$e_a^\top C_{n,\varepsilon}(\mathbf{y}_k) e_b = \frac{1}{n} \sum_{i=1}^n F_{a,b,i,k} = \frac{n-1}{n} \left(\frac{1}{n-1} \sum_{i \neq k, i=1}^n F_{a,b,i,k} \right).$$

Since $\frac{n-1}{n} \rightarrow 1$ as $n \rightarrow \infty$, the error incurred by replacing $\frac{1}{n}$ by $\frac{1}{n-1}$ is of order $\frac{1}{n}$, which is negligible asymptotically. Thus, we can simply focus on analyzing $\frac{1}{n-1} \sum_{i \neq k, i=1}^n F_{a,b,i,k}$. By Bernstein's inequality,

$$\Pr \left\{ \left| \frac{1}{n-1} \sum_{i \neq k, i=1}^n F_{a,b,i,k} - \mathbb{E}[F_{a,b,k}] \right| > \gamma \right\} \leq \exp \left(- \frac{(n-1)\gamma^2}{2e_a^\top \Omega e_b + \frac{4}{3}c\gamma} \right) \leq \exp \left(- \frac{n\gamma^2}{4e_a^\top \Omega e_b + \frac{4}{3}c\gamma} \right).$$

For fixed a, b with $1 \leq a, b \leq d$, we choose γ_1 so that $\frac{\gamma_1}{\varepsilon^{d+2}} \rightarrow 0$ as $\varepsilon \rightarrow 0$, then we have $4e_a^\top \Omega e_b + \frac{4}{3}c\gamma_1 \leq (4C_6 + 2)\varepsilon^{d+4}$. Hence,

$$\exp \left(- \frac{n\gamma_1^2}{4e_a^\top \Omega e_b + \frac{4}{3}c\gamma_1} \right) \leq \exp \left(- C_7 n \gamma_1^2 \varepsilon^{-d-4} \right),$$

where $C_7 = \frac{1}{4C_6 + 2}$.

For fixed a, b with $d+1 \leq a \leq D$ or $d+1 \leq b \leq D$, we choose γ_2 so that $\frac{\gamma_2}{\varepsilon^{d+2\beta} + \varepsilon^{d+4}} \rightarrow 0$ as $\varepsilon \rightarrow 0$, then we have $4e_a^\top \Omega e_b + \frac{4}{3}c\gamma_2 \leq (4C_6 + 2)(\varepsilon^{d+2+2\beta} + \varepsilon^{d+6}) \leq (8C_6 + 4)\varepsilon^{d+2+\min(4,2\beta)}$. Hence,

$$\exp \left(- \frac{n\gamma_2^2}{4e_a^\top \Omega e_b + \frac{4}{3}c\gamma_2} \right) \leq \exp \left(- \frac{C_7}{2} n \gamma_2^2 \varepsilon^{-d-2-\min(4,2\beta)} \right).$$

If $\gamma_1 = C_8 \sqrt{\frac{\log(n)\varepsilon^{d+4}}{n}}$ and $\gamma_2 = C_9 \sqrt{\frac{\log(n)\varepsilon^{d+2+\min(4,2\beta)}}{n}}$ for some constants C_8 and C_9 depending on C_7 and D , then $\exp \left(- C_7 n \gamma_1^2 \varepsilon^{-d-4} \right) = \frac{1}{4D^2 n^3}$ and $\exp \left(- \frac{C_7}{2} n \gamma_2^2 \varepsilon^{-d-2-\min(4,2\beta)} \right) = \frac{1}{4D^2 n^3}$. Hence, for fixed a, b , we have

$$\begin{aligned} \Pr \left\{ \left| \frac{1}{n-1} \sum_{i \neq k, i=1}^n F_{a,b,i,k} - \mathbb{E}[F_{a,b,k}] \right| > C_8 \sqrt{\frac{\log(n)\varepsilon^{d+4}}{n}} \right\} &\leq \frac{1}{4D^2 n^3} \quad \text{when } 1 \leq a, b \leq d, \\ \Pr \left\{ \left| \frac{1}{n-1} \sum_{i \neq k, i=1}^n F_{a,b,i,k} - \mathbb{E}[F_{a,b,k}] \right| > C_9 \sqrt{\frac{\log(n)\varepsilon^{d+2+\min(4,2\beta)}}{n}} \right\} &\leq \frac{1}{4D^2 n^3} \quad \text{otherwise.} \end{aligned}$$

By considering the conditional probability such that $\|\eta_k\|_{\mathbb{R}^D} \leq \varepsilon^\beta$ for $k = 1, \dots, n$ and taking a trivial union bound for all $1 \leq a, b \leq D$ and $1 \leq k \leq n$, we conclude that for all x_k with probability greater than $1 - \frac{1}{n^2}$

$$\begin{aligned} |e_a^\top C_{n,\varepsilon}(\mathbf{y}_k) e_b - \mathbb{E}[F_{a,b,k}]| &< C_8 \sqrt{\frac{\log(n)\varepsilon^{d+4}}{n}} \quad \text{for all } 1 \leq a, b \leq d, \\ |e_a^\top C_{n,\varepsilon}(\mathbf{y}_k) e_b - \mathbb{E}[F_{a,b,k}]| &< C_9 \sqrt{\frac{\log(n)\varepsilon^{d+2+\min(4,2\beta)}}{n}} \quad \text{otherwise.} \end{aligned}$$

The conclusion of the proposition follows.

C.3. Proof of Proposition 3.3. Suppose ε is small enough depending on d, D , the second fundamental form of $\iota(M)$ and the scalar curvature of M . Note that $\sqrt{\frac{\log n}{n\varepsilon^d}} \leq \varepsilon^{\min(\beta-1,1)}$ is equivalent to $\frac{\log n}{n} \leq \varepsilon^{d+2\min(\beta-1,1)}$ and $\sqrt{\frac{\log n}{n\varepsilon^{d-2\min(\beta-1,1)}}} \leq \varepsilon^{2\min(\beta-1,1)}$ is equivalent to $\frac{\log n}{n} \leq \varepsilon^{d+2\min(\beta-1,1)}$. Hence, by Proposition 3.2, if $\varepsilon^{-d-2\min(\beta-1,1)} \leq \frac{n}{\log n}$ and $n \leq \frac{1}{2} \exp(\frac{1}{12\varepsilon^{2(\alpha-\beta)}})$, then for all x_k , with probability greater than $1 - \frac{1}{n^2}$,

$$C_{n,\varepsilon}(\mathbf{y}_k) = \varepsilon^{d+2} \left(\frac{|S^{d-1}|P(x_k)}{d(d+2)} \begin{bmatrix} I_{d \times d} & 0 \\ 0 & 0 \end{bmatrix} + \begin{bmatrix} O(\varepsilon^{\min(\beta-1,1)}) & O(\varepsilon^{2\min(\beta-1,1)}) \\ O(\varepsilon^{2\min(\beta-1,1)}) & O(\varepsilon^{2\min(\beta-1,1)}) \end{bmatrix} \right),$$

where the constant factors depend on d, C^2 norm of P , the second fundamental form of $\iota(M)$ and its derivative and the Ricci curvature of M . Hence,

$$C_{n,\varepsilon}(\mathbf{y}_k) = \varepsilon^{d+2} \frac{|S^{d-1}|P(x_k)}{d(d+2)} \left(\begin{bmatrix} I_{d \times d} + E_1 & 0 \\ 0 & 0 \end{bmatrix} + \begin{bmatrix} E_2 & E_3 \\ E_4 & E_5 \end{bmatrix} \right),$$

where the entries of E_1 are bounded by $C_{10}\varepsilon^{\min(\beta-1,1)}$ and the entries of E_2, E_3, E_4 and E_5 are bounded by $C_{10}\varepsilon^{2\min(\beta-1,1)}$. C_{10} depends on d, P_m, C^2 norm of P , the second fundamental form of $\iota(M)$ and its derivative and the Ricci curvature of M .

The scalar curvature is the trace of the Ricci curvature tensor. We will simplify any dependence on the scalar curvature by the dependence on d and the Ricci curvature. Since $\beta \geq \frac{5}{4}$, if ε is small enough depending on d, D, P_m, C^2 norm of P , the second fundamental form of $\iota(M)$ and its derivative and the Ricci curvature of M , then the operator norms of E_1 and $\begin{bmatrix} E_2 & E_3 \\ E_4 & E_5 \end{bmatrix}$ are bounded by $\frac{1}{3}$. Since $\begin{bmatrix} I_{d \times d} + E_1 & 0 \\ 0 & 0 \end{bmatrix}$ and $\begin{bmatrix} E_2 & E_3 \\ E_4 & E_5 \end{bmatrix}$ are symmetric matrices, based on Weyl's theorem, all the eigenvalues of $I_{d \times d} + E_1$ and the first d largest eigenvalues of $\begin{bmatrix} I_{d \times d} + E_1 & 0 \\ 0 & 0 \end{bmatrix} + \begin{bmatrix} E_2 & E_3 \\ E_4 & E_5 \end{bmatrix}$ are bounded below by $\frac{2}{3}$ and the remaining $D-d$ eigenvalues of $\begin{bmatrix} I_{d \times d} + E_1 & 0 \\ 0 & 0 \end{bmatrix} + \begin{bmatrix} E_2 & E_3 \\ E_4 & E_5 \end{bmatrix}$ are bounded above by $\frac{1}{3}$. Consider the eigen decomposition of $C_{n,\varepsilon}(\mathbf{y}_k)$ as $C_{n,\varepsilon}(\mathbf{y}_k) = U_{n,\varepsilon}(\mathbf{y}_k) \Lambda_{n,\varepsilon}(\mathbf{y}_k) U_{n,\varepsilon}(\mathbf{y}_k)^\top$ with $U_{n,\varepsilon}(\mathbf{y}_k) \in \mathbb{O}(D)$. Then, by Davis-Kahan theorem

$$U_{n,\varepsilon}(\mathbf{y}_k) = \begin{bmatrix} X_1 & 0 \\ 0 & X_2 \end{bmatrix} + O(\varepsilon^{2\min(\beta-1,1)}),$$

where $X_1 \in \mathbb{O}(d), X_2 \in \mathbb{O}(D-d)$. $O(\varepsilon^{2\min(\beta-1,1)})$ represent a D by D matrix whose entries are of order $O(\varepsilon^{2\min(\beta-1,1)})$, where the constant factors depend on d, D, P_m, C^2 norm of P , the second fundamental form of $\iota(M)$ and its derivative and the Ricci curvature of M .

APPENDIX D. PROOF OF THEOREM 3.1

We first define a map from \mathbb{R}^D to \mathbb{R}^d generalizing the map $\mathcal{P}_{\mathbf{y}_k}(\mathbf{y})$.

Definition D.1. Fix $x \in M$. Suppose $U \in \mathbb{O}(D)$. For any vector $\mathbf{a} \in \mathbb{R}^D$, we define a projection map for $\mathbf{y} \in \mathbb{R}^D$ associated with the first d column vectors of U :

$$\mathcal{P}_{U,\iota(x)+\mathbf{a}}(\mathbf{y}) = J^\top U^\top (\mathbf{y} - \iota(x) - \mathbf{a}).$$

Based on the above definition, $\mathcal{P}_{\mathbf{y}_k}(\mathbf{y}) = \mathcal{P}_{U_{n,\varepsilon,\iota(x_k)}+\eta_k}(\mathbf{y})$. We show that, under suitable conditions on \mathbf{a} and U , the map $\mathcal{P}_{U,\iota(x)+\mathbf{a}}(\mathbf{y})$ is a local diffeomorphism when it is restricted on $\iota(M)$. Intuitively, for any $x \in M$, if we have a d dimension subspace of \mathbb{R}^D which does not deviate too far away from the tangent space ι_*T_xM , then for any point $\iota(x) + \mathbf{a} \in \mathbb{R}^D$ that remains close to $\iota(x)$ and any \mathbf{y} around

$\iota(x) + \mathbf{a}$ on $\iota(M)$, the projection of $\mathbf{y} - \iota(x) - \mathbf{a}$ onto the subspace is a diffeomorphism. Hence, the map $\mathcal{P}_{U, \iota(x) + \mathbf{a}}(\mathbf{y})$ can be used to construct a chart. Our next proposition formalizes this argument and serves as a key component in proving Theorem 3.1.

Before we state the proposition. We make the following observation. For any $\mathbf{y} \in \iota(M)$, the map $\mathcal{P}_{U, \iota(x) + \mathbf{a}}(\mathbf{y})$ is invariant under translations of the manifold in \mathbb{R}^D : for any \mathbf{b} , we have

$$\mathcal{P}_{U, \iota(x) + \mathbf{a}}(\mathbf{y}) = J^\top U^\top (\mathbf{y} - \iota(x) - \mathbf{a}) = J^\top U^\top (\mathbf{y} + \mathbf{b} - (\iota(x) + \mathbf{b}) - \mathbf{a})^\top.$$

Moreover, $\mathcal{P}_{U, \iota(x) + \mathbf{a}}(\mathbf{y})$ is invariant under orthogonal transformation in \mathbb{R}^D : for any $V \in \mathbb{O}(D)$,

$$\mathcal{P}_{U, \iota(x) + \mathbf{a}}(\mathbf{y}) = J^\top U^\top (\mathbf{y} - \iota(x) - \mathbf{a}) = J^\top U^\top V^\top V (\mathbf{y} - \iota(x) - \mathbf{a}).$$

Hence, when we discuss the map $\mathcal{P}_{U, \iota(x) + \mathbf{a}}(\mathbf{y})$, we can always translate $\iota(M)$ and apply an orthogonal transformation in \mathbb{R}^D so that $\iota(x) = 0 \in \mathbb{R}^D$ and $\iota_* T_x M$ is generated by $\{e_i\}_{i=1}^d$.

Proposition D.1. *For $x \in M$, suppose we translate $\iota(M)$ and apply an orthogonal transformation in \mathbb{R}^D so that $\iota(x) = 0 \in \mathbb{R}^D$ and $\{Xe_i\}_{i=1}^d$ form a basis of $\iota_* T_x M$ where $X = \begin{bmatrix} X_1 & 0 \\ 0 & X_2 \end{bmatrix} \in \mathbb{O}(D)$ with $X_1 \in \mathbb{O}(d)$ and $X_2 \in \mathbb{O}(D-d)$. Suppose $U \in \mathbb{O}(D)$ and $E = U - X$ with $|E_{ij}| < r$. For any $0 < \xi \leq \frac{3\tau_{\iota(M)}}{16}$ and $r \leq \frac{1}{30d^{\frac{3}{2}}}$, if $\|\mathbf{a}\|_{\mathbb{R}^D} < \frac{\xi}{3}$, then we have the following facts:*

- (1) $\mathcal{P}_{U, \iota(x) + \mathbf{a}}$ is a diffeomorphism from $B_{\frac{\xi}{2}}^{\mathbb{R}^D}(\iota(x) + \mathbf{a}) \cap \iota(M)$ onto its image $O \subset \mathbb{R}^d$. O is homeomorphic to $B_1^{\mathbb{R}^d}(0)$.
- (2) There is a point \mathbf{u}_0 in O such that $0 \in B_R^{\mathbb{R}^d}(\mathbf{u}_0) \subset O \subset B_{\frac{\xi}{2}}^{\mathbb{R}^d}(0)$. Let $A = 1 - d^{\frac{3}{2}}r$ and $B = \frac{8\xi/3 + 2\|\mathbf{a}\|_{\mathbb{R}^D}}{\tau_{\iota(M)}}$. Then $R \geq (\sqrt{A^2 - A^2B} - \sqrt{B - A^2B})(\xi - \|\mathbf{a}\|_{\mathbb{R}^D})$.

D.1. Preliminary lemmas for the proof of Proposition D.1. In order to prove Proposition D.1, we need to define the angle between two subspaces of the same dimension in \mathbb{R}^D .

Definition D.2. *The angle $\phi_{V,W}$ between two subspaces of the same dimension in \mathbb{R}^D , V and W , is defined as*

$$\phi_{V,W} = \max_{\mathbf{v} \in V} \min_{\mathbf{w} \in W} \arccos \left(\frac{|\mathbf{v}^\top \mathbf{w}|}{\|\mathbf{v}\|_{\mathbb{R}^D} \|\mathbf{w}\|_{\mathbb{R}^D}} \right).$$

Based on the definition, we have $0 \leq \phi_{V,W} \leq \frac{\pi}{2}$.

We summarize the basic properties of the angle between two subspaces of the same dimension in the following lemma.

Lemma D.1. *Suppose V, W, Z are three subspaces of the same dimension in \mathbb{R}^D . Then, we have the following properties:*

(1)

$$\cos(\phi_{V,W}) = \min_{\mathbf{v} \in V} \max_{\mathbf{w} \in W} \frac{|\mathbf{v}^\top \mathbf{w}|}{\|\mathbf{v}\|_{\mathbb{R}^D} \|\mathbf{w}\|_{\mathbb{R}^D}}.$$

(2) *If there is a vector $\mathbf{v} \in V$ which is perpendicular to W , then $\phi_{V,W} = \frac{\pi}{2}$.*

(3) *The angle is invariant under orthogonal transformation of \mathbb{R}^D . In other words, if $X \in \mathbb{O}(D)$, then $\phi_{XV, XW} = \phi_{V,W}$.*

(4) *The angle is a metric on the set of all subspaces of the same dimension in \mathbb{R}^D . Specifically, we have*

- (a) (Non-negativeness) $\phi_{V,W} \geq 0$.
- (b) (Identification) $\phi_{V,W} = 0$ implies $V = W$.
- (c) (Symmetry) $\phi_{V,W} = \phi_{W,V}$.
- (d) (Triangle inequality) $\phi_{V,Z} \leq \phi_{V,W} + \phi_{W,Z}$.

Proof. (1) follows from the definition and the fact that cosine is decreasing on $[0, \frac{\pi}{2}]$. (2) and (3) follow directly from the definition. A proof of (4) can be found in [41] \square

We refer the reader to [41] for more discussion about the angle between two subspaces of different dimensions. Next, we prove a lemma which bounds the angle for two sufficiently close subspaces.

Lemma D.2. *Suppose $X \in \mathbb{O}(D)$ such that $X = \begin{bmatrix} X_1 & 0 \\ 0 & X_2 \end{bmatrix}$ with $X_1 \in \mathbb{O}(d)$ and $X_2 \in \mathbb{O}(D-d)$. Suppose $U \in \mathbb{O}(D)$ such that $E = U - X$ with $|E_{ij}| < r$. Let $\{Xe_i\}_{i=1}^d$ be a basis of V and $\{Ue_i\}_{i=1}^d$ be a basis of W . Suppose $\phi_{V,W}$ is the angle between V and W , then $\cos(\phi_{V,W}) \geq 1 - d^{\frac{3}{2}}r$. In particular, if $r \leq \frac{1}{30d^{\frac{3}{2}}}$, then $\cos(\phi_{V,W}) \geq \frac{29}{30}$.*

Proof. We write $E = \begin{bmatrix} E_1 & E_2 \\ E_3 & E_4 \end{bmatrix}$ with $E_1 \in \mathbb{R}^{d \times d}$. Let $\mathbf{u} \in \mathbb{R}^d$ be an arbitrary unit vector. Then $\begin{bmatrix} X_1 \\ 0 \end{bmatrix} \mathbf{u}$ is an arbitrary vector unit in V and $\begin{bmatrix} X_1 + E_1 \\ E_3 \end{bmatrix} \mathbf{u}$ is a unit vector in W . By (1) in Lemma D.1, we have

$$\cos(\phi_{V,W}) \geq \left| \mathbf{u}^\top [X_1^\top, 0] \begin{bmatrix} X_1 + E_1 \\ E_3 \end{bmatrix} \mathbf{u} \right| = |\mathbf{u}^\top X_1^\top (X_1 + E_1) \mathbf{u}| = |1 + \mathbf{u}^\top X_1^\top E_1 \mathbf{u}|$$

By Cauchy-Schwarz inequality, each entry of $X_1^\top E_1$ is bounded by \sqrt{dr} and each entry of $X_1^\top E_1 \mathbf{u}$ is bounded by dr . Hence, $|\mathbf{u}^\top X_1^\top E_1 \mathbf{u}| \leq d^{\frac{3}{2}}r$. The conclusion follows. \square

Suppose $x, y \in M$, then the next lemma describes the angle between the tangent spaces of two points $\iota(x)$ and $\iota(y)$ when they are close in Euclidean distance. The proof is a combination of Proposition 6.2 and Proposition 6.3 in [31].

Lemma D.3. *Suppose $x, y \in M$. Let $\phi_{V,W}$ be the angle between $V = \iota_* T_x M$ and $W = \iota_* T_y M$. If $\|\iota(x) - \iota(y)\| \leq \frac{\tau_{\iota(M)}}{2}$, then $\cos(\phi_{V,W}) \geq \sqrt{1 - \frac{2\|\iota(x) - \iota(y)\|}{\tau_{\iota(M)}}}$. In particular, if $\|\iota(x) - \iota(y)\| \leq \frac{\tau_{\iota(M)}}{4}$, then $\cos(\phi_{V,W}) \geq \frac{1}{\sqrt{2}}$.*

D.2. Proof of Proposition D.1. Proof of part (a) of Proposition D.1

Since we assume $\iota(x) = 0$, we express $\mathcal{P}_{U, \iota(x) + \mathbf{a}}(\mathbf{y})$ as $\mathcal{P}_{U, \mathbf{a}}(\mathbf{y})$ for notation simplicity. By proposition A.1, suppose we choose $0 < \xi_1 \leq \frac{\tau_{\iota(M)}}{4}$, then any $\mathbf{y} \in B_{\xi_1}^{\mathbb{R}^D}(0) \cap \iota(M)$, $\mathcal{P}_{U, \mathbf{a}}(\mathbf{y})$ can be represented in the chart as follows,

$$\mathcal{P}_{U, \mathbf{a}}(\mathbf{y}) = J^\top U^\top \begin{bmatrix} \mathbf{u} \\ G_x(\mathbf{u}) \end{bmatrix} - J^\top U^\top \mathbf{a},$$

where $\mathbf{u} \in V_x \subset B_{\xi_1}^{\mathbb{R}^d}(0) \subset \mathbb{R}^d$. V_x contains 0 and is homeomorphic to $B_1^{\mathbb{R}^d}(0)$.

Since $\iota(M)$ is smooth, $\mathcal{P}_{U, \mathbf{a}}(\mathbf{y})$ is smooth. By Proposition 3.1, $B_{\xi_1}^{\mathbb{R}^D}(0) \cap \iota(M)$ is homeomorphic to $B_1^{\mathbb{R}^d}(0)$. Hence, we can show that $\mathcal{P}_{U, \mathbf{a}}(\mathbf{y})$ is a diffeomorphism from $B_{\xi_1}^{\mathbb{R}^D}(0) \cap \iota(M)$ onto its image by applying the inverse function theorem. Note that

$$D\mathcal{P}_{U, \mathbf{a}}(\mathbf{y}) = J^\top U^\top \begin{bmatrix} I_{d \times d} \\ DG_x(\mathbf{u}) \end{bmatrix}.$$

The column vectors of $\begin{bmatrix} I_{d \times d} \\ DG_x(\mathbf{u}) \end{bmatrix}$ are a basis of the tangent space $V = \iota_* T_{\iota^{-1}(\mathbf{y})} M$, while the column vectors of UJ are a basis of a subspace W . Hence, $D\mathcal{P}_{U, \mathbf{a}}(\mathbf{y})$ is not singular if and only if there is no vector in V that is perpendicular to W . By (2) in Lemma D.1, it is sufficient to show the angle $\phi_{V,W}$ between V

and W is less than $\frac{\pi}{2}$. By Lemma D.2, if $r \leq \frac{1}{30d^{\frac{3}{2}}}$, then $\cos(\phi_{\iota_* T_x M, W}) \geq \frac{29}{30}$. Since $\mathbf{y} \in B_{\xi_1}^{\mathbb{R}^D}(0) \cap \iota(M)$, by Lemma D.3, we have $\cos(\phi_{\iota_* T_x M, V}) \geq \frac{1}{\sqrt{2}}$. By (4) in Lemma D.1 and a straightforward calculation,

$$(41) \quad \phi_{V, W} \leq \phi_{\iota_* T_x M, W} + \phi_{\iota_* T_x M, V} \leq \alpha := \arccos\left(\frac{29}{30}\right) + \arccos\left(\frac{1}{\sqrt{2}}\right) < \frac{\pi}{2}.$$

By the inverse function theorem, $\mathcal{P}_{U, \iota(x) + \mathbf{a}}(\mathbf{y})$ is a diffeomorphism from $B_{\xi_1}^{\mathbb{R}^D}(0) \cap \iota(M)$ onto its image. Choose $\xi = \frac{3\xi_1}{4}$. If $\|\mathbf{a}\|_{\mathbb{R}^D} < \frac{\xi}{3} = \frac{\xi_1}{4}$, then the closure of $B_{\xi}^{\mathbb{R}^D}(\mathbf{a}) \cap \iota(M)$ is contained in $B_{\xi_1}^{\mathbb{R}^D}(0) \cap \iota(M)$. Hence, $\mathcal{P}_{U, \mathbf{a}}(\mathbf{y})$ is a diffeomorphism from the closure of $B_{\xi}^{\mathbb{R}^D}(\mathbf{a}) \cap \iota(M)$ onto its image. By Proposition 3.1, $B_{\xi}^{\mathbb{R}^D}(\mathbf{a}) \cap \iota(M)$ is homeomorphic to $B_1^{\mathbb{R}^d}(0)$.

Proof of part (b) of Proposition D.1

Let $O \subset \mathbb{R}^d$ be the image of $B_{\xi}^{\mathbb{R}^D}(\mathbf{a}) \cap \iota(M)$ under $\mathcal{P}_{U, \mathbf{a}}(\mathbf{y})$. Then, O is homeomorphic to $B_1^{\mathbb{R}^d}(0)$. Let \bar{O} be the closure of O in \mathbb{R}^d . Suppose $\Phi : \bar{O} \rightarrow \mathbb{R}^D$ is the inverse of $\mathcal{P}_{U, \mathbf{a}}(\mathbf{y})$. Then the restriction of Φ on O is a chart of $\iota(M)$. Since $\|\mathbf{a}\|_{\mathbb{R}^D} < \frac{\xi}{3}$, we have $0 = \iota(x) \in B_{\xi}^{\mathbb{R}^D}(\mathbf{a}) \cap \iota(M)$. Hence, $\mathbf{u}_0 = \mathcal{P}_{U, \mathbf{a}}(0) = \mathcal{P}_{U, \mathbf{a}}(\iota(x)) \in O$. Based on the definition of $\mathcal{P}_{U, \mathbf{a}}$ in Definition D.1, Φ can be expressed as

$$\Phi(\mathbf{u}) = \mathbf{a} + U \begin{bmatrix} \mathbf{u} \\ F(\mathbf{u}), \end{bmatrix}$$

where $F(\mathbf{u}) : \bar{O} \rightarrow \mathbb{R}^{D-d}$ is a smooth function. For any $\mathbf{u} \in O$, $\Phi(\mathbf{u}) \in B_{\xi_1}^{\mathbb{R}^D}(0) \cap \iota(M)$. Hence, we apply the same argument as in the proof of part (a). Recall that W is the subspace generated by the column vectors of UJ . If $V(\mathbf{u})$ is the tangent space of $\iota(M)$ at $\Phi(\mathbf{u})$ for $\mathbf{u} \in O$. By Lemma D.2, $\cos(\phi_{\iota_* T_x M, W}) \geq 1 - d^{\frac{3}{2}}r$. By Lemma D.3, we have $\cos(\phi_{\iota_* T_x M, V(\mathbf{u})}) \geq \sqrt{1 - \frac{2(\xi_1 + \|\mathbf{a}\|_{\mathbb{R}^D})}{\tau_{\iota(M)}}}$. Hence, by (4) in Lemma D.1,

$$(42) \quad \phi_{V(\mathbf{u}), W} \leq \phi_{\iota_* T_x M, W} + \phi_{\iota_* T_x M, V(\mathbf{u})} \leq \arccos\left(\sqrt{1 - \frac{2(\xi_1 + \|\mathbf{a}\|_{\mathbb{R}^D})}{\tau_{\iota(M)}}}\right) + \arccos(1 - d^{\frac{3}{2}}r).$$

In particular, by (41), for $\mathbf{u} \in O$,

$$(43) \quad \cos(\phi_{V(\mathbf{u}), W}) \geq \cos(\alpha) > 0.5$$

Suppose $B_R^{\mathbb{R}^d}(\mathbf{u}_0)$ is the largest open ball centered at \mathbf{u}_0 and contained in O , i.e. there is \mathbf{u}_1 on the boundary of O such that $\|\mathbf{u}_0 - \mathbf{u}_1\|_{\mathbb{R}^d} = R$. Thus, we have

$$\|\iota(x) - \Phi(\mathbf{u}_1)\|_{\mathbb{R}^D}^2 = \|\Phi(\mathbf{u}_0) - \Phi(\mathbf{u}_1)\|_{\mathbb{R}^D}^2 = \|\mathbf{u}_0 - \mathbf{u}_1\|_{\mathbb{R}^d}^2 + \|F(\mathbf{u}_0) - F(\mathbf{u}_1)\|_{\mathbb{R}^{D-d}}^2.$$

Since $B_R^{\mathbb{R}^d}(\mathbf{u}_0)$ is contained in O , any point on the segment between \mathbf{u}_0 and \mathbf{u}_1 is in O . By the mean value inequality, there is $\mathbf{u}^* \in O$ on the segment between \mathbf{u}_0 and \mathbf{u}_1 such that

$$\|F(\mathbf{u}_0) - F(\mathbf{u}_1)\|_{\mathbb{R}^{D-d}} \leq \|DF(\mathbf{u}^*)\mathbf{v}\|_{\mathbb{R}^{D-d}} \|\mathbf{u}_0 - \mathbf{u}_1\|_{\mathbb{R}^d}^2,$$

where $\mathbf{v} = \frac{\mathbf{u}_0 - \mathbf{u}_1}{\|\mathbf{u}_0 - \mathbf{u}_1\|_{\mathbb{R}^d}}$. In other words,

$$(44) \quad \|\iota(x) - \Phi(\mathbf{u}_1)\|_{\mathbb{R}^D} \leq R \sqrt{1 + \|DF(\mathbf{u}^*)\mathbf{v}\|_{\mathbb{R}^{D-d}}^2}.$$

Based on the definition of Φ , $U \begin{bmatrix} \mathbf{v} \\ DF(\mathbf{u}^*)\mathbf{v} \end{bmatrix}$ is a vector in $V(\mathbf{u}^*)$, the tangent space of $\iota(M)$ at $\Phi(\mathbf{u}^*)$.

Hence, $\frac{1}{\sqrt{1 + \|DF(\mathbf{u}^*)\mathbf{v}\|_{\mathbb{R}^{D-d}}^2}} \begin{bmatrix} \mathbf{v} \\ DF(\mathbf{u}^*)\mathbf{v} \end{bmatrix}$ is a unit vector in $U^\top V(\mathbf{u}^*)$. By (3) in Lemma D.1, $\phi_{U^\top V(\mathbf{u}^*), U^\top W} =$

$\phi_{V(\mathbf{u}^*),W}$. Observe that any unit vector in $U^\top W$ is in the form of $\begin{bmatrix} \mathbf{w} \\ 0 \end{bmatrix}$, where \mathbf{w} is a unit vector in \mathbb{R}^d .

We choose the \mathbf{w} such that $\begin{bmatrix} \mathbf{w} \\ 0 \end{bmatrix}^\top \frac{1}{\sqrt{1+\|DF(\mathbf{u}^*)\mathbf{v}\|_{\mathbb{R}^{D-d}}^2}} \begin{bmatrix} \mathbf{v} \\ DF(\mathbf{u}^*)\mathbf{v} \end{bmatrix}$ attains the maximum, then we have

$$\begin{aligned} \cos(\phi_{V(\mathbf{u}^*),W}) &= \cos(\phi_{U^\top V(\mathbf{u}^*),U^\top W}) \leq \begin{bmatrix} \mathbf{w} \\ 0 \end{bmatrix}^\top \frac{1}{\sqrt{1+\|DF(\mathbf{u}^*)\mathbf{v}\|_{\mathbb{R}^{D-d}}^2}} \begin{bmatrix} \mathbf{v} \\ DF(\mathbf{u}^*)\mathbf{v} \end{bmatrix} \\ &= \frac{\mathbf{w}^\top \mathbf{v}}{\sqrt{1+\|DF(\mathbf{u}^*)\mathbf{v}\|_{\mathbb{R}^{D-d}}^2}} \leq \frac{1}{\sqrt{1+\|DF(\mathbf{u}^*)\mathbf{v}\|_{\mathbb{R}^{D-d}}^2}}. \end{aligned}$$

By (44), we have $\|\iota(x) - \Phi(\mathbf{u}_1)\|_{\mathbb{R}^D} \leq \frac{R}{\cos(\phi_{V(\mathbf{u}^*),W})}$. Note that since \mathbf{u}_1 is on the boundary of O , $\Phi(\mathbf{u}_1)$ is on the boundary of $B_{\frac{R}{\xi}}^{\mathbb{R}^D}(\mathbf{a}) \cap \iota(M)$. Hence,

$$\xi = \|\mathbf{a} - \Phi(\mathbf{u}_1)\|_{\mathbb{R}^D} = \|\iota(x) + \mathbf{a} - \Phi(\mathbf{u}_1)\|_{\mathbb{R}^D} \leq \|\iota(x) - \Phi(\mathbf{u}_1)\|_{\mathbb{R}^D} + \|\mathbf{a}\|_{\mathbb{R}^D} \leq \frac{R}{\cos(\phi_{V(\mathbf{u}^*),W})} + \|\mathbf{a}\|_{\mathbb{R}^D}.$$

We conclude that $R \geq (\xi - \|\mathbf{a}\|_{\mathbb{R}^D}) \cos(\phi_{V(\mathbf{u}^*),W})$. By (42), we have

$$\cos(\phi_{V(\mathbf{u}^*),W}) \geq (1-d^{\frac{3}{2}}r) \sqrt{1 - \frac{2(\xi_1 + \|\mathbf{a}\|_{\mathbb{R}^D})}{\tau_{\iota(M)}}} - \sqrt{\frac{2(\xi_1 + \|\mathbf{a}\|_{\mathbb{R}^D})}{\tau_{\iota(M)}}} \sqrt{1 - (1-d^{\frac{3}{2}}r)^2}.$$

The lower bound for R follows by substituting $\xi_1 = \frac{4\xi}{3}$.

To show that $0 \in O \subset \mathbb{R}^d$, we prove that $\|\mathbf{u}_0\|_{\mathbb{R}^d} < R$. First, by (43),

$$R \geq (\xi - \|\mathbf{a}\|_{\mathbb{R}^D}) \cos(\phi_{V(\mathbf{u}^*),W}) \geq \cos(\alpha)(\xi - \|\mathbf{a}\|_{\mathbb{R}^D}) > 0.5(\xi - \|\mathbf{a}\|_{\mathbb{R}^D}).$$

Moreover, $\|\mathbf{u}_0\|_{\mathbb{R}^d} \leq \|\mathbf{a}\|_{\mathbb{R}^D}$. Since $\|\mathbf{a}\|_{\mathbb{R}^D} < \frac{\xi}{3}$, we have $\|\mathbf{a}\|_{\mathbb{R}^D} < 0.5(\xi - \|\mathbf{a}\|_{\mathbb{R}^D})$. The conclusion follows.

D.3. Proof of Theorem 3.1. Based on Proposition 3.3, for all $x_i, i = 1, \dots, n$, with probability greater than $1 - \frac{1}{n^2}$, we have $\|\eta_i\|_{\mathbb{R}^D} \leq \varepsilon^\beta$. When ε is small enough, we have $\varepsilon^\beta < \varepsilon < \frac{\tau_{\iota(M)}}{16}$. Hence, we have $\|\eta_i\|_{\mathbb{R}^D} \leq \varepsilon^\beta < \delta < \frac{\tau_{\iota(M)}}{16}$. If $\mathbf{y}_i \in B_\delta^{\mathbb{R}^D}(\mathbf{y}_k)$, then by triangle inequality

$$\|\iota(x_i) - \mathbf{y}_k\|_{\mathbb{R}^D} = \|\mathbf{y}_i - \eta_i - \mathbf{y}_k\|_{\mathbb{R}^D} \leq \|\mathbf{y}_i - \mathbf{y}_k\|_{\mathbb{R}^D} + \|\eta_i\|_{\mathbb{R}^D} < 3\delta.$$

Hence, $\iota(x_i) \in B_{3\delta}^{\mathbb{R}^D}(\mathbf{y}_k)$. Moreover,

$$U_{n,\varepsilon}(\mathbf{y}_k) = \begin{bmatrix} X_1 & 0 \\ 0 & X_2 \end{bmatrix} + E.$$

By Proposition 3.3, $|E_{ij}| < C\varepsilon^{2\min(\beta-1,1)}$, where C is a constant depending on d, D, P_m, C^2 norm of P , the second fundamental form of $\iota(M)$ and its derivative and the Ricci curvature of M . Since $\beta \geq \frac{5}{4}$, $2\min(\beta-1,1) \geq \frac{1}{2}$. Hence, when ε is small enough depending on d, D, P_m, C^2 norm of P , the second fundamental form of $\iota(M)$ and its derivative and the Ricci curvature of M , $C\varepsilon^{2\min(\beta-1,1)} \leq \frac{1}{30d^{\frac{3}{2}}}$.

Note that $\mathcal{P}_{\mathbf{y}_k}(\mathbf{y}) = \mathcal{P}_{U_{n,\varepsilon,\iota(x_k)} + \eta_k}(\mathbf{y})$. The conditions in Proposition D.1 are satisfied with $\xi = 3\delta$, $\mathbf{a} = \eta_k$ and $r = C\varepsilon^{2\min(\beta-1,1)}$. (1) and (2) of Theorem 3.1 follows. Since $\|\eta_i\|_{\mathbb{R}^D} \leq \varepsilon^\beta$, we have $B = \frac{8/3(3\delta)+2\|\eta_k\|_{\mathbb{R}^D}}{\tau_{\iota(M)}} \leq \frac{8\delta+2\varepsilon^\beta}{\tau_{\iota(M)}}$. (3) of Theorem 3.1 follows.

APPENDIX E. PROOF OF PROPOSITION 3.4

Since $\mathcal{Y}_{true} \subset \iota(M)$, $\text{dist}(\mathbf{y}_i, \iota(M)) \leq \text{dist}(\mathbf{y}_i, \mathcal{Y}_{true})$ for all i . Hence, $GRMSE(\mathcal{Y}, \iota(M)) \leq GRMSE(\mathcal{Y}, \mathcal{Y}_{true})$. Let $N_r(x)$ be the number of samples in $B_r^{\mathbb{R}^D}(\iota(x)) \cap \mathcal{Y}_{true}$. Based on (3) in Theorem 2.4 in [43], if $r \rightarrow 0$ as $m \rightarrow \infty$, then with probability greater than $1 - \frac{1}{m^2}$,

$$\sup_{x \in M} \left| \frac{N_r(x)}{mr^d} - q(x) \right| \leq C \sqrt{\frac{\log m}{mr^d}},$$

where C is a constant depending on d, D, C^1 norm of q , the curvature of M and the second fundamental form of $\iota(M)$. Hence, if $\frac{q_{\min}}{2} mr^d \geq 1$ and $\frac{\log m}{mr^d} \leq \frac{q_{\min}^2}{4C^2}$, then $N_r(x) \geq \frac{q_m}{2} mr^d \geq 1$. Note that $\frac{q_{\min}}{2} mr^d \geq 1$ and $\frac{\log m}{mr^d} \leq \frac{q_{\min}^2}{4C^2}$ are satisfied when $r^d \geq \max(\frac{2}{q_{\min} m}, \frac{4C^2 \log m}{q_{\min}^2 m})$. Hence, we choose $r^d = \max(\frac{2}{q_{\min}}, (\frac{2C}{q_{\min}})^2) \frac{\log m}{m}$.

Since M is compact, for any \mathbf{y}_i , let $\iota(x'_i)$ be the point that realizes $\text{dist}(\mathbf{y}_i, \iota(M))$. Then, with probability greater than $1 - \frac{1}{m^2}$, there is a point $\iota(x_j) \in \mathcal{Y}_{true}$ such that $\iota(x_j) \in B_r^{\mathbb{R}^D}(\iota(x'_i))$. Hence,

$$\begin{aligned} \text{dist}(\mathbf{y}_i, \mathcal{Y}_{true}) - r &\leq \|\mathbf{y}_i - \iota(x_j)\|_{\mathbb{R}^D} - r \leq \|\mathbf{y}_i - \iota(x_j)\|_{\mathbb{R}^D} - \|\iota(x'_i) - \iota(x_j)\|_{\mathbb{R}^D} \\ &\leq \|\iota(x'_i) - \mathbf{y}_i\|_{\mathbb{R}^D} = \text{dist}(\mathbf{y}_i, \iota(M)). \end{aligned}$$

In conclusion, we have $0 \leq \text{dist}(\mathbf{y}_i, \mathcal{Y}_{true}) - \text{dist}(\mathbf{y}_i, \iota(M)) \leq r$. Consequently,

$$0 \leq \text{dist}(\mathbf{y}_i, \mathcal{Y}_{true})^2 - \text{dist}(\mathbf{y}_i, \iota(M))^2 \leq r(\text{dist}(\mathbf{y}_i, \mathcal{Y}_{true}) + \text{dist}(\mathbf{y}_i, \iota(M))) \leq 2r \text{dist}(\mathbf{y}_i, \iota(M)) + r^2.$$

By the definition of $GRMSE$,

$$GRMSE(\mathcal{Y}, \mathcal{Y}_{true})^2 - GRMSE(\mathcal{Y}, \iota(M))^2 \leq 2r \frac{1}{n} \sum_{i=1}^n \text{dist}(\mathbf{y}_i, \iota(M)) + r^2 \leq 2r GRMSE(\mathcal{Y}, \iota(M)) + r^2.$$

The conclusion follows.

APPENDIX F. BRIEF REVIEW OF THE DIFFUSION MAP

We provide a briefly review of the Diffusion Map (DM). Given samples $\{\mathbf{y}_i\}_{i=1}^n \subset \mathbb{R}^D$, the DM constructs a normalized graph Laplacian $L \in \mathbb{R}^{n \times n}$ by using the kernel $k(\mathbf{y}, \mathbf{y}') = \exp(-\frac{\|\mathbf{y} - \mathbf{y}'\|_{\mathbb{R}^D}^2}{\varepsilon_{DM}^2})$ as shown in the following steps.

- (1) Let $W_{ij} = \frac{k(\mathbf{y}_i, \mathbf{y}_j)}{q(\mathbf{y}_i)q(\mathbf{y}_j)} \in \mathbb{R}^{n \times n}$, $1 \leq i, j, \leq n$, where $q(\mathbf{y}_i) = \sum_{j=1}^n k(\mathbf{y}_i, \mathbf{y}_j)$.
- (2) Define an $n \times n$ diagonal matrix D as $D_{ii} = \sum_{j=1}^n W_{ij}$, where $i = 1, \dots, n$.
- (3) The normalized graph Laplacian L is defined as $L = \frac{D^{-1}W - I}{\varepsilon_{DM}^2} \in \mathbb{R}^{n \times n}$.

Suppose $(\mu_j, V_j)_{j=0}^{n-1}$ are the eigenpairs of $-L$ with $\mu_0 \leq \mu_1 \leq \dots \leq \mu_{n-1}$ and V_i normalizing in ℓ^2 . Then, $\mu_0 = 0$ and V_0 is a constant vector. The map (V_1, \dots, V_ℓ) provides the coordinates of the data set $\{\mathbf{y}_i\}_{i=1}^n$ in a low dimensional space \mathbb{R}^ℓ .

When $\{\mathbf{y}_i = \iota(x_i)\}_{i=1}^n$ are samples from an isometrically embedded submanifold $\iota(M) \subset \mathbb{R}^D$, then [8] shows that $-L$ approximates the Laplace-Beltrami (LB) operator of M pointwisely. In particular, when the boundary of M is not empty, $-L$ pointwisely approximates the LB operator with Neumann boundary condition. Moreover, when M is a closed manifold, the spectral convergence rate of $-L$ to the LB operator is discussed in [12, 7, 6]. Suppose the eigenvectors of $-L$ are normalized properly. [12] show that the first K eigenpairs of $-L$ approximate the corresponding eigenpairs of the LB operator over $\{x_i\}_{i=1}^n$ whenever ε_{DM} is small enough depending on K and n is large enough depending on ε_{DM} . Based on the results in spectral geometry, by choosing ℓ sufficiently large, the DM (V_1, \dots, V_ℓ) approximates the discretization of an embedding of $\iota(M)$ into \mathbb{R}^ℓ .

APPENDIX G. DETERMINE THE DIMENSION OF THE DATA SET

Suppose the data points $\{\mathbf{y}_i\}_{i=1}^n \subset \mathbb{R}^D$ satisfy the Assumption 2.1. In this section, we describe a method to estimate the dimension d of the underlying manifold M by using diffusion map. Let $C_{n,\varepsilon}(\mathbf{y}_k)$ be the local covariance matrix at \mathbf{y}_k constructed by $\{\mathbf{y}_i\}_{i=1}^n$ as defined in (1). Suppose $\lambda_{n,\varepsilon,i}(\mathbf{y}_k)$ is the i th largest eigenvalue of $C_{n,\varepsilon}(\mathbf{y}_k)$. Then, we define the mean of the i th eigenvalues of the the local covariance matrices as

$$(45) \quad \bar{\lambda}_{\varepsilon,i} = \frac{1}{n} \sum_{k=1}^n \lambda_{n,\varepsilon,i}(\mathbf{y}_k).$$

We demonstrate our method by using the following example. Consider the surface of the ellipsoid in \mathbb{R}^3 described by the equation

$$\frac{x^2}{4} + \frac{y^2}{2.25} + z^2 = 1$$

We sample 800 points $\{(x'_i, y'_i, z'_i)\}_{i=1}^{800}$ uniformly on the surface. Let R be an orthogonal matrix of \mathbb{R}^3 .

We rotate the surface by using R , i.e. we get 800 points $\{(x''_i, y''_i, z''_i)\}_{i=1}^{800}$ where $\begin{bmatrix} x''_i \\ y''_i \\ z''_i \end{bmatrix} = R \begin{bmatrix} x'_i \\ y'_i \\ z'_i \end{bmatrix}$. Hence,

$\iota(x_i) = (0, \dots, 0, x''_i, y''_i, z''_i, 0, \dots, 0) \in \mathbb{R}^{30}$ (x''_i , y''_i , and z''_i are the 14th, 15th, and 16th coordinates, respectively) is a point on a surface of the ellipsoid $\iota(M)$ in \mathbb{R}^{30} . Suppose $\{\eta_i\}_{i=1}^{800}$ are i.i.d samples from $\mathcal{N}(0, \sigma^2 I_{30 \times 30})$ where $\sigma = 0.05$. Then $\mathbf{y}_i = \iota(x_i) + \eta_i$ is a noisy data point around the submanifold $\iota(M)$ in \mathbb{R}^{30} . We choose the bandwidths $\varepsilon = 0.3, 0.4, 0.5, 0.6$ and find $\{\bar{\lambda}_{\varepsilon,i}\}_{i=1}^{30}$ by using $\{\iota(x_i)\}_{i=1}^{800}$. We show the plot of $\{\bar{\lambda}_{\varepsilon,i}\}_{i=1}^{30}$ for different ε in Fig 8 . We can see that there are two large eigenvalues. In other words, for this example, when there is no noise, the eigenvalues of the local covariance matrices constructed from $\{\iota(x_i)\}_{i=1}^{800}$ are sufficient to determine the dimension of the underlying manifold.

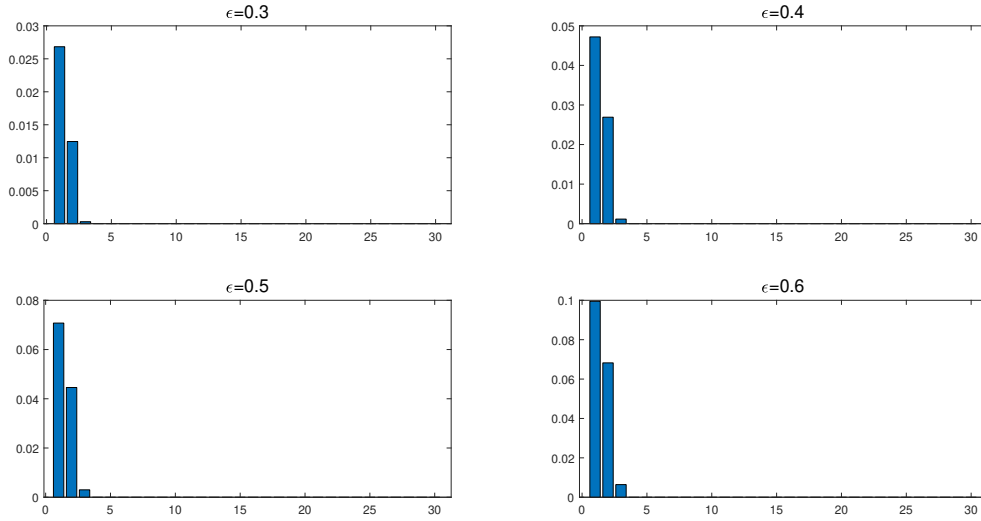


FIGURE 8. We choose the bandwidths $\varepsilon = 0.3, 0.4, 0.5, 0.6$ and find $\{\bar{\lambda}_{\varepsilon,i}\}_{i=1}^{30}$ by using $\{\iota(x_i)\}_{i=1}^{800}$. In the above plots, the horizontal axis indicates the $i = 1, \dots, 30$ and the vertical axis indicates the value of corresponding $\bar{\lambda}_{\varepsilon,i}$.

Next, we choose the bandwidths $\{\varepsilon = 0.1\ell\}_{\ell=1}^{30}$ and find $\{\bar{\lambda}_{\varepsilon,i}\}_{i=1}^{30}$ by using $\{\mathbf{y}_i\}_{i=1}^{800}$. We show the plot of $\{\bar{\lambda}_{\varepsilon,i}\}_{i=1}^{30}$ for $\varepsilon = 0.5, 1, \dots, 3$ in Fig 9. Due to the noise, we cannot determine the dimension of $\iota(M)$ correctly by using the eigenvalues of the local covariance matrices constructed from $\{\mathbf{y}_i\}_{i=1}^{800}$.

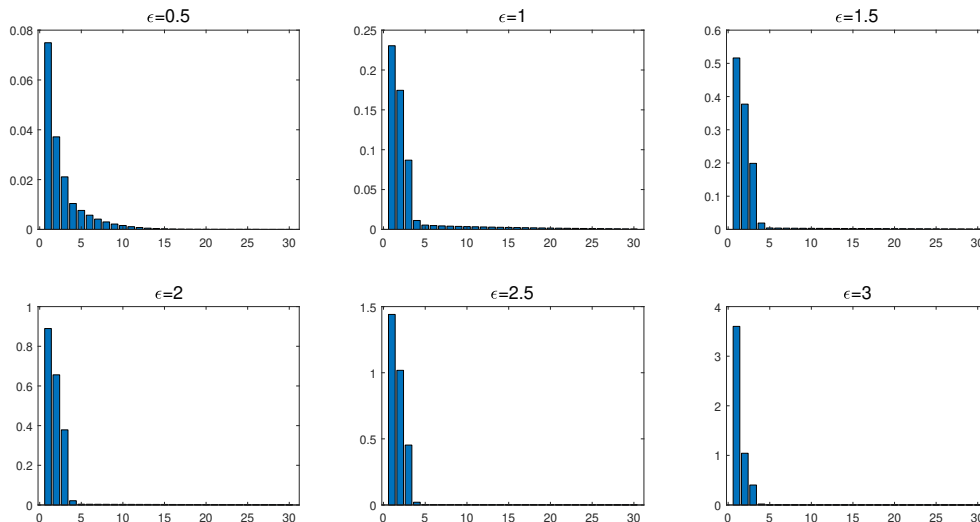


FIGURE 9. For $\{\varepsilon = 0.1\ell\}_{\ell=1}^{30}$, we find $\{\bar{\lambda}_{\varepsilon,i}\}_{i=1}^{30}$ by using $\{\mathbf{y}_i\}_{i=1}^{800}$. We plot $\{\bar{\lambda}_{\varepsilon,i}\}_{i=1}^{30}$ for $\varepsilon = 0.5, 1, \dots, 3$. In the above plots, the horizontal axis indicates $i = 1, \dots, 30$ and the vertical axis indicates the value of the corresponding $\bar{\lambda}_{\varepsilon,i}$.

The robustness of diffusion map to noise is discussed in [14, 36, 13, 10]. Based on the description of the algorithm in Section F, we construct the normalized graph Laplacian $L \in \mathbb{R}^{n \times n}$ by using the kernel $k(\mathbf{y}, \mathbf{y}') = \exp(-\frac{\|\mathbf{y}-\mathbf{y}'\|_{\mathbb{R}^D}^2}{\varepsilon_{DM}^2})$ and the noisy data points $\{\mathbf{y}_i\}_{i=1}^{800}$. We choose $\varepsilon_{DM} = 2$ and let $(\mu_j, V_j)_{j=0}^{n-1}$ be the eigenpairs of $-L$ with $\mu_0 \leq \mu_1 \leq \dots \leq \mu_{n-1}$ and V_i normalizing in ℓ^2 . We reconstruct the noisy data points $\{\mathbf{y}_i\}_{i=1}^{800}$ in \mathbb{R}^{2+j} by using $(V_1, \dots, V_{2+j}) \in \mathbb{R}^{800 \times (2+j)}$ and denote these data points in \mathbb{R}^{2+j} as \mathcal{X}_j for $j = 1, \dots, 4$. For each $j = 1, \dots, 4$, the diffusion map (V_1, \dots, V_{2+j}) can be regarded as an approximation of a discretization of an embedding of $\iota(M)$ into \mathbb{R}^{2+j} over the clean data point $\{\iota(x_i)\}_{i=1}^{800}$ on $\iota(M)$. Hence, \mathcal{X}_j are the samples around an embedded submanifold N_j in \mathbb{R}^{2+j} homeomorphic to M . The dimension of M is the same as the dimension of N_j . For each $j = 1, \dots, 4$, we construct the local covariance matrices by using \mathcal{X}_j with $\varepsilon = 0.3 + 0.1j$ and calculate $\{\bar{\lambda}_{\varepsilon,i}^j\}_{i=1}^{2+j}$. We plot $\{\bar{\lambda}_{\varepsilon,i}^j\}_{i=1}^{2+j}$ for each j in Figure 10. We can see that in each plot there are 2 large eigenvalues. Therefore, the dimension of the underlying manifold N_j and the dimension of M are 2.

APPENDIX H. AN EXAMPLE FOR SELECTION OF ε AND δ IN THE MRGAP

In this section, we illustrate our my method for selecting the parameters ε and δ in the MrGap algorithm. We consider $\iota(M)$ which is the unit circle in \mathbb{R}^2 . We uniformly sample 100 points on the circle, each added by Gaussian noise with $\sigma = 0.06$. Let $\mathcal{Y} = \{\mathbf{y}_i\}_{i=1}^{100}$ be the noisy data around the circle. We also sample \mathcal{Y}_{true} consisting of 10^5 points on the circle. We use \mathcal{Y}_{true} to approximate the GRMSE from samples to $\iota(M)$ with $GRMSE(\mathcal{Y}, \mathcal{Y}_{true}) = 0.0588$. Let $\varepsilon = \{0.1, 0.2, \dots, 1.8\}$ and $\delta = \{0.1, 0.2, \dots, 1.8\}$. We consider all pairs $(\varepsilon_i, \delta_j)$ with $\varepsilon \leq \delta$. Therefore, there are 171 distinct pairs. For each pair $(\varepsilon_i, \delta_j)$, we maximize $L_{ij} = \sum_{k=1}^n \log p_k(\mathbf{Z}_k | A, \rho, \sigma)$ in (12) over A, ρ, σ . We choose $(\varepsilon_i, \delta_j)$ corresponding to the largest L_{ij} . When $\varepsilon = 1.4$ and $\delta = 1.4$, $\frac{L_{ij}}{100}$ achieves maximum 338 over

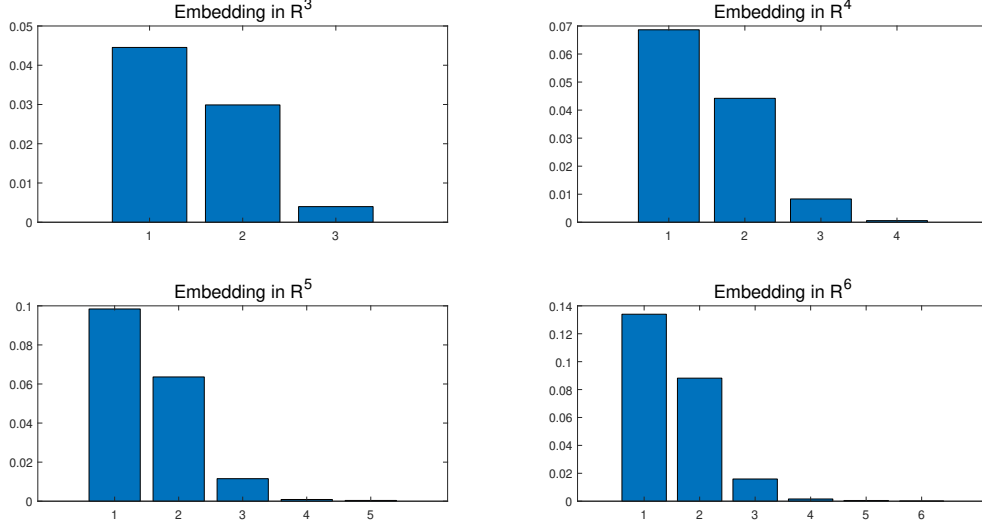


FIGURE 10. $\mathcal{X}_1, \dots, \mathcal{X}_4$ constructed by diffusion map are the samples around the embeddings of M in $\mathbb{R}^3, \dots, \mathbb{R}^6$, respectively. For each $j = 1, \dots, 4$, we construct the local covariance matrices by using \mathcal{X}_j with $\varepsilon = 0.3 + 0.1j$ and calculate $\{\bar{\lambda}_{\varepsilon,i}^j\}_{i=1}^{2+j}$. We plot $\{\bar{\lambda}_{\varepsilon,i}^j\}_{i=1}^{2+j}$ for each j . The top two plots correspond to $j = 1, 2$. The bottom two plots correspond to $j = 3, 4$. In the above plots, the horizontal axis indicates $i = 1, \dots, 2 + j$ and the vertical axis indicates the value of the corresponding $\bar{\lambda}_{\varepsilon,i}^j$.

all pairs of $(\varepsilon_i, \delta_j)$. The corresponding GP parameters are $A^{(0)} = 0.9$, $\rho^{(0)} = 1.2$ and $\sigma^{(0)} = \sqrt{0.008}$. For $\varepsilon = 1.4$ and $\delta = 1.4$, suppose \mathcal{X}_1 is the denoised output after the first round of the iteration in Algorithm 1. Then, $GRMSE(\mathcal{X}_1, \mathcal{Y}_{true}) = 0.0251$. We plot the $\frac{L_{ij}}{100}$ and the corresponding first round denoised outputs for different pairs of $(\varepsilon_i, \delta_j)$ in Figure 11.

APPENDIX I. EXPLORATION OF THE PROPERTIES OF MRGAP ON NUMERICAL EXAMPLES

I.1. **Cassini Oval in \mathbb{R}^3 .** We consider a Cassini Oval $\iota(M)$ in \mathbb{R}^3 parametrized by $\theta \in [0, 2\pi)$,

$$(46) \quad \begin{aligned} X(\theta) &= \sqrt{\cos(2\theta) + \sqrt{\cos(2\theta)^2 + 0.2 \cos(\theta)}}, \\ Y(\theta) &= \sqrt{\cos(2\theta) + \sqrt{\cos(2\theta)^2 + 0.2 \sin(\theta)}}, \\ Z(\theta) &= 0.3 \sin(\theta + \pi). \end{aligned}$$

We uniformly sample points $\{\theta_i\}_{i=1}^{102}$ on $[0, 2\pi)$ to obtain non-uniform samples $\{X(\theta_i), Y(\theta_i), Z(\theta_i)\}_{i=1}^{102}$ on $\iota(M)$. Suppose $\eta_i \sim \mathcal{N}(0, \sigma^2 I_{3 \times 3})$, with $\sigma = 0.04$, $\mathbf{y}_i = (X(\theta_i), Y(\theta_i), Z(\theta_i))^\top + \eta_i$ for $i = 1, \dots, 102$, and $\mathcal{Y} = \{\mathbf{y}_i\}_{i=1}^{102}$. We uniformly sample $\{\phi_i\}_{i=1}^{10^5}$ on $[0, 2\pi)$ to obtain $\mathcal{Y}_{true} = \{X(\phi_i), Y(\phi_i), Z(\phi_i)\}_{i=1}^{10^5}$. We use \mathcal{Y}_{true} to approximate the GRMSE from samples to $\iota(M)$ with $GRMSE(\mathcal{Y}, \mathcal{Y}_{true}) = 0.059$. We plot \mathcal{Y} and \mathcal{Y}_{true} in Figure 12.

We apply the MrGap algorithm with $\varepsilon = 0.3$ and $\delta = 0.6$. We iterate Steps 1-3 of Algorithm 1 twice. The estimated covariance parameters in the last round of the iterations are $A^{(1)} = 0.048$, $\rho^{(1)} = 0.3$ and $\sigma^{(1)} = \sqrt{2} \times 10^{-5}$. The denoised outputs are $\mathcal{X}_1 = \{\hat{\mathbf{y}}_i\}_{i=1}^{102}$, with $GRMSE(\mathcal{X}_1, \mathcal{Y}_{true}) = 0.0224$. The plot of \mathcal{X}_1 and \mathcal{Y}_{true} is in Figure 13. When we apply Algorithm 2, we choose $K = 20$, i.e. we

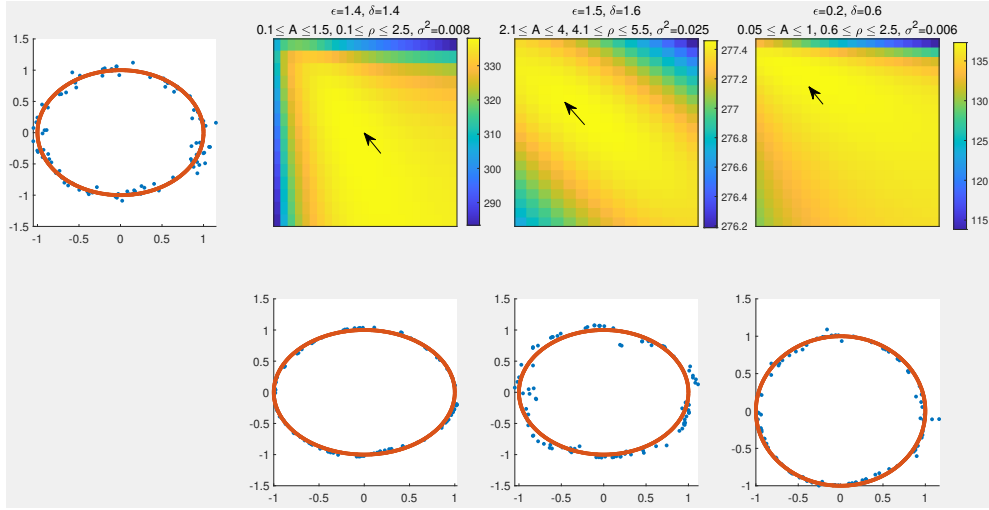


FIGURE 11. Top row: The first plot shows the noisy data \mathcal{Y} and the samples on the unit circle \mathcal{Y}_{true} . $GRMSE(\mathcal{Y}, \mathcal{Y}_{true}) = 0.0588$. For each pair $(\varepsilon_i, \delta_j)$, suppose $\frac{L_{ij}}{100}$ achieves maximum with A_{ij} , ρ_{ij} and σ_{ij} . In the second to the fourth plot, we fix $\frac{L_{ij}}{100}$ and we plot $\frac{L_{ij}}{100}$ over A and ρ in a neighborhood around A_{ij} and ρ_{ij} . The horizontal axis is ρ and the vertical axis is A . The arrows indicate the locations of the maximums. The maximums of $\frac{L_{ij}}{100}$ in the plots are 338, 277.46, and 137.3 respectively. Bottom row: The plots of the first round denoised outputs correspond to ε_i , δ_j , A_{ij} , ρ_{ij} and σ_{ij} in the top row. The GRMSE between the first round denoised outputs and \mathcal{Y}_{true} are 0.0251, 0.0769, and 0.0366 respectively.

construct 102 charts and we interpolate 20 points in each chart. The outputs are $\mathcal{X}_2 = \{\tilde{\mathbf{y}}_i\}_{i=1}^{2040}$ with $GRMSE(\mathcal{X}_2, \mathcal{Y}_{true}) = 0.0216$. We plot \mathcal{X}_2 and \mathcal{Y}_{true} in Figure 14.

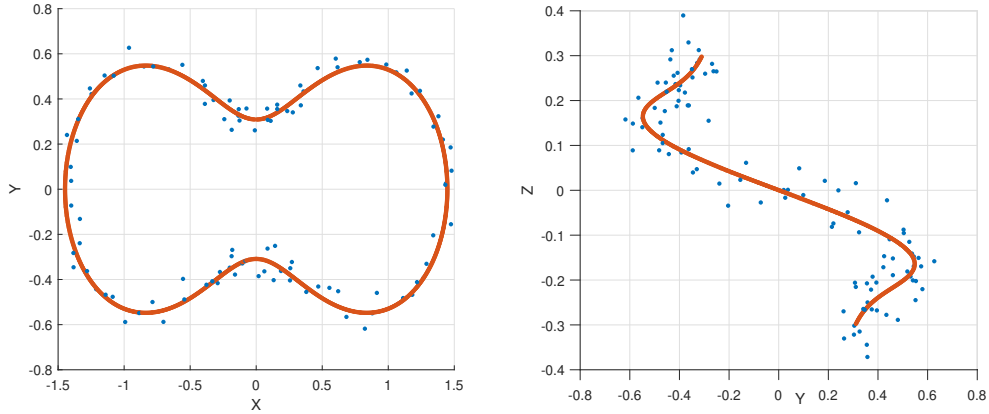


FIGURE 12. \mathcal{Y} contains 102 noisy points around the Cassini Oval $\iota(M)$ and \mathcal{Y}_{true} contains 10^5 points on $\iota(M)$. The left and the right panels show the XY plot and YZ plot of \mathcal{Y} and \mathcal{Y}_{true} respectively. The blue points are \mathcal{Y} and the red points are \mathcal{Y}_{true} . We use \mathcal{Y}_{true} to estimate the GRMSE from samples to $\iota(M)$ with $GRMSE(\mathcal{Y}, \mathcal{Y}_{true}) = 0.059$.

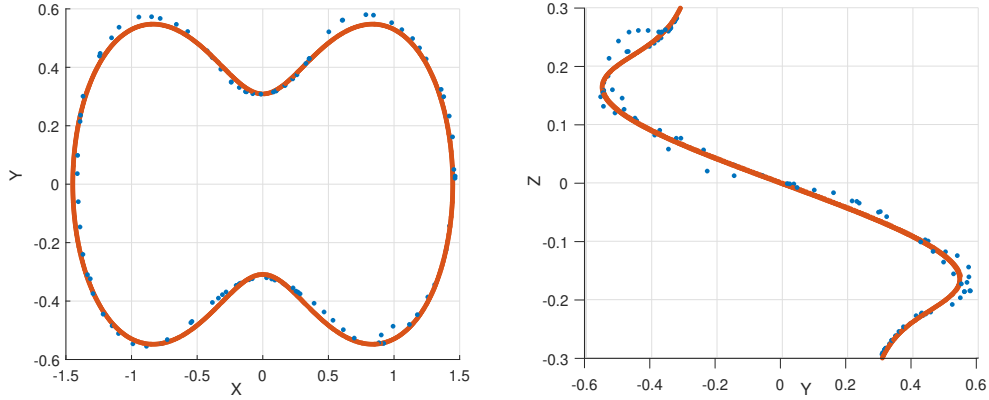


FIGURE 13. \mathcal{X}_1 contains 102 denoised points by the MrGap algorithm. The left and the right panels show the XY plot and YZ plot of \mathcal{X}_1 and \mathcal{Y}_{true} respectively. The blue points are \mathcal{X}_1 and the red points are \mathcal{Y}_{true} . We use \mathcal{Y}_{true} to estimate the GRMSE from samples to $\iota(M)$ with $GRMSE(\mathcal{X}_1, \mathcal{Y}_{true}) = 0.0224$.

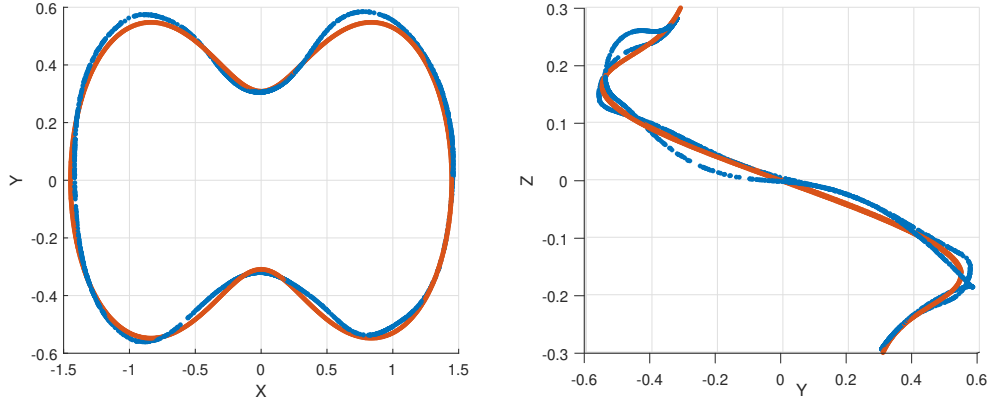


FIGURE 14. \mathcal{X}_2 contains 2040 interpolated points by the MrGap algorithm. The left and the right panels show the XY plot and YZ plot of \mathcal{X}_2 and \mathcal{Y}_{true} respectively. The blue points are \mathcal{X}_2 and the red points are \mathcal{Y}_{true} . We use \mathcal{Y}_{true} to estimate the GRMSE from samples to $\iota(M)$ with $GRMSE(\mathcal{X}_2, \mathcal{Y}_{true}) = 0.0216$.

I.2. Stability of Algorithm 2 under different orders of interpolations. Suppose $\{\hat{\mathbf{y}}_i\}_{i=1}^n$ are the final denoised output from Algorithm 1. Recall that Algorithm 2 iteratively interpolates points around each $\hat{\mathbf{y}}_i$ based on the index order i . In this subsection, we demonstrate through a numerical simulation that the output of Algorithm 2 remains stable regardless of the interpolation order.

Let $\mathcal{Y} = \{\mathbf{y}_i\}_{i=1}^{102}$ be the noisy data points around the Cassini Oval in subsection I.1. Suppose $\{\mathbf{y}_i^{(1)}\}_{i=1}^{102}$ are the output after applying the first round of the iterations in Algorithm 1 to \mathcal{Y} . Next, we generate 100 different permutations of $\{\mathbf{y}_i^{(1)}\}_{i=1}^{102}$. We denote these permutations as $\{\mathcal{Y}_j^{(1)}\}_{j=1}^{100}$. For each permutation $\mathcal{Y}_j^{(1)}$, we apply Algorithm 2 with $\varepsilon = 0.3$ and $\delta = 0.6$. We choose $K = 20$ and we apply the same estimated covariance parameters in the last round of the iterations of Algorithm 1 i.e. $A^{(1)} = 0.048$, $\rho^{(1)} = 0.3$ and $\sigma^{(1)} = \sqrt{2} \times 10^{-5}$. Therefore, for each permutation $\mathcal{Y}_j^{(1)}$, we construct

$\tilde{\mathcal{X}}_j$ consisting of 2040 interpolation points. Let \mathcal{Y}_{true} be the 10^5 points sampled on the Cassini Oval described in subsection I.1. We evaluate the performance of each group of interpolation through an estimation the GRMSE between $\tilde{\mathcal{X}}_j$ and the Cassani Oval through \mathcal{Y}_{true} . Let $\mathcal{E}_j = GRMSE(\tilde{\mathcal{X}}_j, \mathcal{Y}_{true})$ for $j = 1, \dots, 100$. The mean of $\{\mathcal{E}_j\}_{j=1}^{100}$ is 0.0213 with a small standard deviation 2.16×10^{-4} .

I.3. Performance of MrGap on data with a different distribution. In this subsection, we explore the performance of the MrGap algorithm when the clean data are highly non-uniformly distributed on $\iota(M)$. We consider the Cassini Oval $\iota(M)$ in \mathbb{R}^3 parametrized by $[X(\theta), Y(\theta), Z(\theta)]^\top$ in (46). We generate non-uniform sample points $\{\theta_i\}_{i=1}^{102}$ on $[0, 2\pi)$ to obtain non-uniform samples $\{X(\theta_i), Y(\theta_i), Z(\theta_i)\}_{i=1}^{102}$ on $\iota(M)$. Suppose $\eta_i \sim \mathcal{N}(0, \sigma^2 I_{3 \times 3})$, with $\sigma = 0.04$, $\mathbf{y}_i = (X(\theta_i), Y(\theta_i), Z(\theta_i))^\top + \eta_i$ for $i = 1, \dots, 102$, and $\mathcal{Y} = \{\mathbf{y}_i\}_{i=1}^{102}$. We uniformly sample $\{\phi_i\}_{i=1}^{10^5}$ on $[0, 2\pi)$ to obtain $\mathcal{Y}_{true} = \{X(\phi_i), Y(\phi_i), Z(\phi_i)\}_{i=1}^{10^5}$. We use \mathcal{Y}_{true} to approximate the GRMSE from samples to $\iota(M)$ with $GRMSE(\mathcal{Y}, \mathcal{Y}_{true}) = 0.0529$. We plot \mathcal{Y} and \mathcal{Y}_{true} in Figure 15. We apply the MrGap algorithm with $\varepsilon = 0.7$ and $\delta = 0.7$. We iterate Steps 1-3 of Algorithm 1 twice. The estimated covariance parameters in the last round of the iterations are $A^{(1)} = 0.24$, $\rho^{(1)} = 0.6$ and $\sigma^{(1)} = \sqrt{2} \times 10^{-5}$. The denoised outputs are $\mathcal{X}_1 = \{\hat{\mathbf{y}}_i\}_{i=1}^{102}$, with $GRMSE(\mathcal{X}_1, \mathcal{Y}_{true}) = 0.0223$. The plot of \mathcal{X}_1 and \mathcal{Y}_{true} is in Figure 15. When we apply Algorithm 2, we choose $K = 30$, i.e. we construct 102 charts and we interpolate 30 points in each chart. The outputs are $\mathcal{X}_2 = \{\tilde{\mathbf{y}}_i\}_{i=1}^{3060}$ with $GRMSE(\mathcal{X}_2, \mathcal{Y}_{true}) = 0.0206$. The plot of \mathcal{X}_2 and \mathcal{Y}_{true} is in Figure 15. Since the clean data are highly non-uniformly distributed on $\iota(M)$, there are large gaps between the interpolations. However, in regions where the curvature is small and the data is sparse, the interpolations, while not fully covering the manifold, still accurately reflect its local geometry.

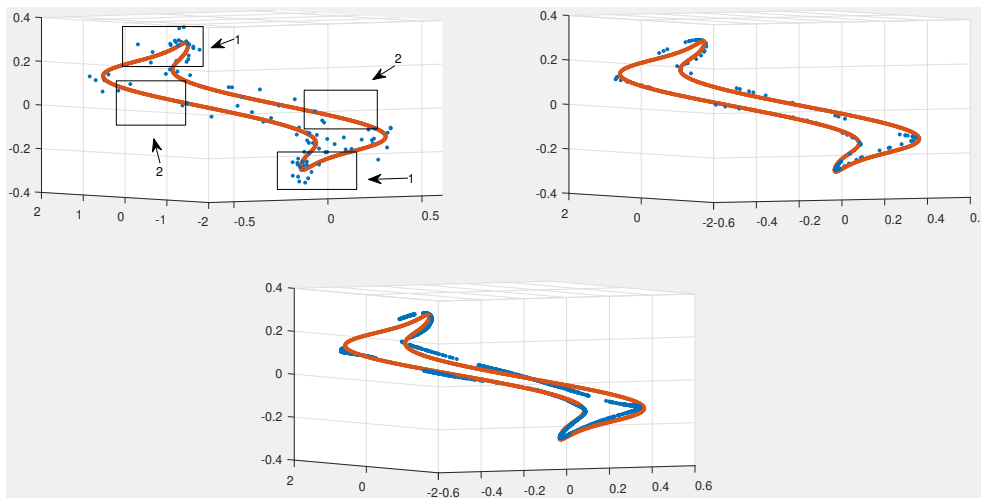


FIGURE 15. \mathcal{Y} contains 102 noisy points around the Cassini Oval $\iota(M)$ and \mathcal{Y}_{true} contains 10^5 points on $\iota(M)$. Left Panel: The plot of \mathcal{Y} and \mathcal{Y}_{true} . The blue points are \mathcal{Y} and the red points are \mathcal{Y}_{true} . We use \mathcal{Y}_{true} to estimate the GRMSE from samples to $\iota(M)$ with $GRMSE(\mathcal{Y}, \mathcal{Y}_{true}) = 0.0529$. Unlike the noisy data in subsection I.1, this noisy data set is more dense over regions 1 and there are large gaps over regions 2. Right Panel: The plot of \mathcal{X}_1 and \mathcal{Y}_{true} . The blue points are \mathcal{X}_1 and the red points are \mathcal{Y}_{true} . $GRMSE(\mathcal{X}_1, \mathcal{Y}_{true}) = 0.0223$. Bottom Panel: The plot of \mathcal{X}_2 and \mathcal{Y}_{true} . The blue points are \mathcal{X}_2 and the red points are \mathcal{Y}_{true} . $GRMSE(\mathcal{X}_2, \mathcal{Y}_{true}) = 0.0206$.

I.4. Noisy data set around a submanifold with small reach. We consider $\iota(M)$ which is a 2-d Cassini Oval with small reach. For $\theta \in [0, 2\pi)$,

$$X(\theta) = \sqrt{\cos(2\theta) + \sqrt{\cos(2\theta)^2 + 0.7 \cos(\theta)}},$$

$$Y(\theta) = \sqrt{1.07 \cos(2\theta) + \sqrt{\cos(2\theta)^2 + 0.2 \sin(\theta)}}.$$

Let \mathcal{Y}_{true} be the collection of 10^5 points on $\iota(M)$. Suppose $\mathbf{y}_i = \iota(x_i) + \eta_i$.

In the first example, we show that to reconstruct $\iota(M)$ properly, it is necessary that η_i is small compared to the reach. Suppose $\mathcal{Y} = \{\mathbf{y}_i\}_{i=1}^{102}$ in which $\eta_i \sim \mathcal{N}(0, \sigma^2 I_{3 \times 3})$, with $\sigma = 0.04$. We plot \mathcal{Y} and \mathcal{Y}_{true} in Figure 16. We choose $\varepsilon = 0.6$ and $\delta = 0.6$ by maximizing the sum of the marginal likelihood functions in the first round of the iteration in Algorithm 1. We iterate Steps 1-3 of Algorithm 1 twice. The estimated covariance parameters in the last round of the iterations are $A^{(1)} = 0.1$, $\rho^{(1)} = 0.5$ and $\sigma^{(1)} = \sqrt{0.012}$. We apply Algorithm 2 with the covariance parameters and output \mathcal{X}_2 consisting of 612 points. The denoised outputs \mathcal{X}_1 and the interpolations \mathcal{X}_2 are shown in Figure 16. Given the large noise and small reach, \mathcal{Y} is more likely to distribute around a figure 8 curve rather than a simple closed curve. Thus, MrGap improperly connects two regions on $\iota(M)$, resulting in the denoised points and interpolations falling along the figure 8 curve.

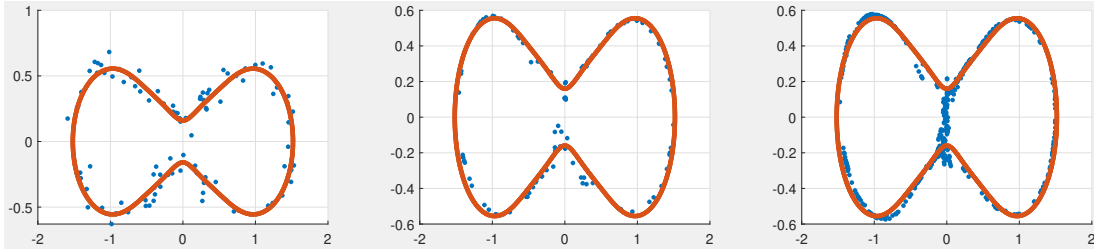


FIGURE 16. Left: The plot of \mathcal{Y} (blue) and \mathcal{Y}_{true} (red). Middle: The plot of \mathcal{X}_1 (blue) and \mathcal{Y}_{true} (red). Right: The plot of \mathcal{X}_2 (blue) and \mathcal{Y}_{true} (red)

In the second example, we apply the same $\iota(M)$. We demonstrate that regions with large curvature cannot be adequately reconstructed when the surrounding data is too sparse. Suppose $\mathcal{Y} = \{\mathbf{y}_i\}_{i=1}^{30}$ in which $\eta_i \sim \mathcal{N}(0, \sigma^2 I_{3 \times 3})$, with $\sigma = 0.04$. We plot \mathcal{Y} and \mathcal{Y}_{true} in Figure 17. We choose $\varepsilon = 0.6$ and $\delta = 0.6$ by maximizing the sum of the marginal likelihood functions in the first round of the iteration in Algorithm 1. We iterate Steps 1-3 of Algorithm 1 twice. The estimated covariance parameters in the last round of the iterations are $A^{(1)} = 0.24$, $\rho^{(1)} = 1$ and $\sigma^{(1)} = \sqrt{0.0005}$. We apply Algorithm 2 with the covariance parameters and output \mathcal{X}_2 consisting of 600 points. The denoised outputs \mathcal{X}_1 and the interpolations \mathcal{X}_2 are shown in Figure 17. The highlighted regions in the figure have large curvature. Due to the lack of samples in these areas, interpolations either fail to reconstruct the region or produce a flatter representation compared to the actual curve.

APPENDIX J. COMPARISON OF MRGAP WITH PRINCIPAL GRAPH METHOD ON CASSINI OVAL

We compare the performance of MrGap on the noisy samples from the Cassini Oval $\iota(M)$ described in subsection I.1 with the principal graph method of [26]. The principal graph method treats the data as vertices of a weighted graph and solves a minimization problem involving a number of nearest neighbors mn and tuning parameters σ_p , γ_p and λ_p . Recall that the Cassini Oval data set \mathcal{Y} consists of 102 noisy points near the curve and \mathcal{Y}_{true} consists of 10^5 points on the curve for us to estimate the GRMSE. \mathcal{X}_1 is the denoised output of the MrGap with $GRMSE(\mathcal{X}_1, \mathcal{Y}_{true}) = 0.0224$. We plot \mathcal{X}_1 and \mathcal{Y}_{true} in Figure

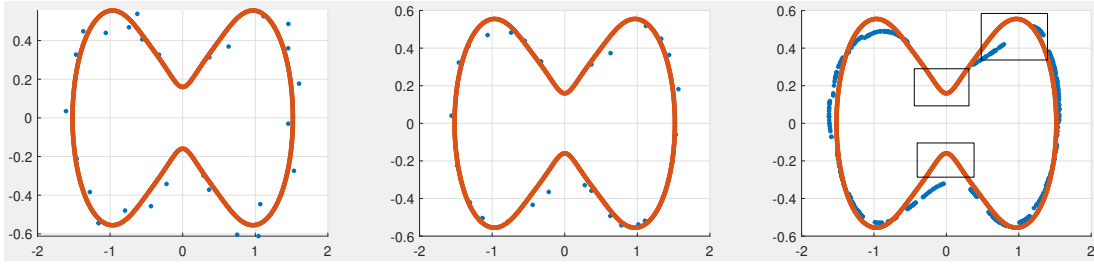


FIGURE 17. Left: The plot of \mathcal{Y} (blue) and \mathcal{Y}_{true} (red). Middle: The plot of \mathcal{X}_1 (blue) and \mathcal{Y}_{true} (red). Right: The plot of \mathcal{X}_2 (blue) and \mathcal{Y}_{true} (red)

13. For the principal graph method, we choose $nn = 5$, $\sigma_p = 0.01$, $\gamma_p = 0.5$ and $\lambda_p = 1$ based on the suggestion in the code. We iterate the algorithm for 20 times to acquire 102 denoised data points \mathcal{X}_p , obtaining $GRMSE(\mathcal{X}_p, \mathcal{Y}_{true}) = 0.0322$, which is 44% higher than $GRMSE(\mathcal{X}_1, \mathcal{Y}_{true})$. We plot \mathcal{X}_p and \mathcal{Y}_{true} in Figure 18. The principal graph algorithm generates a curve which fits \mathcal{Y} . We plot the curve and \mathcal{Y}_{true} in Figure 19. In the MrGap algorithm, we glue charts together by applying GP to construct a smooth manifold. However, in the principal graph method, there may be non smoothness generated as indicated in Figure 19.

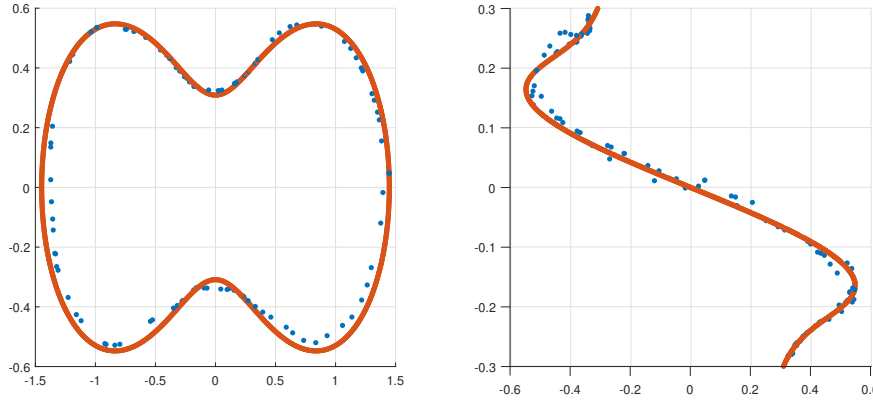


FIGURE 18. \mathcal{X}_p contains 102 denoised points on the Cassini Oval $\iota(M)$ by the principal graph algorithm. The left and the right panels show the XY plot and YZ plot of \mathcal{X}_p and \mathcal{Y}_{true} respectively. The blue points are \mathcal{X}_p and the red points are \mathcal{Y}_{true} . We use \mathcal{Y}_{true} to estimate the GRMSE from samples to $\iota(M)$ with $GRMSE(\mathcal{X}_p, \mathcal{Y}_{true}) = 0.0322$.

APPENDIX K. PERFORMANCE OF MRGAP UNDER DIFFERENT ASSUMPTIONS ON THE MANIFOLD AND THE NOISE

In the following subsections, we explore the performance of the MrGap under different assumptions on the noisy data. First, we assume that the noisy data are distributed around $\iota(M)$ which is an embedded submanifold with boundary in the Euclidean space. Then, we consider the case when the noise is not Gaussian.

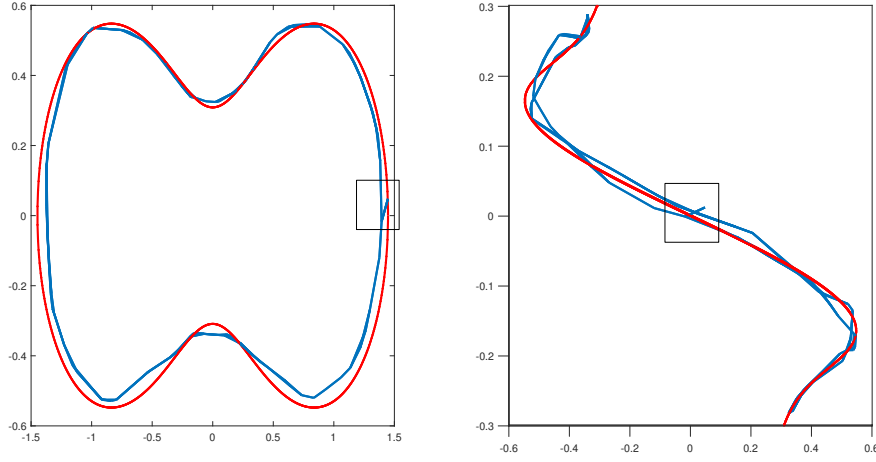


FIGURE 19. The blue curve is the curve which fits the noisy data set \mathcal{Y} by applying the principal graph algorithm. The red points are \mathcal{Y}_{true} . The left and the right panels show the XY plot and YZ plot of the fitting curve and \mathcal{Y}_{true} respectively. The fitting curve is not smooth at the indicated position.

K.1. MrGap on manifold with boundary. Let $\iota(M)$ be a half torus in \mathbb{R}^3 parametrized by $u \in [0, 2\pi)$ and $v \in (-\frac{\pi}{2}, \frac{\pi}{2})$

$$(47) \quad \begin{aligned} X(u, v) &= (3 + 0.8 \cos(u)) \cos(v), \\ Y(u, v) &= (3 + 0.8 \cos(u)) \sin(v), \\ Z(u, v) &= 0.8 \sin(u). \end{aligned}$$

We randomly sample 400 points $\{\iota(x_i)\}_{i=1}^{400}$ based on the uniform density function on $\iota(M)$. Let $\eta_i \sim \mathcal{N}(0, \sigma^2 I_{3 \times 3})$, with $\sigma = 0.12$, $\mathbf{y}_i = \iota(x_i) + \eta_i$ for $i = 1, \dots, 400$, and $\mathcal{Y} = \{\mathbf{y}_i\}_{i=1}^{400}$. We randomly sample 79585 points based on the uniform density function on $\iota(M)$ to form \mathcal{Y}_{true} . We calculate the GRMSE from \mathcal{Y} to \mathcal{Y}_{true} which is $GRMSE(\mathcal{Y}, \mathcal{Y}_{true}) = 0.1159$. We plot \mathcal{Y} in Figure 20. We apply the MrGap algorithm with $\varepsilon = 1$ and $\delta = 1$. We iterate Steps 1-3 of Algorithm 1 twice. The estimated covariance parameters in the last round of the iterations are $A^{(1)} = 1.3$, $\rho^{(1)} = 5$ and $\sigma^{(1)} = \sqrt{0.002}$. The final denoised outputs are $\mathcal{X}_1 = \{\hat{\mathbf{y}}_i\}_{i=1}^{400}$ with $GRMSE(\mathcal{X}_1, \mathcal{Y}_{true}) = 0.0646$. We plot \mathcal{X}_1 in Figure 20. Note that η_i can be decomposed into two components: η_i^\top which is tangent to $\iota(M)$ at $\iota(x_i)$ and η_i^\perp which is perpendicular to $\iota(M)$ at $\iota(x_i)$. Due to the boundary property of the manifold, when $\iota(x_i)$ is near the boundary of $\iota(M)$, the δ neighborhood around the corresponding noisy data \mathbf{y}_i may contain fewer data points than when $\iota(x_i)$ is away from the boundary. Since MrGap relies on GP to reconstruct a chart associated with \mathbf{y}_i , we may have fewer predictors and responses for the GP regression, potentially diminishing the effectiveness of reducing η_i^\top . Thus, the denoised data points may lie on an outward extension of $\iota(M)$ from the boundary as we shown in region 1 of Figure 20. At last, we choose $K = 20$ in applying algorithm 2. The outputs are $\mathcal{X}_2 = \{\hat{\mathbf{y}}_i\}_{i=1}^{8000}$ with $GRMSE(\mathcal{X}_2, \mathcal{Y}_{true}) = 0.0634$. We plot \mathcal{X}_2 in Figure 20.

K.2. MrGap on data with bounded noise. Let $\iota(M)$ be a half torus in \mathbb{R}^3 described by (47). Suppose \mathcal{Y}_{true} consists of 79585 points on $\iota(M)$. $\iota(M)$ is contained in a larger box $[-4.3, 4.3] \times [-4.3, 4.3] \times [-1.2, 1.2]$ in \mathbb{R}^3 . We sample 3000 points \mathcal{Y}_b non-uniformly from this box. \mathcal{Y} consists of 319 points $\{\mathbf{y}_i\}_{i=1}^{319}$ such that if $\mathbf{y}_i \in \mathcal{Y}_b$ and $GRMSE(\mathbf{y}_i, \mathcal{Y}_{true}) < 0.25$, then $\mathbf{y}_i \in \mathcal{Y}$. Hence, \mathcal{Y} are the points around $\iota(M)$ with bounded non-isotropic noise. We calculate the GRMSE from \mathcal{Y} to \mathcal{Y}_{true} which is $GRMSE(\mathcal{Y}, \mathcal{Y}_{true}) = 0.1201$. We apply the MrGap algorithm with $\varepsilon = 1$ and $\delta = 1$. We iterate

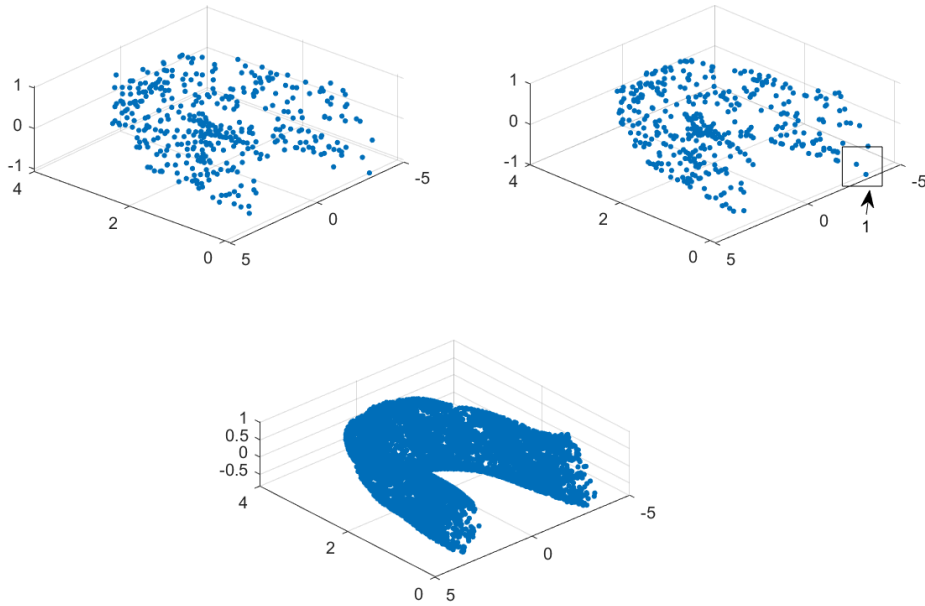


FIGURE 20. \mathcal{Y} contains 400 noisy points around the half torus $\iota(M)$ and \mathcal{Y}_{true} contains 79585 points on the torus $\iota(M)$. \mathcal{X}_1 contains 400 denoised points on $\iota(M)$ by the MrGap algorithm. \mathcal{X}_2 contains 8000 interpolated points on $\iota(M)$ by the MrGap algorithm. We use \mathcal{Y}_{true} to estimate the GRMSE from samples to $\iota(M)$. Top left: Original data \mathcal{Y} with $GRMSE(\mathcal{Y}, \mathcal{Y}_{true}) = 0.1159$. Top right: Fits from MrGap \mathcal{X}_1 with $GRMSE(\mathcal{X}_1, \mathcal{Y}_{true}) = 0.0646$. Region 1 includes the denoised points on an extension $\iota(M)$ from the boundary. Bottom: Interpolated fits from MrGap \mathcal{X}_2 with $GRMSE(\mathcal{X}_2, \mathcal{Y}_{true}) = 0.0634$.

Steps 1-3 of Algorithm 1 twice. The estimated covariance parameters in the last round of the iterations are $A^{(1)} = 0.6$, $\rho^{(1)} = 3$ and $\sigma^{(1)} = \sqrt{0.002}$. The final denoised outputs are $\mathcal{X}_1 = \{\hat{\mathbf{y}}_i\}_{i=1}^{319}$ with $GRMSE(\mathcal{X}_1, \mathcal{Y}_{true}) = 0.0698$. At last, we choose $K = 20$ in applying algorithm 2. The outputs are $\mathcal{X}_2 = \{\hat{\mathbf{y}}_i\}_{i=1}^{6380}$ with $GRMSE(\mathcal{X}_2, \mathcal{Y}_{true}) = 0.0524$.

REFERENCES

- [1] Eddie Aamari and Clément Levrard. Nonasymptotic rates for manifold, tangent space and curvature estimation. *The Annals of Statistics*, 47(1):177–204, 2019.
- [2] Yariv Aizenbud and Barak Sober. Non-parametric estimation of manifolds from noisy data. *arXiv preprint arXiv:2105.04754*, 2021.
- [3] Mauricio A Alvarez, Lorenzo Rosasco, Neil D Lawrence, et al. Kernels for vector-valued functions: A review. *Foundations and Trends® in Machine Learning*, 4(3):195–266, 2012.
- [4] Mikhail Belkin and Partha Niyogi. Laplacian eigenmaps for dimensionality reduction and data representation. *Neural computation*, 15(6):1373–1396, 2003.
- [5] Jean-Daniel Boissonnat, André Lieutier, and Mathijs Wintraecken. The reach, metric distortion, geodesic convexity and the variation of tangent spaces. *Journal of applied and computational topology*, 3(1):29–58, 2019.
- [6] Jeff Calder, Nicolas Garcia Trillos, and Marta Lewicka. Lipschitz regularity of graph Laplacians on random data clouds. *SIAM Journal on Mathematical Analysis*, 54(1):1169–1222, 2022.
- [7] Xiuyuan Cheng and Nan Wu. Eigen-convergence of Gaussian kernelized graph Laplacian by manifold heat interpolation. *Applied and Computational Harmonic Analysis*, 61:132–190, 2022.
- [8] Ronald R Coifman and Stéphane Lafon. Diffusion maps. *Applied and Computational Harmonic Analysis*, 21(1):5–30, 2006.

- [9] Chandler Davis and William Morton Kahan. The rotation of eigenvectors by a perturbation. iii. *SIAM Journal on Numerical Analysis*, 7(1):1–46, 1970.
- [10] Xiucui Ding and Hau-Tieng Wu. Impact of signal-to-noise ratio and bandwidth on graph Laplacian spectrum from high-dimensional noisy point cloud. *arXiv preprint arXiv:2011.10725*, 2020.
- [11] Manfredo P Do Carmo. *Riemannian geometry*. Springer Science & Business Media, 2013.
- [12] David B. Dunson, Hau-Tieng Wu, and Nan Wu. Spectral convergence of graph Laplacian and heat kernel reconstruction in L^∞ from random samples. *Applied and Computational Harmonic Analysis*, 55:282–336, 2021.
- [13] David B. Dunson, Hau-Tieng Wu, and Nan Wu. Graph based Gaussian processes on restricted domains. *Journal of the Royal Statistical Society: Series B (Statistical Methodology)*, 84(2):414–439, 2022.
- [14] Noureddine El Karoui and Hau-Tieng Wu. Graph connection Laplacian methods can be made robust to noise. *The Annals of Statistics*, 44(1):346–372, 2016.
- [15] Brittany Terese Fasy, Fabrizio Lecci, Alessandro Rinaldo, Larry Wasserman, Sivaraman Balakrishnan, and Aarti Singh. Confidence sets for persistence diagrams. *The Annals of Statistics*, 42(6):2301 – 2339, 2014.
- [16] Herbert Federer. Curvature measures. *Transactions of the American Mathematical Society*, 93(3):418–491, 1959.
- [17] Charles Fefferman, Sergei Ivanov, Yaroslav Kurylev, Matti Lassas, and Hariharan Narayanan. Fitting a putative manifold to noisy data. 75:688–720, 2018.
- [18] Charles Fefferman, Sergei Ivanov, Matti Lassas, and Hariharan Narayanan. Fitting a manifold of large reach to noisy data. *arXiv preprint arXiv:1910.05084*, 2019.
- [19] Christopher Genovese, Marco Perone-Pacífico, Isabella Verdinelli, and Larry Wasserman. Minimax manifold estimation. *Journal of Machine Learning Research*, 13(43):1263–1291, 2012.
- [20] Trevor Hastie and Werner Stuetzle. Principal curves. *Journal of the American Statistical Association*, 84(406):502–516, 1989.
- [21] Daniel N Kaslovsky and François G Meyer. Non-asymptotic analysis of tangent space perturbation. *Information and Inference: a Journal of the IMA*, 3(2):134–187, 2014.
- [22] Slav Kirov and Dejan Slepčev. Multiple penalized principal curves: analysis and computation. *Journal of Mathematical Imaging and Vision*, 59(2):234–256, 2017.
- [23] Patrik Lauha, Panu Somervuo, Petteri Lehtikoinen, Lisa Geres, Tobias Richter, Sebastian Seibold, and Otso Ovaskainen. Domain-specific neural networks improve automated bird sound recognition already with small amount of local data. *Methods in Ecology and Evolution*, 13(12):2799–2810, 2022.
- [24] John M Lee. *Introduction to Smooth Manifolds*. Springer, 2012.
- [25] Petteri Lehtikoinen, Meeri Rannisto, Ulisses Camargo, Aki Aintila, Patrik Lauha, Esko Piirainen, Panu Somervuo, and Otso Ovaskainen. A successful crowdsourcing approach for bird sound classification. *Citizen science*, 8(1), 2023.
- [26] Qi Mao, Li Wang, Ivor W Tsang, and Yijun Sun. Principal graph and structure learning based on reversed graph embedding. *IEEE Transactions on Pattern Analysis and Machine Intelligence*, 39(11):2227–2241, 2016.
- [27] Kun Meng and Ani Eloyan. Principal manifold estimation via model complexity selection. *Journal of the Royal Statistical Society: Series B (Statistical Methodology)*, 83(2):369–394, 2021.
- [28] Kun Meng, Jinyu Wang, Lorin Crawford, and Ani Eloyan. Randomness and statistical inference of shapes via the smooth euler characteristic transform. *arXiv preprint arXiv:2204.12699*, 2022.
- [29] James R Munkres. *Analysis on manifolds*. CRC Press, 2018.
- [30] Andrew Ng, Michael Jordan, and Yair Weiss. On spectral clustering: Analysis and an algorithm. *Advances in neural information processing systems*, 14, 2001.
- [31] Partha Niyogi, Stephen Smale, and Shmuel Weinberger. Finding the homology of submanifolds with high confidence from random samples. *Discrete & Computational Geometry*, 39(1-3):419–441, 2008.
- [32] Otso Ovaskainen, Ulisses Moliterno de Camargo, and Panu Somervuo. Animal sound identifier (asi): software for automated identification of vocal animals. *Ecology letters*, 21(8):1244–1254, 2018.
- [33] Carl Edward Rasmussen. Gaussian processes in machine learning. In *Summer School on Machine Learning*, pages 63–71. Springer, 2003.
- [34] Andrew Robinson and Katharine Turner. Hypothesis testing for topological data analysis. *Journal of Applied and Computational Topology*, 1:241–261, 2017.
- [35] Sam T Roweis and Lawrence K Saul. Nonlinear dimensionality reduction by locally linear embedding. *Science*, 290(5500):2323–2326, 2000.
- [36] Chao Shen and Hau-Tieng Wu. Scalability and robustness of spectral embedding: landmark diffusion is all you need. *arXiv preprint arXiv:2001.00801*, 2020.
- [37] Amit Singer and H-T Wu. Vector diffusion maps and the connection Laplacian. *Communications on Pure and Applied Mathematics*, 65(8):1067–1144, 2012.
- [38] Alexander Smola, Sebastian Mika, Bernhard Schölkopf, Robert Williamson, et al. Regularized principal manifolds. *Journal of Machine Learning Research*, 1:179–209, 2001.
- [39] Joshua B Tenenbaum, Vin De Silva, and John C Langford. A global geometric framework for nonlinear dimensionality reduction. *Science*, 290(5500):2319–2323, 2000.

- [40] Laurens Van der Maaten and Geoffrey Hinton. Visualizing data using t-SNE. *Journal of Machine Learning Research*, 9(11):2579–2605, 2008.
- [41] Per Åke Wedin. On angles between subspaces of a finite dimensional inner product space. In *Matrix Pencils*, pages 263–285. Springer, 1983.
- [42] Hau-Tieng Wu and Nan Wu. Think globally, fit locally under the manifold setup: Asymptotic analysis of locally linear embedding. *The Annals of Statistics*, 46(6B):3805–3837, 2018.
- [43] Hau-Tieng Wu and Nan Wu. Strong uniform consistency with rates for kernel density estimators with general kernels on manifolds. *Information and Inference: A Journal of the IMA*, 11(2):781–799, 2021.
- [44] Hau-Tieng Wu and Nan Wu. When locally linear embedding hits boundary. *Journal of Machine Learning Research*, 24(69):1–80, 2023.
- [45] Zhigang Yao, Jiaji Su, Bingjie Li, and Shing-Tung Yau. Manifold fitting. *arXiv preprint arXiv:2304.07680*, 2023.
- [46] Yi Yu, Tengyao Wang, and Richard J Samworth. A useful variant of the davis–kahan theorem for statisticians. *Biometrika*, 102(2):315–323, 2015.

DAVID B DUNSON, DEPARTMENT OF STATISTICAL SCIENCE, DUKE UNIVERSITY, DURHAM, NC
Email address: `dunson@duke.edu`

NAN WU, DEPARTMENT OF MATHEMATICAL SCIENCES, THE UNIVERSITY OF TEXAS AT DALLAS, RICHARDSON, TX
Email address: `nan.wu@utdallas.edu`